THE CHARACTERISATION OF THE CORROSION AND DEGRADATION OF ATOMISED FERROSILICON IN A DENSE MEDIUM CIRCUIT

Andries Mans, B.Eng (Minerals)

Dissertation submitted in fulfilment of the requirements for the degree Magister in Engineering at the School of Chemical and Minerals Engineering at the Potchefstroom University of Christian Higher Education

Supervisor: Prof F.B. Waanders

Co-Supervisor: Mr. Q.P. Campbell

Potchefstroom

2003

Declaration

I, Andries Mans, hereby declare that the dissertation with title: **The characterisation of the corrosion and degradation of atomised Ferrosilicon in a dense medium circuit**, which is done for the completion of the degree Magister in Engineering, is my own work.

Signature: _____ Date: _____

Abstract

The Kumba Resources Sishen Iron Ore Mine is one of the biggest iron ore producers in South Africa, where beneficiation of the iron ore is done using a dense medium separation process. Ferrosilicon is used as the dense medium separation material.

About 7 years ago, Kumba Resources decided to produce its own ferrosilicon, whereas the previous supplier was Samancor. The new ferrosilicon produced by Kumba Resources, however, had different characteristics and thus caused different problems in the dense medium separation process, as was the case with the previously used ferrosilicon.

A study was undertaken to identify the changes that occur in the new ferrosilicon and to understand the reasons why certain losses occur. Tests were done in the laboratory to identify the effect of attrition on the ferrosilicon used as a dense medium separation material, and the results obtained via the use of SEM analyses and Mössbauer spectroscopy, were compared with the results obtained from samples taken in the Sishen plant itself.

No definite change could be observed in the magnetic properties of the ferrosilicon during use, but rather a difference in magnetic recoverability of individual particles was found. The difference in the magnetic recoverability was assigned to the fact that the chemical compositions of individual size fractions may be different from the bulk chemical composition. Furthermore, due to a difference in magnetic recoverability, it was found that one of the main pathways of loss for the ferrosilicon was the inefficient magnetic recovery of the ferrosilicon. The abrasion process that takes place during normal use of the ferrosilicon, was also identified as a large contributing factor to the loss of ferrosilicon.

It is recommended that manufacturers should ensure that the bulk chemical composition of the ferrosilicon produced be an accurate reflection of the chemical composition of individual ferrosilicon particles. This would ensure more efficient reclaiming of the used ferrosilicon.

Opsomming

Die Kumba Resources Sishen Ystererts Myn is een van die grootste produsente van ystererts in Suid-Afrika. Die veredeling van die ystererts vind plaas deur gebruik te maak van 'n digte medium skeidings proses, met ferrosilikon as digte medium materiaal.

Ongeveer 7 jaar gelede het Kumba Resources besluit om hul eie ferrosilikon te produseer. Die nuwe ferrosilikon het egter ander eienskappe as die vorige vervaardiger, Samancor, se ferrosilikon, wat veroorsaak dat ander probleme ondervind word met die nuwe ferrosilikon tydens die digte medium skeidings proses.

'n Studie is onderneeem om die veranderinge wat plaasvind in die eienskappe van die nuwe ferrosilikon, tydens die gebruik daarvan as digte medium materiaal, te identifiseer en om die redes te verstaan waarom sekere verliese van ferrosilikon plaasvind. Toetse op die invloed van verwering, korrosie en slytasie op ferrosilikon is gedoen, en die resultate hiervan, verkry met behulp van SEM analises en Mössbauer spektroskopie, is vergelyk met die resultate verkry uit die monsters geneem in die Sishen aanleg.

Geen verandering in die magnetiese eienskappe is waargeneem nie, maar daar is wel 'n verskil in magnetiese herwinbaarheid uitgewys tussen verskillende ferrosilikon partikels. The verskil in magnetiese herwinbaarheid kan toegeskryf word aan die verskil in chemiese samestelling waargeneem by verskillende grootte fraksies, in vergelyking met die chemiese samestelling van die ferrosilicon as geheel. Verder is gevind dat een van die grootste bydraende faktore tot die verlies van ferrosilikon die oneffektiewe magnetiese herwinning van ferrosilikon is, veroorsaak deur die verskil in magnetiese herwinbaarheid. Die afslyting van onreëlmatighede op die ferrosilikon is ook geïdentifiseer as een van die grootste bydraende faktore wat verliese bepaal.

'n Aanbeveling, dat vervaardigers seker moet maak dat die individuele chemiese samestelling van die ferrosilikon partikels streng moet ooreenstem met die chemiese samestelling van die ferrosilikon partikels as geheel, is gemaak wat sal verseker dat meer effektiewe herwinning van die ferrosilikon sal plaasvind.

Acknowledgements

I would like to thank a few people for their help and contributions to the completion of this project. Without their help, all this could not have been done.

First of all, many thanks must go to my mentor and supervisor **Prof. F.B. Waanders** for the guidance he gave me, the encouragement he gave and the patience he had during the completion of this project.

I would like to thank the staff of PU for CHE, School for Chemical and Minerals Engineering, for the help I received in setting up the experiments and for the maintenance done on the set-up. Furthermore, I would especially like to thank **Dr. L.R. Tiedt** of the Laboratory for electron microscopy at the PU for CHE, for the SEM analysis made and time spent refining the microphotographs.

A special word of thanks to the following people for the moral support during this project. Firstly to my wife **Lizelle**, I know it was hard to be without a husband for days at a time. To **Marco le Roux**, while busy with his own masters degree, he always had time to listen to some new theory regarding the results I obtained, and sometimes helping me to see something from a different angle.

Finally, and most important, all that was done would not have been possible without the guidance of my creator and saviour, **God**, in whom my strength lies.

Contents

List of Figures

List of Tables

CHAPTER 1: INTRODUCTION

The Kumba Resources Iron Ore Mine at Sishen is one of the biggest iron ore producers in South Africa [1]. Ferrosilicon is used in the dense medium separation of the iron ore at the Sishen iron ore mine. Dense medium separation can be described as a process of separation between the valuable mineral (iron ore in this case) and the gangue material and is based on differences in the mineral densities. The manner of separation occurs by using a medium with a density between that of the gangue and the ore, so that separation occurs within the medium to produce a sink and float product. Depending on which of the gangue or ore has the highest density, the sink or float streams, respectively, is seen as the product. The dense medium is used in the form of dissolved salts in water, or more commonly a suspension, in water, of finely divided high-density particles, such as the case with ferrosilicon.

Up to about 7 years ago, the primary manufacturer of ferrosilicon in South Africa, was Samancor and Sishen bought the ferrosilicon from this company. Kumba Resources however started to produce its own ferrosilicon at a plant situated near Pretoria, South Africa. The new ferrosilicon, produced by Kumba, differs in characteristics from the Samancor ferrosilicon, with particle shape one of the biggest differences. The reason for the change being made from the milled ferrosilicon, supplied by Samancor, to the newer atomised ferrosilicon, supplied by Kumba, lies in the particle shape, supposed to minimise operating cost. The difference in characteristics causes a difference in the operating characteristics during dense medium separation, which in turn causes Kumba plant problems different than that experienced with the Samancor ferrosilicon [1]. With the current set-up of the dense medium separation plants at Kumba, the changes in ferrosilicon characteristics cause a collectively bigger loss of ferrosilicon due to differences in, amongst others, magnetic recoverability and medium stability during the dense medium separation process. Although the pathways of losses are similar in some ways, with respect to the Kumba and Samancor ferrosilicon, the changes in characteristics have different effects on the overall pathway of loss. The pathways of losses of ferrosilicon are called medium losses, collectively.

The current total loss of ferrosilicon can be very high, which contributes greatly to the running cost of the plant. The cost of ferrosilicon was about R6 000/ton in the year 2001. At the current rate of addition of new ferrosilicon to the system, due to the continued loss during dense medium separation, the loss could be as high as 150 t of ferrosilicon, which relates to a loss of about R900 000 per month. Although this figure seems to be high, the Sishen plant compares relatively well with respect to other similar plants, where the Sishen plant loss is about 150 – 250 g ferrosilicon/ton ore while similar plants report losses of 500 g ferrosilicon/ton ore (up to 3000g/t in some cases) [2]. It could thus be understood that any way to reduce this loss should be investigated and employed to counter these losses.

The losses of ferrosilicon that occur are due to the adhesion of the ferrosilicon to the separation products (adhesion to iron ore and waste) as well as being present in discard streams originating from process equipment. Pathways for these losses are: attraction (adhesion) of the ferrosilicon to the ore and waste products (with ore porosity and inefficient washing playing a major role), medium properties (size, shape, density and magnetic susceptibility which influence the recoverability etc.), magnetic separation and classification inefficiencies (unrecovered ferrosilicon exiting the dense medium separation circuit) and corrosion and abrasion of the medium (producing very fine or even possibly soluble ferrosilicon). Other pathways that are easier to rectify are: poor housekeeping (ferrosilicon spilled and washed away), excessive circuit loading during the addition of fresh medium (causing spillage of ferrosilicon) and storage of the ferrosilicon medium during plant downtime.

In the current study four possible problems regarding ferrosilicon losses are investigated, which are: particle size distribution before and after use, to determine abrasion influence, change in particle density due to abrasion, possible magnetic property changes that can occur during use and changes that occur while storing the ferrosilicon medium during plant downtime.

- One of the biggest problems [1] relating to the losses is currently identified as the change in the particle size distribution of the ferrosilicon. This means that the finer particle content in the ferrosilicon medium decrease over time, which causes problems in the viscosity and stability of this medium. A decrease (and not an increase) of finer particle content occur due to the continuous loss of the finer particles through insufficient magnetic recovery of the ferrosilicon medium, according to Myburgh [1]. Although abrasion of the ferrosilicon medium does occur, which should produce more of the finer particles, the loss through insufficient magnetic recovery seems to counter this effect.

- A change in density can not be identified due to the fact that the density of the ferrosilicon medium continuously changes in the Sishen plant.

- A problem especially occurring during shutdown time, is the settling and packing of the ferrosilicon medium occurring in the storage containers. The ferrosilicon settles to the bottom of the container and after about a day, it "solidifies", due to possible oxidation, to such an extent that the container has to be emptied by means of jackhammers. Currently lime is used as an inhibitor (about 150 kg per 45 tons of medium, depending on the amount of downtime) to counter this chemical corrosion effect. More examples of the addition of inhibitors are noted by other authors [3] as being very successful.

- The magnetic properties of the medium are also thought to change over time, which could explain the change in the magnetic recoverability of the ferrosilicon. Some work has been done on the magnetic properties (saturation magnetisation value) of ferrosilicon [4][5] and on the link between the saturation magnetism value for a given sample and the magnetic recoverability of that sample [3]. However, no work could be found to indicate a possible change (or lack thereof) in the saturation magnetisation value (magnetic property of the ferrosilicon) during the use of the ferrosilicon, which would indicate a change in magnetic recoverability of the ferrosilicon.

Previous [2-11] work on the identification of the relevant ferrosilicon properties has already been done. Due to the different dense medium separation properties, various types of ferrosilicon have been developed and utilized, resulting in investigations being done only on specific types of differently manufactured ferrosilicon. No real investigation on comparable materials has thus been conducted and a need has arisen to know which changes occur during usage, where these changes occur, what the reasons for these changes are and what these changes could cause at the Kumba Resources mine at Sishen. The knowledge of these changes and subsequent corrective actions taken, can have a positive effect on the beneficiation rate of iron ore at the Sishen plant.

With these questions in mind, the following hypothesis can be formulated.

Hypotheses

1. A particle size distribution change occurs during usage of the ferrosilicon, to produce a medium with less fine particles, which will change the dense medium separation efficiency.
2. A change in medium density occurs during usage of the medium.
3. A definite magnetic property change occurs in the ferrosilicon particles, which affects losses through the magnetic recovery circuit.
4. During plant downtime, the addition of lime to the storage cones act as an oxidizer, which inhibits the active corrosion of the ferrosilicon.

CHAPTER 2: LITERATURE REVIEW

2.1 Introduction

A dense medium suspension consisting of water and ferrosilicon is used in most high-density mineral separation processes. The properties of the suspension (the dense medium or DMS-medium) and practices in a plant employing this separation technique, determine the losses of medium that could possible occur during the whole process. The chemical and physical properties of the ferrosilicon determine the behaviour of the suspension and the loss mechanisms, which in turn determine the separation performance and consumption of the dense medium separation material in the plant.

It is believed that the replacement of lost medium (ferrosilicon) constitutes about 20 – 40 % of the total running cost of a DMS plant [2][10]. These losses can be reduced by making minor changes to the plant configuration and improving plant practices, and this is usually accompanied by minimal capital expenditure. Good initial plant design and correct equipment selection can however eliminate this expenditure and ensure acceptable low medium losses.

The pathway for DMS-medium losses can be grouped into the following two routes [2]:

- Adherence to the products of separation, even after drainage, washing and screening.
- Losses in the final effluent streams during the dewatering of the medium, using magnetic separators and also hydrocyclones, settling cones and other solid-liquid separation devices, as well as spillage washed away during housekeeping.

The causes of the losses down these pathways are the following [2][10]:

- Attraction between the ore and medium particles, also ore porosity and poor washing and screening.
- Properties of the medium which include particle size, shape, magnetic susceptibility, ect.

- Inefficient separation and classification, eg. during magnetic separation, hydrocyclones, ect.
- Corrosion and abrasion of the medium.
- Poor housekeeping.
- Circuit overloading during addition of fresh medium.
- Plant downtime.

The emphasis in this study was on the property changes that could possibly occur during the use of the atomised ferrosilicon as dense medium separation material. These are: particle size distribution before and after use to determine abrasion influence, change in particle density possibly due to abrasion, possible magnetic property changes that can occur during use and changes that occur while storing the ferrosilicon medium during plant downtime.

The Sishen Iron Ore mine, part of the Kumba Resources group, uses atomised ferrosilicon in their dense medium separation plants for the beneficiation of iron ore. About 7 years ago, Kumba Resources decided to produce their own ferrosilicon. Due to the difference in characteristics of the new ferrosilicon and the previously used ferrosilicon, some problems in its use became apparent. A need arose to characterise the new self-produced ferrosilicon. With the current study, it is hoped that some light will be shed on this ferrosilicon question.

With much of the previous work done on the wider spectrum of the ferrosilicon alloy as subject [2-11], very little work exists on the specific ferrosilicon alloy with a silicon content in the 12-16 wt% silicon range. Most of the work done on the ferrosilicon alloy in this range, is usually done by the end users themselves and published data is very scarce or incomplete. Furthermore, the work that does exist for the ferrosilicon in this range, was done on steam atomised ferrosilicon, while the ferrosilicon used in this study was nitrogen gas atomised ferrosilicon. At the high temperatures involved in atomising the ferrosilicon, there is thermodynamically the possibility of a chemical reaction between the steam and the molten ferrosilicon, and a difference in the abrasion and chemical

corrosion characteristics between the steam atomised and the nitrogen atomised ferrosilicon may exist.

To understand the use and losses that occur due to basic property changes of ferrosilicon in a dense medium separation process, it is necessary to discuss the physical parameters of the ferrosilicon, such as:

- Internal structure
  - Microstructure
- External structure
  - Atomised vs. Milled ferrosilicon
  - Surface appearance
  - Hardness
  - Magnetic properties

2.2 Properties of ferrosilicon

The properties of ferrosilicon vary greatly and the properties needed depend mainly on the use thereof. The biggest consideration in the manufacturing of ferrosilicon is the silicon content in the final alloy, with alloy compositions ranging from about 3 wt% silicon to about 50 wt% silicon.

2.2.1 Internal structure and properties of ferrosilicon alloys

A discussion of the internal structure of the ferrosilicon alloys will follow with specific discussions of the phase diagram and microstructure.

2.2.1.1 Phase diagram and crystal structure

In **Figure 2.1** the phase diagram of the ferrosilicon system is shown [14]. Most ferrosilicon used in the industry [6] has the chemical composition of Fe_xSi ($3 \geq x \geq 0.43$) with a corresponding silicon content of between 14 and 54 wt%. For use in the dense medium separation industry, the silicon content in the ferrosilicon alloy has a narrower range of between 14 and 20 wt% silicon. The silicon content determine (among others) corrosion susceptibility and the density of the final product.

From **Figure 2.1** and the relevant enlargement of the area of interest, it can be seen that only a small area of the ferrosilicon phase diagram is applicable to the manufacturing of the dense medium separation material. Furthermore, from **Figure 2.1** and **Table 2.1** it can be seen that the relevant phases, of interest to the dense medium separation process, are the α_1, Fe_2Si, Fe_5Si_3 and FeSi phases.

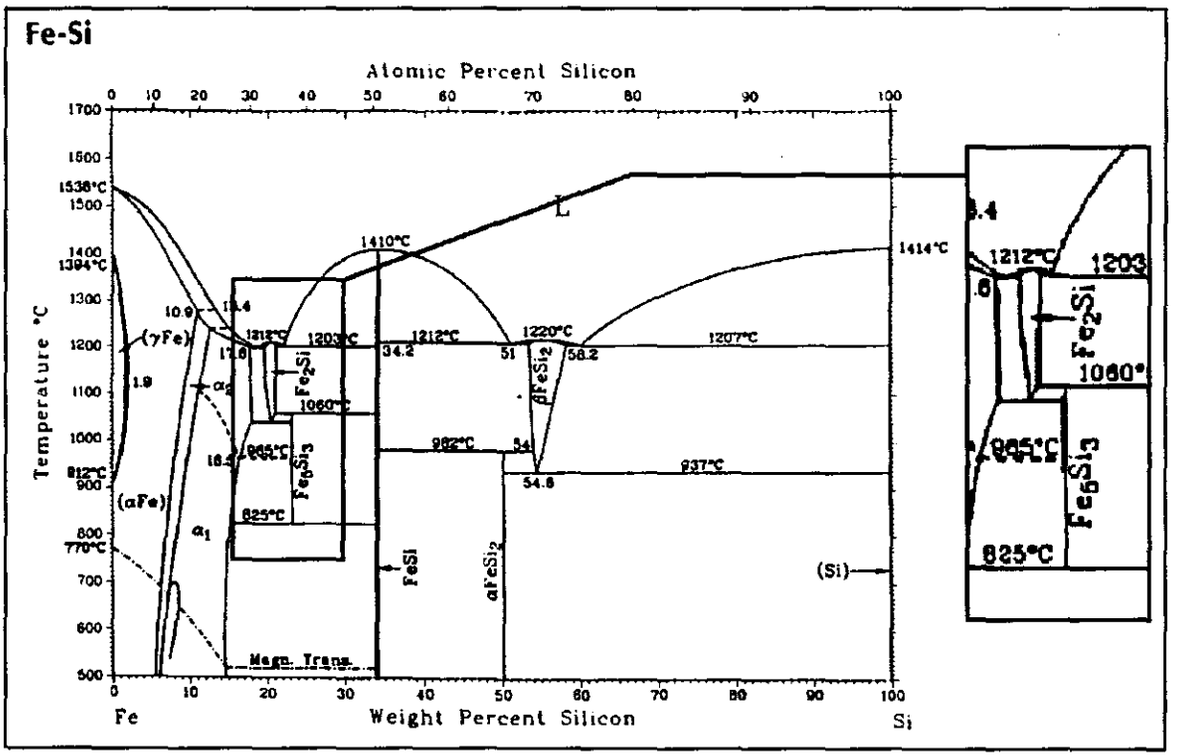

Figure 2.1: The phase diagram of the ferrosilicon system [14].

Table 2.1: Possible phases occurring in the ferrosilicon system [14]. Those relevant to dense medium separation material are given in bold.

Phase	Composition (wt% Si)
(γFe)	0 to 10.9
(αFe)	0 to 1.63
α_2	~5 to 12
α_1	**~5 to 18**
Fe_2Si	**~20.1**
Fe_5Si_3	**23.2**
FeSi	**~34**
$BFeSi_2$	53.4 to 58.2
$AFeSi_2$	50.2
(Si)	100

Microstructure

Williams *et al.* [11] reported a dual phase structure in the atomised as well as the milled ferrosilicon powders investigated, with the microstructure of the atomised ferrosilicon much finer, due to the faster cooling rate at which it was (cooled down) formed. Atomised ferrosilicon particles are normally not subjected to further heat treatment, which means that a dual metastable phase may be present [11]. A metastable phase is formed when the initial alloy at production temperature has two or more phases in equilibrium. During normal cooling (slow cooling), a solid phase is formed with the appropriate solid phase(s), which would then be in equilibrium at that temperature. The compositions of the phases change due to the migration of the different atoms between the solid state already formed and the remaining liquid state. This migration of atoms is a slow process, especially when migration takes place through a solid state. Thus, sufficient time is required for cooling to ensure the alloy with equilibrium phases. However, when rapid cooling takes place (as in the case of ferrosilicon production), there is not sufficient time for the equilibrium phases to form, and the two or more phases that were in equilibrium at the initial temperature, are solidified to form the metastable phase in the

alloy. This phase can be removed by heating the alloy to a sufficient temperature (temperature before it was cooled) and cooling it at a much slower rate [22].

This multi phase dendritic structure comprising of dendrites, Fe_3Si, and interdendrites, Fe_2Si as has been reported by Hunt *et al.* [3]. These authors made use of an electron probe micro-analyser, a scanning electron microscope (SEM) and a petrological microscope to determine these phases. The interdendrites are lines of weakness, along which the ferrosilicon particle can break to expose silicon rich areas, which can enhance corrosion rates. The increased cooling rate, used in the production of atomised ferrosilicon, decreases the microsegregation and dendrite arm spacing [11], which in turn ensured a more consistent homogeneity of the particles. Particle size may also have an effect on the microstructure [11] as the microstructure varies with particle size, due to the cooling rate.

Nkosibomvu *et al.* [4] indicated that the ferrosilicon they studied had a two-phase microstructure, with dendrites (possibly Fe_3Si with 74 - 78 wt% Fe and 18 - 22 wt% Si) being the major phase with an eutectic phase (75 - 80 wt% Fe and 13 - 18 wt% Si) crystallised between the dendrites. This eutectic phase had two phases, with one phase having the same composition as the dendrites.

Stearns [5] showed that ferrosilicon alloys are disordered when the silicon content is below 5 wt% Si, with ordering starting to take place at 8 wt% Si. According to Stearns [5] ordering is in the form of the Fe_3Al-type structure of which a lattice diagram is given in **Figure 2.2.** Nkosibomvu *et al.* [4] also described this Fe_3Al body centred cubic structure that forms in the 14 wt% silicon ferrosilicon alloy and they postulated that it is due to kinetic ordering.

In a ferrosilicon alloy with 14 wt% silicon the correct iron to silicon ratio is obtained to produce the Fe_3Si lattice with the Fe_3Al structure. If more silicon atoms are present, more of the D sites will be filled with silicon, with the inverse also holding, up to a minimum of 8 wt% silicon. With a silicon content of less than 8 wt% silicon, the alloy will have no D-type sites, and the silicon will be situated in any A-type site with equal probability [5].

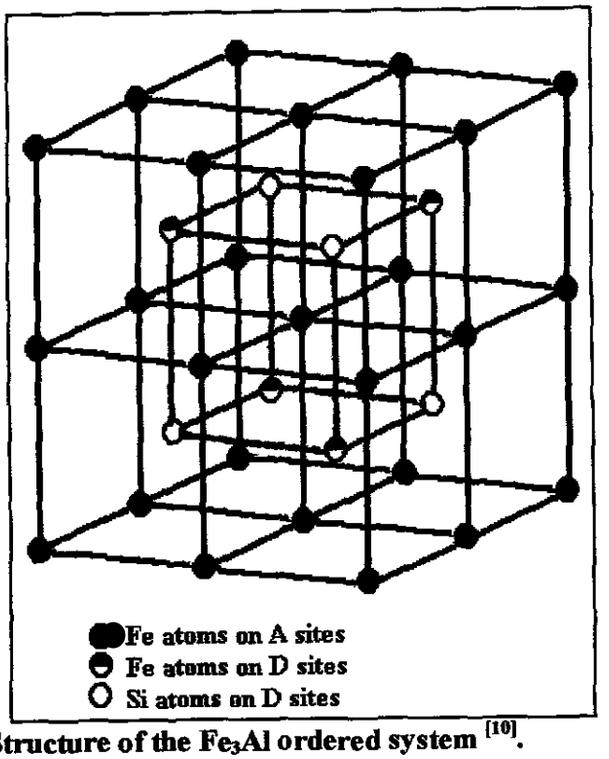

Figure 2.2: Structure of the Fe_3Al ordered system [10].

Most of the commercially available ferrosilicon powders are produced using processes that are not described in detail. However it is known that parameters of importance are melting temperature and the rates of production and cooling, which influences the quantity and quality of the final product microstructure. Although the ferrosilicon produced by Kumba are deemed to be unique, and the exact details (melt temperature, rate of production and cooling rate) of the production method is unknown, it seems to be safe to say that a dual phase, as described by the above-mentioned workers, can be expected to exist in the ferrosilicon in this study. It should be remembered that in all methods of atomised ferrosilicon production, some form of rapid cooling is essential to ensure the spherical shape of the particles. Some similarities should be expected due to the fact that the basic parameters for atomised ferrosilicon production are the same for all manufacturing methods.

2.2.2 External structure and properties of ferrosilicon alloys

The external structure of the ferrosilicon particle is of great importance to the dense medium separation process, because it influences dense medium stability, viscosity and abrasion characteristics, amongst others. A brief discussion of the external properties of the ferrosilicon particles will follow, with specific references to the difference between milled and atomised ferrosilicon, surface properties of the particle, hardness of individual particles and its magnetic properties.

2.2.2.1 Atomised vs. Milled ferrosilicon

Ferrosilicon is one of the most frequently used powders to be utilised in dense medium separation (DMS) processes. The two basic forms of these powders are either atomised or milled ferrosilicon material. The production mechanism of these two powders is basically the same. No details on the manufacturing techniques will be given in this study, with the only difference between the two being the fact that atomised ferrosilicon is produced by spraying the molten ferrosilicon alloy into a cooling medium (steam) to produce the atomised spheres. The subsequent milled ferrosilicon is produced by granulation of the ferrosilicon alloy in water and subsequent milling to produce the milled ferrosilicon powders [11]. Milling is performed to produce a powder with the correct size distribution. Although the initial production of the milled and atomised ferrosilicon is very similar, the milled ferrosilicon is still cheaper to produce and is thus widely used in the industry.

The use of ferrosilicon powders, either milled or atomised, was studied by Ferrara and Schena [12]. These authors came to the conclusion that for relative densities (RD) higher than 3 g/cm^3 in the dense medium separation process, the use of atomised ferrosilicon powders should be the first choice as dense medium, even though the milled powder is much cheaper. The reasons being:

- Milled ferrosilicon can only be used for separation processes with the relative density of the dense medium being less than about 3 g/cm^3, due to the low tolerance of the ferrosilicon to contamination from the ore being benificiated.
- Higher amounts of contamination (ore abrasion products) can be tolerated by atomised ferrosilicon. Relative densities of up to 3.2 g/cm^3 can be reached with contaminant (very fine slimes produced by the abrasion of the ore being benificiated) content even reaching a value of up to 15% in the dense medium.
- Although the stability of milled ferrosilicon suspensions is much better than that of the atomised ferrosilicon suspensions, the increase in viscosity of the former can have a detrimental effect on the plant operation.

The above-mentioned corresponds to the experience at the Sishen mine, where relative densities of up to 4g/cm^3 are used in the dense medium separation process and maintained relatively easy, with contaminants in the dense medium reaching values of up to 5 % (optimum being 3 %) [1].

2.2.2.2 Discussion of important surface properties of ferrosilicon powders

The properties of the individual particles are determined, as discussed earlier, by the parameters used in the ferrosilicon production method, and a discussion follows regarding the surface properties of the ferrosilicon particles.

Surface appearance

The particle shape of the ferrosilicon powders is the biggest physical difference that can be observed between the milled and atomised ferrosilicon, as can be seen from **Figure 2.3**.

As can be seen from **Figure 2.3(a)** the atomised particles consist of mainly spheroid particles, with the bigger particles even having protruding segments. These protrusions

may have been produced in the atomisation chamber during manufacturing [9], as a result of particle collisions while the material was still molten, giving rise to fusion of the particles. The smaller particles normally have a smooth surface in comparison to the coarser particles. Cavities and fractures may also occur in atomised ferrosilicon powders during production due to the rapid cooling of the powders. The cavities usually appear in the form of spherical holes or cores in the centre of the particle, which greatly influence the apparent density and hardness of the particle. Williams *et al.* [11] showed that the probability of a particle to have a cavity inclusion increases with particle size.

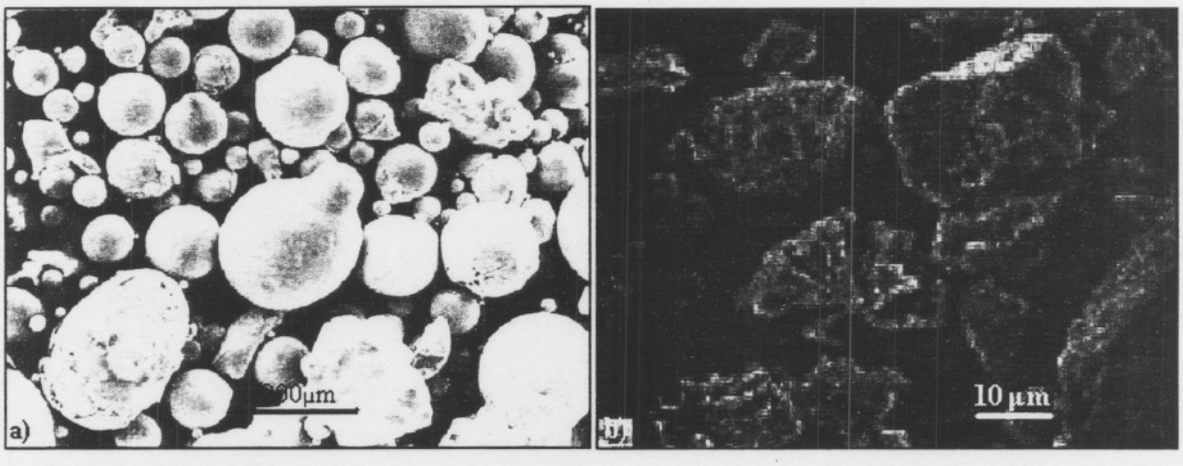

Figure 2.3: SEM microphotograph of (a) atomised and (b) milled ferrosilicon powders. Note the clear difference in the spheroid characteristic of the particles.

From **Figure 2.3(b)** the definite irregular shape of the milled ferrosilicon particles can be clearly seen. Williams and Kelsall [10] reported that at high magnification of cross-sectional views of the milled ferrosilicon particles, the poor mechanical integrity of the powders become apparent with many cracks visible. These cracks and fractures were produced either during the cooling phase of production or during the milling of the coarse ferrosilicon particles to obtain the required particle size distribution. Due to possible disintegration along the cracks, a significant change in particle shape and particle size distribution could thus take place in the dense medium separation process, which in turn could pose a problem with continuously changing dense medium properties.

The ferrosilicon produced by Kumba compares relatively well, with regard to the amount of protrusions, with the atomised ferrosilicon produced by other manufacturers, according to Myburgh [1]. This could reduce the effect of abrasion on the particle size distribution.

Hardness

Ferrosilicon containing 15 wt% silicon is hard and brittle, with a tensile strength of about 110 MPa [11] and a hardness of about 1000 HV_{50}. The Vickers microhardness technique, used by Williams *et al.* [11] resulted in the hardness values shown in **Figures 2.4** and **2.5**.

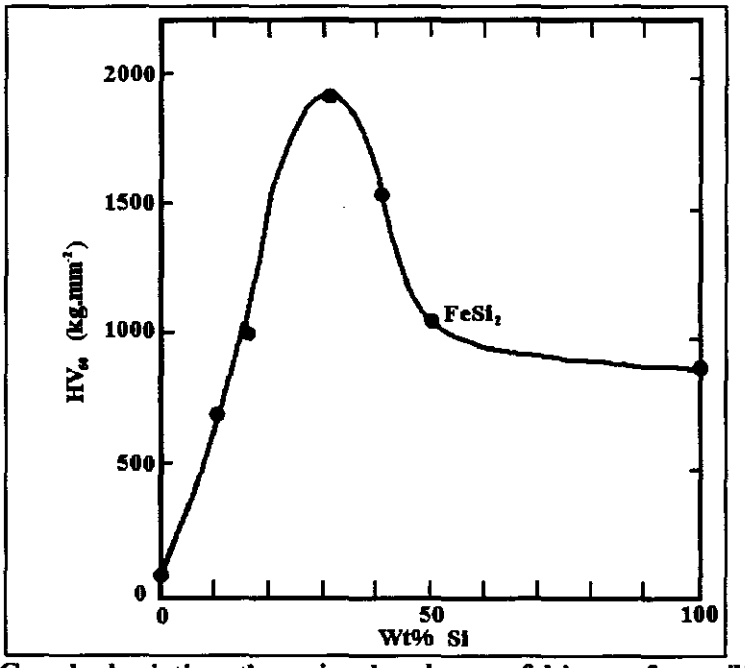

Figure 2.4: Graph depicting the microhardness of binary ferrosilicon alloys as function of silicon content [11].

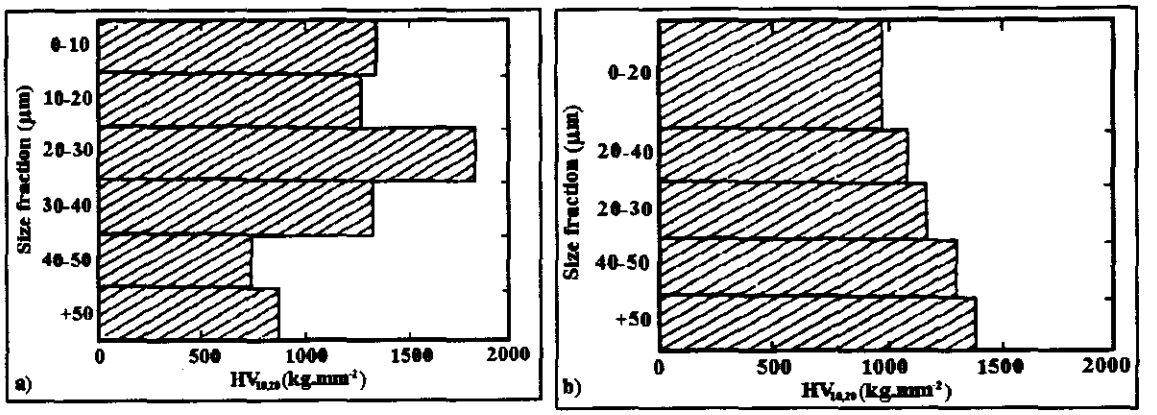

Figure 2.5(a) and (b): Graphs of microhardness of (a) atomised and (b) milled particles as a function of size [11].

From **Figure 2.4** it can be seen that the hardness values increased with higher silicon content, with a maximum at about 30 wt% Si. A decrease with a further increase in the silicon content can also be seen. It should be noted that these values where obtained for ferrosilicon alloys in brick form, and not the powder form used in dense medium separation processes. It is interesting to note that a change in microhardness (**Figure 2.5(a)**) occurs with respect to particle size in the atomised ferrosilicon powder investigated. The difference in microhardness can be assigned to the inclusion of micropores in the larger particles as was observed by William *et al.* [11]. Nkosibomvu *et al.* [4] described two kinds of pores, a majority of small irregular pores associated with solidification shrinkage and much larger spherical voids caused by gas generation during solidification of the particle. For the increasing microhardness with respect to particle size of the milled ferrosilicon (**Figure 2.5(b)**), Williams *et al.* [11] explained that the increase in hardness is due to the fact that fractures in the smaller particles may have traversed the entire particle, with the larger particles showing less fractures, and thus resulting in higher hardness values.

When the microhardness of particles without any micropores or fractures were measured [11], the correlation between the microhardness and the silicon content were the same as seen in **Figure 2.4**.

Passivation/Depassivation of the ferrosilicon particle surface

According to Williams and Kelsall [9], the chemical analyses of the surface of atomised particles shows a surface content of up to 54 wt% silicon [9]. With further investigation, they suggested that the surface of the atomised ferrosilicon particle may even consist of a mixture of SiO_2-Fe(II/III) oxide film, with a depth measured to be about 50 nm. Other authors [3][10][11] made suggestions as to the chemical composition of this surface layer, with little or no correlation between these findings. The few correlating suggestions can however be summarised as follows:

- A film does exist on the ferrosilicon powders, with a higher silicon ratio in the film than in the whole particle.
- Iron does occur in or on the film, in the form of hydroxides, oxides or as ions.
- Some sort of passivation/depassivation occurs.
- Atomised ferrosilicon has a thicker initial passive layer than milled ferrosilicon, but after a short time of use in the dense medium separation plant, the passive layers become the same for both the atomised and milled ferrosilicon.

The significance of these suggestions are that it is expected that both the milled and atomised ferrosilicon would act the same, with respect to corrosion susceptibility, after some use in the dense medium separation process.

Magnetic properties

It is clear form **Figure 2.6** that an increase in silicon content yields a decrease in the magnetisation, which is technologically undesirable for dense medium separation materials because it influences the magnetic recovery efficiency. In the silicon content region of 15 – 20 wt% silicon, typical for the ferrosilicon used in the dense medium separation process, Satmagan values of 55 - 70 % were obtained.

The magnetic properties of the ferrosilicon alloy are of great significance to dense medium separation plants and determine the ability to reclaim and reuse the ferrosilicon. Satmagan values (saturation magnetisation, σ_{sat}) were experimentally determined by Nkosibomvu *et al* [4] and the results are shown in **Figure 2.7**.

In a study done by Hunt *et al.* [3] to find a correlation between the Satmagan value for a given sample and the magnetic separator efficiency, they found that with a reduction in Satmagan value, the efficiency of the magnetic separator was also reduced. At a Satmagan value of about 58% and higher, no decrease in ferrosilicon loss was observed. Furthermore, in their work they also found that the effluent ferrosilicon particles were always the smaller size fractions and the Satmagan value was always lower than the Satmagan value of the feed. This can be ascribed to the fact that for a certain sample of ferrosilicon, not all the particles will have the same chemical composition [3] (which indirectly determines the Satmagan value). Satmagan values for the smaller size fractions of the samples used in the work by Hunt *et al.* [3] was lower than the bulk Satmagan value of the ferrosilicon used.

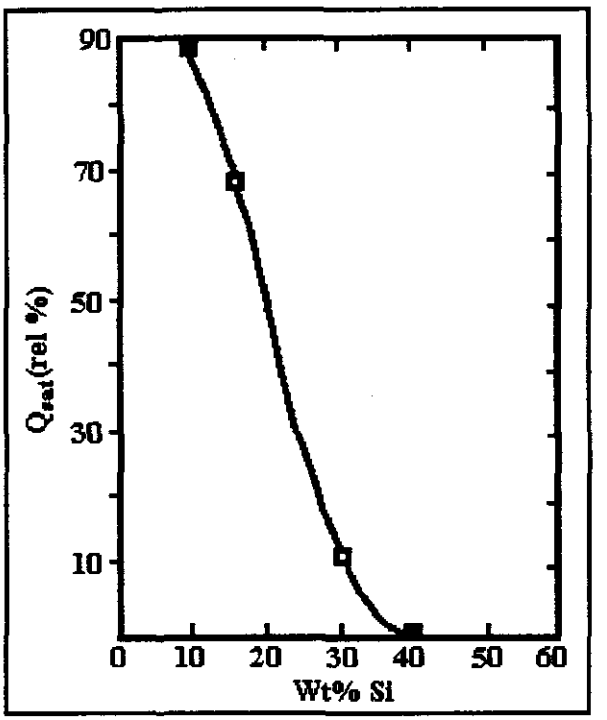

Figure 2.6: Experimentally determined magnetisation for ferrosilicon alloys as function of silicon content [11].

A study of the internal structure of the ferrosilicon powders was done by Nkosibomvu *et al.*[4] using Mössbauer spectroscopy as major analytical method. In this study the relationship between the magnetic field distribution peaks in a Mössbauer

spectrum and the Satmagan value for five ferrosilicon samples were determined. It was initially expected that the higher the overall iron content of the sample, the higher the Satmagan value would be, which was not the case. A relationship was however found by Nkosibomvu *et al.* [4], which is depicted in **Figure 2.7**, which shows a maximum to occur.

The Mössbauer results showed two sextets with hyperfine magnetic fields of 19.7 ± 0.5 T and 31.3 ± 0.5 T respectively with the ratio of the peak intensities of the two hyperfine magnetic fields increasing with an increase in Satmagan value. Stearns [5] showed in his work that the annealed ferrosilicon alloy powders started to become ordered when the silicon content was above 14.6 wt% Si. This means that any ferrosilicon alloy powder with a silicon content of more than 15 wt% silicon, would show some degree of ordering into the Fe_3Al type structure, the amount of ordering only being dependent of the annealing that could take place during the production or use thereof. The Satmagan values obtained via Mössbauer spectroscopy corresponds with the data obtained by Williams *et al.* [11].

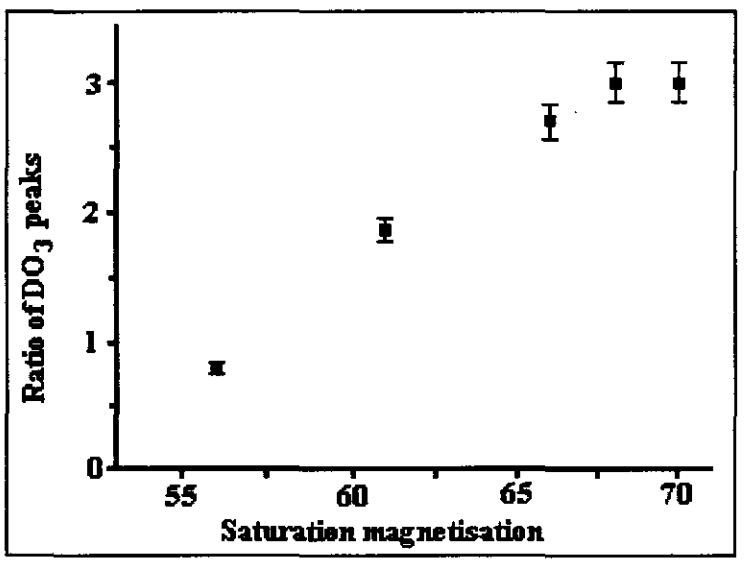

Figure 2.7: The effect of the relative peak intensity ratio of the two sextets to the Satmagan value [4], with DO_3 indicating the degree of ordering.

The amount of sextets with different hyperfine magnetic field strengths, as obtained from a Mössbauer spectrum of ferrosilicon, is an indication of the ordering of the alloy and the

ratio of the two sextet peak intensities are an indication of the Satmagan value of the alloy. The change in the hyperfine magnetic field strengths could show an increase in ordering but not necessarily a change in Satmagan value (or indirectly the magnetic properties) of a sample.

Thus, to summarise, the Mössbauer results will give an indication of the Satmagan value (and thus the amount of ordering) for the given ferrosilicon sample, which indicates the efficiency of its magnetic recoverability. The cooling rate however determines the amount of ordering in the alloy. As a consequence, the cooling rate will thus indirectly determine the magnetic recoverability of the ferrosilicon.

2.3 Classification of ferrosilicon

In order to obtain a classification system for ferrosilicon powders, different tests were designed and used to classify certain powders [13]. These techniques were designed to produce a standardised test with which to determine the corrosion characteristics of different ferrosilicon alloys and to enable a comparison to other ferrosilicon alloys. With the standard test in place, manufactures could then use the test and determine a standardised corrosion "value" which would make it easier for the user to buy equivalent ferrosilicon alloys.

The best known test for this purpose is the Rust Index test [13], which was designed to give qualitative answers to the properties and thus the uses of different ferrosilicon powders. The test consists of a repeated wetting and drying cycle of a small sample (in the standard test a precise sample of 20g is used) of ferrosilicon powder. After five cycles, the weight percentage gain of the sample was deemed the "Rust Index" of the particular sample. Using this test produced problems, as the reproducibility of the conventional Rust Index test was unsatisfactory and Guerney [13] identified the following problems with this testing method:

- The container shape and size and the amount of water used in the test effects the results. Due to the fact that a certain amount of water is added to the sample, the shape and size of the container will determine the duration that the sample will be covered by water during these repeated wetting and drying cycles. The duration that the sample is thus covered with water, determines the final results of the test. Guerney [13] showed that the higher the solids to water ratio was, the lower the Rust Index value was for a sample of the same ferrosilicon.
- Atomised ferrosilicon gave results that differed from the initial unused powder results, with respect to powder that had been used in a dense medium. The used atomised ferrosilicon however gave the same results as used or unused milled ferrosilicon. The difference in test results, according to Guerney [13], could be due to a thicker initial passive layer on the atomised ferrosilicon which was both removed and replaced by a new layer, or which changed to the new layer, after use.
- Furnace type, different airflow characteristics and temperature profiles in the furnace has an effect on the drying rate of the samples, which can change the final Rust Index value.
- The sample weight had an effect on the Rust Index value. Guerney [13] showed that the higher the sample weight was (sample weights were varied between 5 and 100g, with the standard being 20g), the lower the Rust Index value was. This had the same effect as with the changing of the amount of water. The higher the solids to water ratio, the lower the Rust Index value.
- PH had an effect on the Rust Index value. This is simply due to the fact that in an acidic solution (pH < 6) the rate of corrosion sharply increases, while in a basic solution (pH > 6), the corrosion rate stayed the same as for a neutral (pH = 6) solution.

From the above results it can be understood why the Rust Index test is not a very reliable method of testing. Although further work is being done on an improved Rust Index test, no new test is as yet available for the purpose of qualitative ferrosilicon powder characterisation.

[illegible] the corresponding magnetic properties of the system. The ease with which Mössbauer spectrums can be obtained and the thoroughness, with which it explains the surrounding structure of the iron particle, makes Mössbauer spectroscopy the ideal tool to characterise ferrosilicon.

2.3.1.2 Basic Mössbauer principle

The basic principle of the Mössbauer effect is as follows:
Adding energy to the nucleus of an atom at ground state A, leaves the nucleus in an excited state, call it state B, after which spontaneous relaxation takes place. (Refer to **Figure 2.8**). When relaxation takes place and to return to the ground state (the state the nucleus was in before it was in excited state and also the most stable state), quantized amounts of monoenergetic γ-rays are emitted [17]. This is because the relaxation takes place in quantized steps. When this γ-ray passes through a sample containing the same element, this element, which has about the same energy levels, absorbs the γ-ray and is excited to state B. The amount of energy absorbed by the atom is then less than the total energy of the γ-ray, because energy was used to excite the atom to state B. Those γ-rays not absorbed by other atoms, continue in a straight line without a decrease in energy. [16] Both these emitted γ-rays have the same frequency but differ in energy because of absorption and re-emission. The γ-ray emission spectrum [15] is characteristic for each nucleus and is thus useful in the identification of isotopes.

In atoms of the same element but of different mass numbers (e.g. isotopes of the same element), different amounts of energy is needed to excite the atom to its excited state. [17] This means that the γ-rays emitted by a ^{57}Fe source will only excite another atom with a mass number of 57. The amount of energy needed by other isotopes with the mass number not equal to 57, is so different that no absorption would take place. The secondary γ-rays produced is then detected and any difference in energy between emitted and secondary γ-rays can tell something about the surrounding of the nucleus. [16]

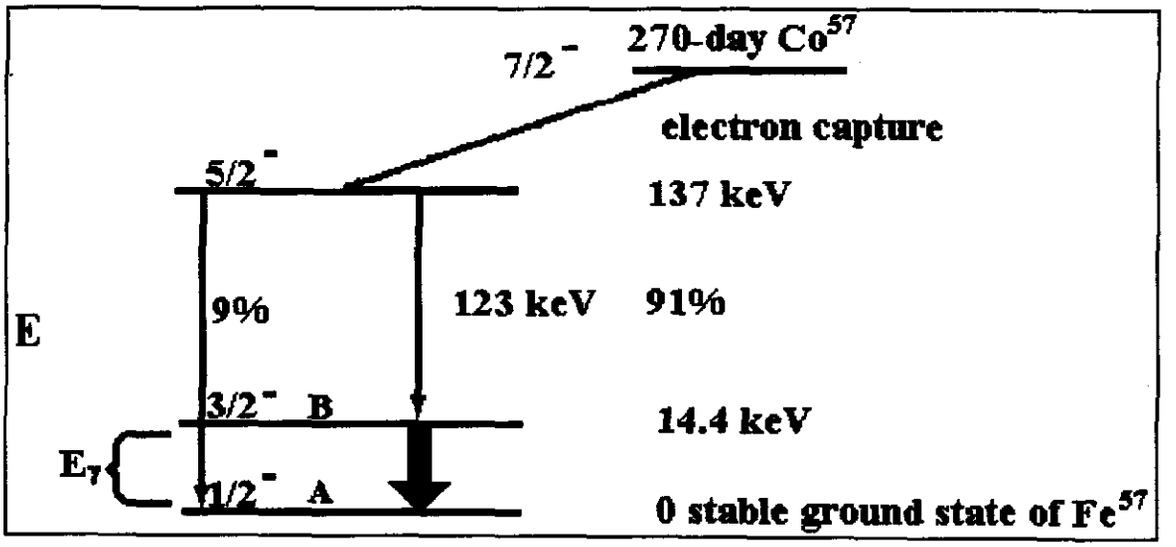

Figure 2.8: Decay scheme of ^{57}Fe. The E_γ = 14.4 keV transition (3/2 → 1/2) is used in the present Mössbauer experiment [16].

The source used in Mössbauer spectroscopy is radioactive ^{57}Co with a half-life of 270 days. The source will relax to the excited state of ^{57}Fe due to electron absorption and when the excited ^{57}Fe relaxes to the ground state, a low energy γ-ray is produced with energy E_γ = 14.4 keV. The emission of γ-rays from the source is then used to excite the target atoms to result in the Mössbauer-effect.

2.3.1.3 Mössbauer spectrum interpretation

The spectrum is obtained by plotting the count rate as a function of the source movement, as shown in **Figure 2.9**.

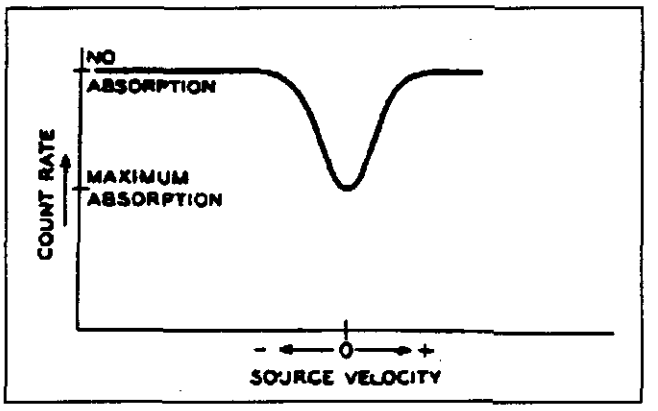

Figure 2.9: A typical Mössbauer spectrum [16].

The different effects that are present in the MS spectrum can be summarised as follows:

- Isomer shifting

  The total electron density on the Mössbauer atom is represented as the Isomer shift and is measured relative to that in a standard material. The nucleus interacts with the electrons in a manner, which raises the energy levels by an amount that is proportional, both to the size of the nucleus and to the magnitude of the electron density. According to Frauenfelder [16], the isomer shift is determined by the interaction between the nucleus and the charge distribution of electrons in the region of the nucleus. The isomer shift depends on the fact that the spacing of the nuclear energy levels depend on the chemical environment of the nucleus. A γ-ray of different energy will be produced due to the isomer effect. The shift can either be positive or negative relative to the appropriate standard material [17], and a typical spectrum is illustrated in **Figure 2.10**.

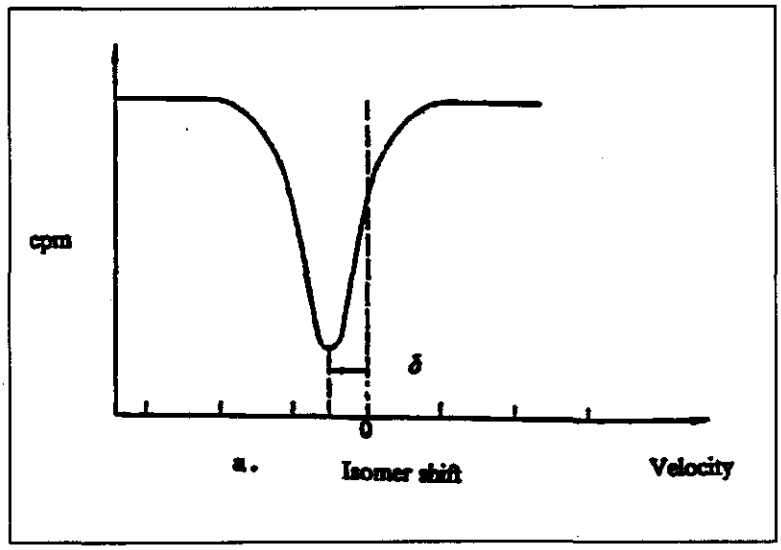

Figure 2.10: Schematic representation of the isomer shift [16].

- Electric quadrupole splitting

  When the atom is no longer symmetrical due to the effect an ionic bond (thus an internal or external magnetic field [17]) has on its electron cloud, the quadrupole splitting effect is encountered.

  When nuclei spin, the spin is characterised by the spin quantum number, I, which may be integral (including zero), or half-integral. From this, the, magnetic quantum number, m, can be determined, which is an indication of the possible orientation of the spin axis of the nuclei when it is applied in a magnetic field. [15] The values for m can be $+I$, $+(I - 1)$, $+(I - 2)$, ..., $-(I - 1)$, $-I$. Thus, for each value of I, $2I + 1$ orientations are possible. Each of these orientations corresponds to a different (quantized) energy, so that these nuclei can be exited from one orientation to a higher energy orientation by application of radiation of appropriate frequency.

  Thus quadrupole splitting separation occurs because the $I = 3/2$ state is split into two sublevels by the presence of an electric-field gradient (see **Figure 2.11**). A typical spectrum is shown in **Figure 2.12**.

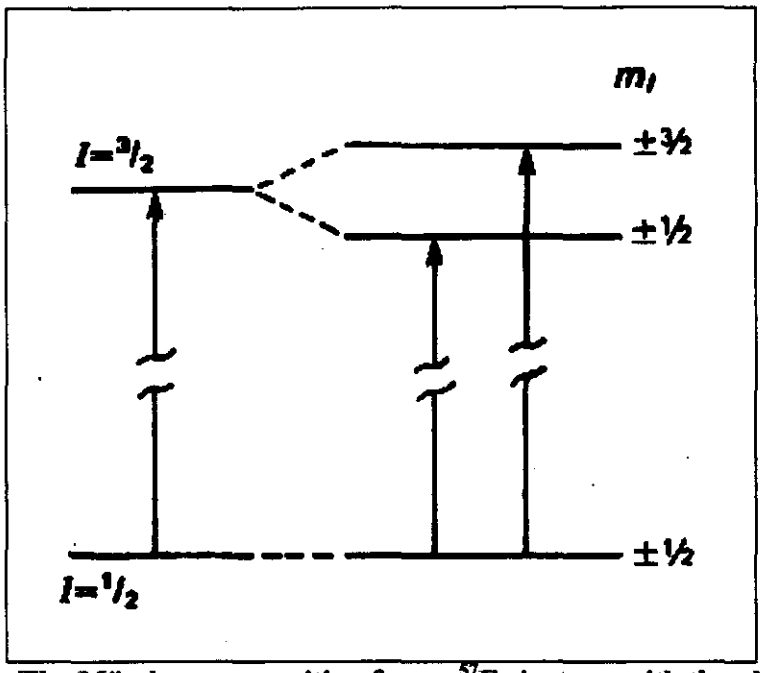

Figure 2.11: The Mössbauer transition for an ^{57}Fe isotope with the absorption of energy from the I =1/2 state to the I =3/2 state to produce the doublet spectra shown in Figure 2.12. [17]

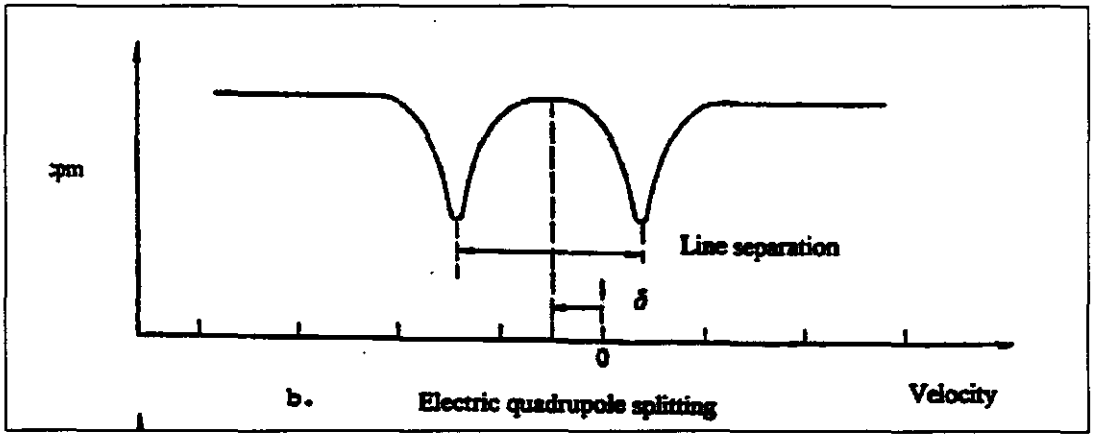

Figure 2.12: Schematic representation of the electric quadrupole splitting [16].

- Nuclear Zeeman splitting (Hyperfine magnetic interactions)

  The magnetic hyperfine interaction arises from the coupling of the nuclear magnetic moment with effective magnetic fields at the nucleus and results in splitting of the

nuclear ground and excited states if they have a nuclear spin larger than zero. Thus it is an optical effect in which the γ-rays are polarised due to the effect of a magnetic field [17] (see **Figure 2.13**) to produce the sextet spectrum as shown in **Figure 2.14**.

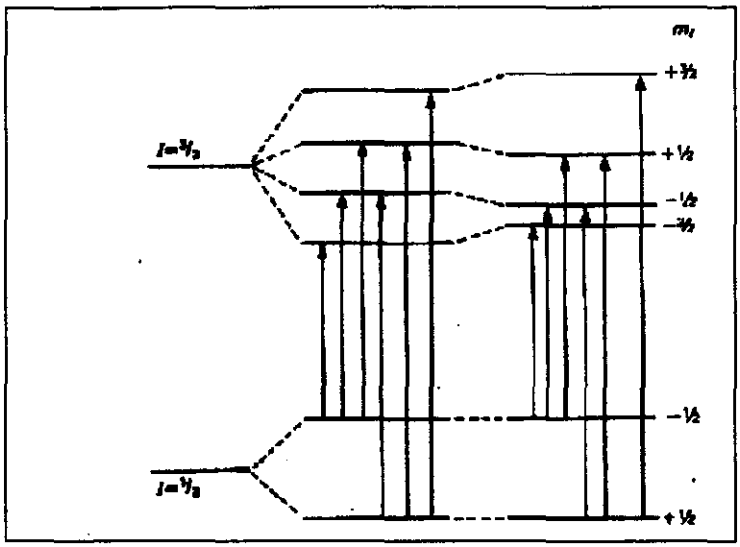

Figure 2.13: Zeeman splitting of energy levels for ^{57}Fe [16].

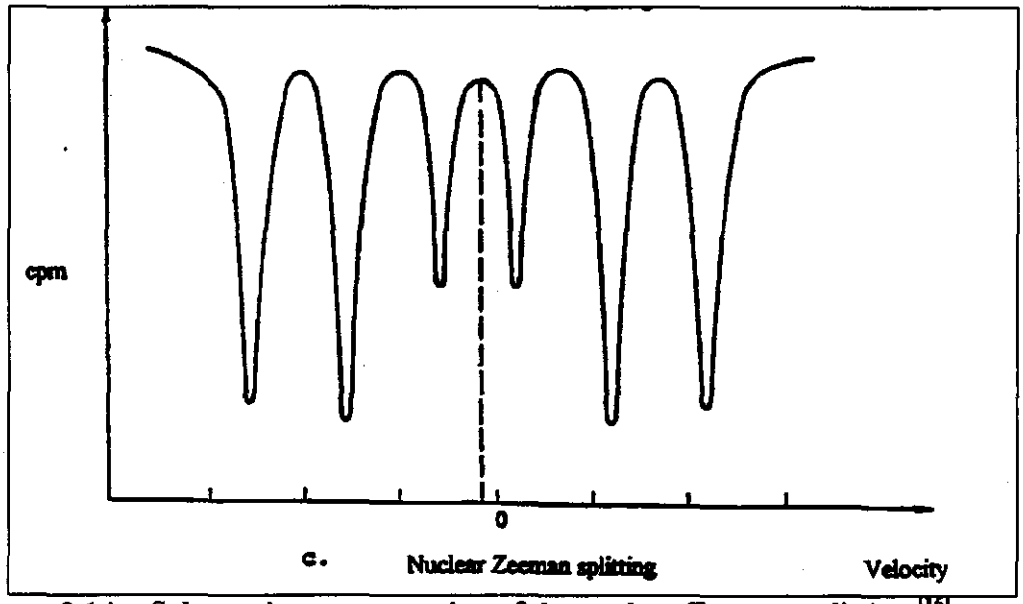

Figure 2.14: Schematic representation of the nuclear Zeeman splitting [16].

2.3.2 Scanning Electron Microscopy

SEM is the acronym for Scanning Electron Microscope. The SEM is used to produce a surface picture of a scanned particle surface using a tightly focused electron beam, as well as determine the chemical content of the sample.

When the surface of the solid is scanned, several types of signals are produced which are backscattered, secondary and Auger electrons, X-ray fluorescence photons and other photons of various energies. Backscattered and secondary electrons are the signals used in the Scanning Electron Microscope.

Furthermore, by scanning at discrete positions on a raster, a digital image can be compiled using the co-ordinates of the position as well as the energy intensity at that position. To determine the element or oxide amounts in each sample, the SEM was fitted with Energy Dispersive Analyses of the X-rays (EDAX).

2.3.2.1 Instrumentation

The basic SEM consists of the following parts and a schematic diagram is shown in **Figure 2.15**: [18]

- Electron gun

  The electron gun consists of a heated tungsten filament, 0.1 mm in diameter and bent into a hairpin shape with a sharp tip. A large potential difference (1 – 50 kV) between the anode and cathode causes the emitted electrons to converge at the crossover point d_0. The partly focused beam continues to the magnetic condenser lens.
- Magnetic condenser lens

  The magnetic condenser lens may consist of more than one lens and is responsible for the throughput of the electron beam to the objective lens.
- Magnetic objective lens

This lens(es) is responsible for impinging the electron beam on the surface of the sample.

- Two pairs of electromagnetic coils

  These two pairs are responsible for deflecting the electron beam in the X and Y direction respectively. Changing the electrical signal in the coil pairs deflects the electron beam and thus the whole surface of the sample can be scanned.

- Cathode ray tube

  Using the same signals used in the coils to scan the sample surface, the cathode ray tube can also be controlled. With the method of scanning, a signal map is produced which corresponds to a particular location on the sample and also with a particular location on the cathode ray tube, which then displays the image of the sample.

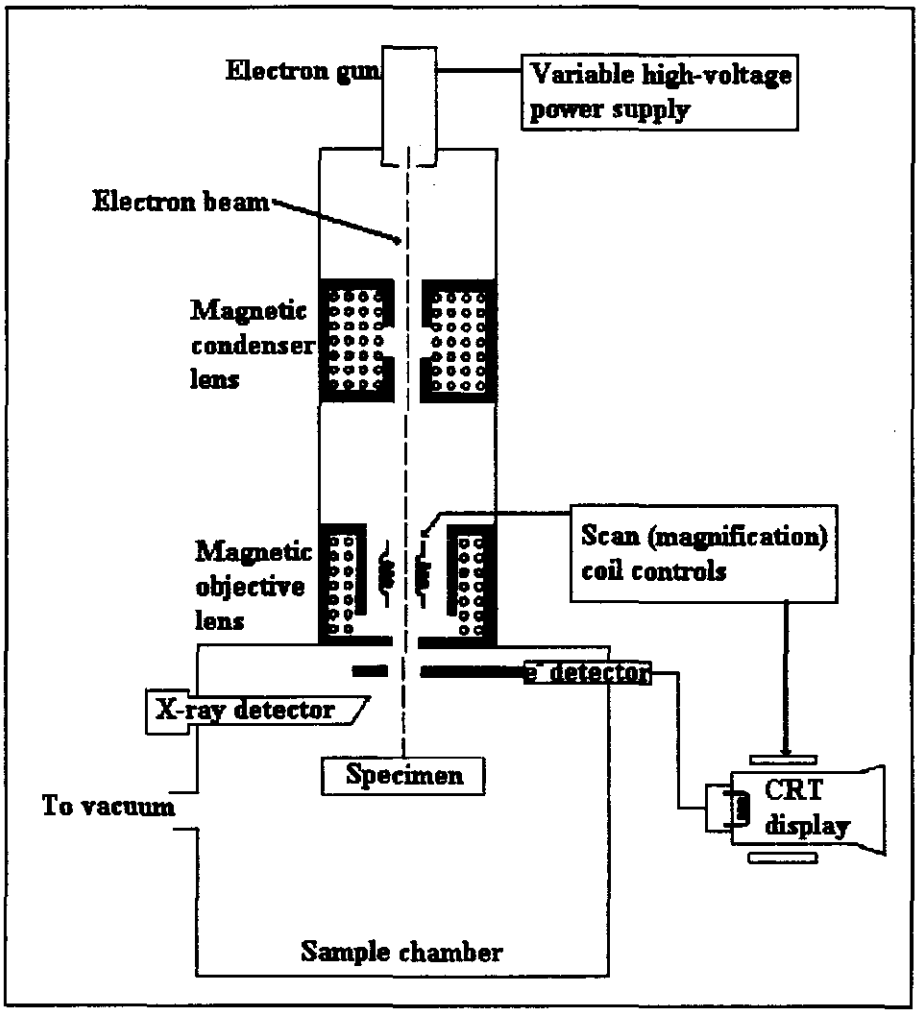

Figure 2.15: Schematic diagram of a typical SEM set-up [18]

2.3.2.2 Uses [18]

The SEM produces morphologic and topographic information about the surface of the sample. A typical photomicrograph of the sample is thus obtained. This is usually also the first step needed in the understanding of the behaviour of the surfaces. The SEM is also used in the qualitative and quantitative analysis of samples (EDAX), which is to show "what" and "how much" of an element is present in the sample.

CHAPTER 3: EXPERIMENTAL SETUP AND MATERIALS USED

3.1 Introduction

As mentioned, no real standard procedures regarding the properties exist for the testing of ferrosilicon. Most of the work done was conducted with test systems, designed for the testing of a particular property of the alloy powder. Properties that were tested by previous workers included corrosion type testing (which includes corrosion susceptibility, passivation/activation and corrosion in acid/alkali mediums amongst others), adhesion/cohesion properties (agglomeration, adhesion to the ore and waste product), size distribution (initial and change during use) and hardness (with respect to breakdown during usage). Furthermore, investigators also conducted sampling and tests in a plant environment, to better understand the environmental conditions during use and to better predict possible future changes to be made to the plant to ensure a reduction in ferrosilicon loss.

Actual ferrosilicon, as used in the Sishen mine of Kumba Resources, was obtained for this investigation to ensure results that could be directly related to the particular plant environment at the mine.

3.2 Ferrosilicon used

The ferrosilicon currently used at the Sishen mine was produced by Iscor at the Pretoria works. Due to the high relative densities used in each dense medium separation plant, Sishen uses atomized ferrosilicon because of personal positive experience in the field of ferrosilicon usage.

The ferrosilicon used had the following initial properties:

- Measured density of 7.177 g/cm^3
- Particle size distribution: 99.55% of the particles were smaller than 404.21 μm and 85.94% of the particles were smaller than 56.09 μm, with the average size being 30.66 μm (d_{50} = 30.66 μm).
- Silicon content of 14.11 wt% silicon, with traces of aluminium, potassium and calcium (total of 4.61 wt%), the balance being iron.

3.3 Mössbauer spectroscopy and SEM analyses

The ferrosilicon was analyzed at room temperature using transmission Mössbauer Spectroscopy and Scanning Electron Microscopy (SEM).

Mössbauer spectroscopy is the name given to a technique based on the absorption and recoilles re-emission of γ-rays by the nuclei as discussed under section **2.3.1.2**. The basis of the Mössbauer effect is the emission of γ-rays by radioactive nuclei (e.g. ^{57}Co, E_γ = 14.4keV), the subsequent absorption of these γ-rays by a target and the recoilles re-emission by the target. This amounts to the recording of the transitions between energy states in iron atoms and emission immediately follows sample radiation and gives rise to a spectrum which is characterized by the chemical "environment" in which the iron atoms are present in the sample. The success of the technique for characterizing the crystal chemistry of the sample depends on the ranges of the "chemical shift" (δ in mm.s^{-1}), "quadrupole splitting" (Δ in mm.s^{-1}) and "hyperfine magnetic field" (T) in the spectra.

All Mössbauer spectra were obtained with the aid of a Halder Mössbauer spectrometer, capable of operating in conventional constant acceleration mode using a proportional counter filled with Xe-gas to 2 atm. The samples were placed between Perspex plates and then irradiated with γ-rays from a 50 mCi ^{57}Co(Rh) radioactive source to obtain a room temperature Mössbauer spectrum. The data was collected in a multi-channel analyzer (MCA) to obtain a spectrum of count rate against source velocity. A least-squares fitting

program was used and by superimposing Lorentzian line shape, the isomer shifts, quadrupole splitting and/or hyperfine magnetic field of each constituent was determined with reference to the centroid of the spectrum of a standard α-iron foil at room temperature. The amount of each constituent present was determined from the areas under the relevant peaks. The Mössbauer spectrometer was calibrated using α-iron as the reference and a schematic diagram of the set-up is shown in **Figure 3.1**.

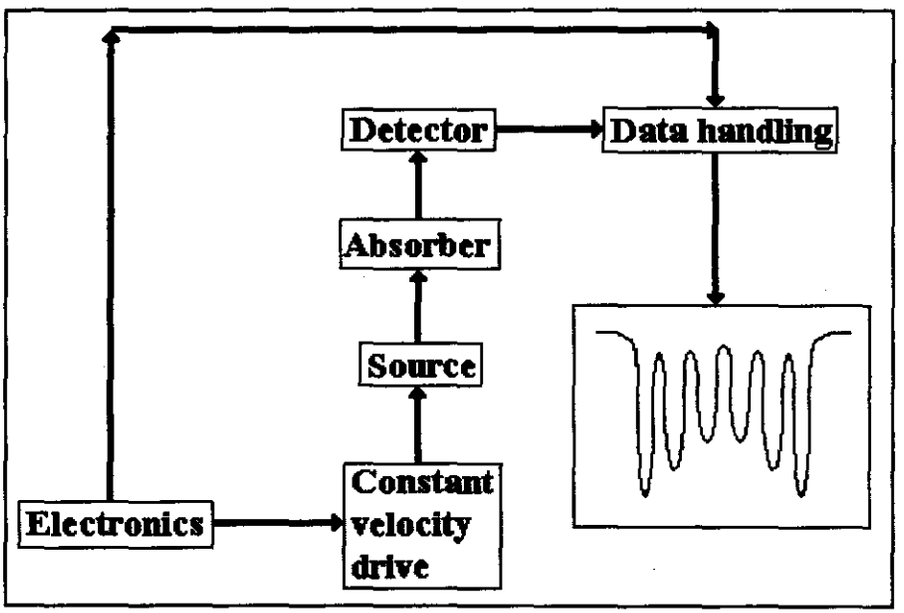

Figure 3.1: Schematic diagram of the experimental Mössbauer set-up where "absorber" indicates the ferrosilicon sample and "source" indicates the ^{57}Co(Rh) radioactive source.

A Philip model XL30 DX41 Scanning Electron Microscope fitted with an energy dispersive X-ray spectrometer (EDAX) was used for the SEM analyses.

3.4 Test set-up used in the characterization of the ferrosilicon

Test systems were designed to simulate the plant environment as closely as possible while also testing certain characteristics of the ferrosilicon. It was nearly impossible to isolate one property change without other factors influencing the outcome, as was seen in the experiments. An example of this, was the particle size distribution that changes during the use of the ferrosilicon. This effect cannot be studied independently, as some type of corrosion may take place simultaneously, which could also influence the particle size distribution.

A short descriptive explanation of the system used for the characterization of the ferrosilicon that has been used, is given in section **3.4.1**.

3.4.1 The attrition system

An elementary attrition system was used, consisting of a pump, piping with six bends (elbow fittings) and a sump into and from which the slurry was continuously pumped. The sampling from this system was simplified with the availability of a secondary system connected to the first system, which consists of a hydrocyclone from which both top and bottom outlet streams returned to the sump to ensure no slurry loss occurred during sampling. Daily sampling was done by simultaneously taking a sample from the top and bottom outlets of the cyclone to ensure that a representative sample was taken. These samples were then allowed to settle somewhat, before recovery of the magnetic solids was performed, using a bench scale wet magnetic separator. Non magnetics were retained for analyses while the magnetic fraction was wet sieved to determine the particle size distribution. A simple schematic representation of the attrition system is shown in **Figure 3.2**.

The dense medium, used in the system, was prepared using tap water (about 250 L) and enough ferrosilicon (about 30 kg) to produce a medium with relative density of about 1.1

g/cm^3, which could be easily handled by the system without continuous breakdowns. Although a relative density of up to 4g/cm^3 is used in the Sishen plant, the aim of the system was not to test dense medium stability, but rather to see the effect of attrition on the ferrosilicon particles. Thus, the relative density used in the test system was appropriate for the application of the system.

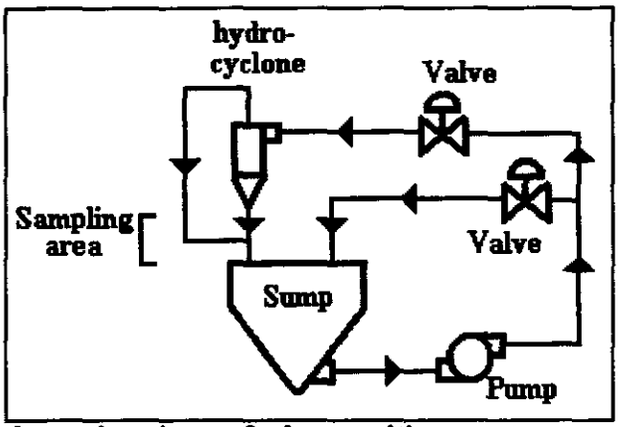

Figure 3.2: A schematic view of the attrition system used in the present experiments.

3.4.2 Wet sieve technique

The wet sieve technique was used during the attrition system experiments as a means to determine the particle size distribution. The sieve series used had a top size of 450 μm and a bottom size of 37.5 μm, with an aperture size reduction factor of $\sqrt{2}$.

With each sample taken from the attrition system, the wet sieve technique was applied to determine the particle size distribution. The top size sieve was taken, and with the use of water, the undersize particles were washed through the sieve and over the bench scale magnetic separator, to recover these undersize particles. This was continued until no more undersize particles reported to the magnetic separator, after which the next smaller size sieve was used, and the process repeated. Each of the oversize particle fractions were dried in air and weighed, to determine the particle size distribution of the sample.

3.4.3 Samples taken at the Sishen plant

The ferrosilicon samples that were collected at the Sishen plant were taken to determine the characteristics of the ferrosilicon which adhered to the final product (the final iron ore product as well as the waste product) and to investigate the possible change in properties (e.g. magnetic properties) which might have occurred during magnetic recovery of the diluted dense medium. See **Figure 3.3** for a schematic diagram of the Sishen iron-ore beneficiation plant.

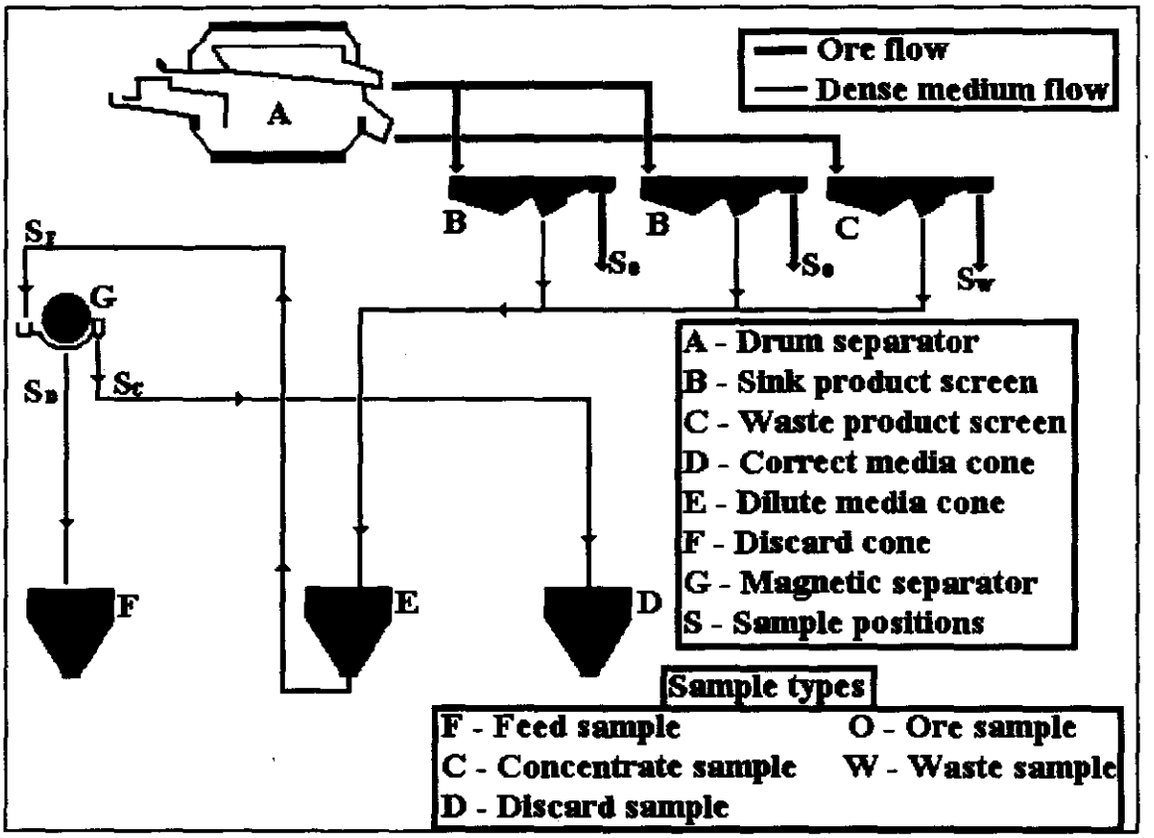

Figure 3.3: A Schematic representation of the Sishen plant with respect to the equipment involved and the positions were the samples were taken.

Ore samples were taken from the product washing screens and thoroughly cleaned to remove all possible ferrosilicon, which were then analyzed using Mössbauer spectrometry to determine if possible difference in ordering in the ferrosilicon as well as

a possible change in magnetic characteristics occurred during the process of dense medium separation (and thus the use of ferrosilicon).

Samples of the diluted dense medium feed, the concentrate dense medium and the dilute (discard) streams were taken of the primary magnetic separators. These samples were analysed using Mössbauer spectroscopy, to determine if possible changes in ordering and magnetic properties might have occurred in the ferrosilicon during its use as dense medium material.

CHAPTER 4: RESULTS AND DISCUSSION

4.1 Introduction

The results obtained can be divided into three categories:

- Initial characteristics of the received ferrosilicon powders from the Sishen plant,
- Results from laboratory tests, and
- Results from samples taken from the Sishen plant itself.

4.2 Characteristics of the unused ferrosilicon

By characterizing the unused ferrosilicon, a better indication of the changes that occur in the ferrosilicon characteristics, during its use as dense medium separation material, can be obtained.

4.2.1 Density and particle size distribution

Stereopicnometric analysis of the density of the ferrosilicon yielded a density of 7.177 g/cm^3. A particle size distribution was determined using a Malvern Mastersizer (model X). The ferrosilicon used in this investigation had a particle size distribution smaller than 404 μm, whilst about 98% of the particles were smaller than 272 μm and 86% than 56 μm. The average particle size was determined to be 30 μm. A graphic representation of the particle size distribution results is shown in **Figure 4.1**.

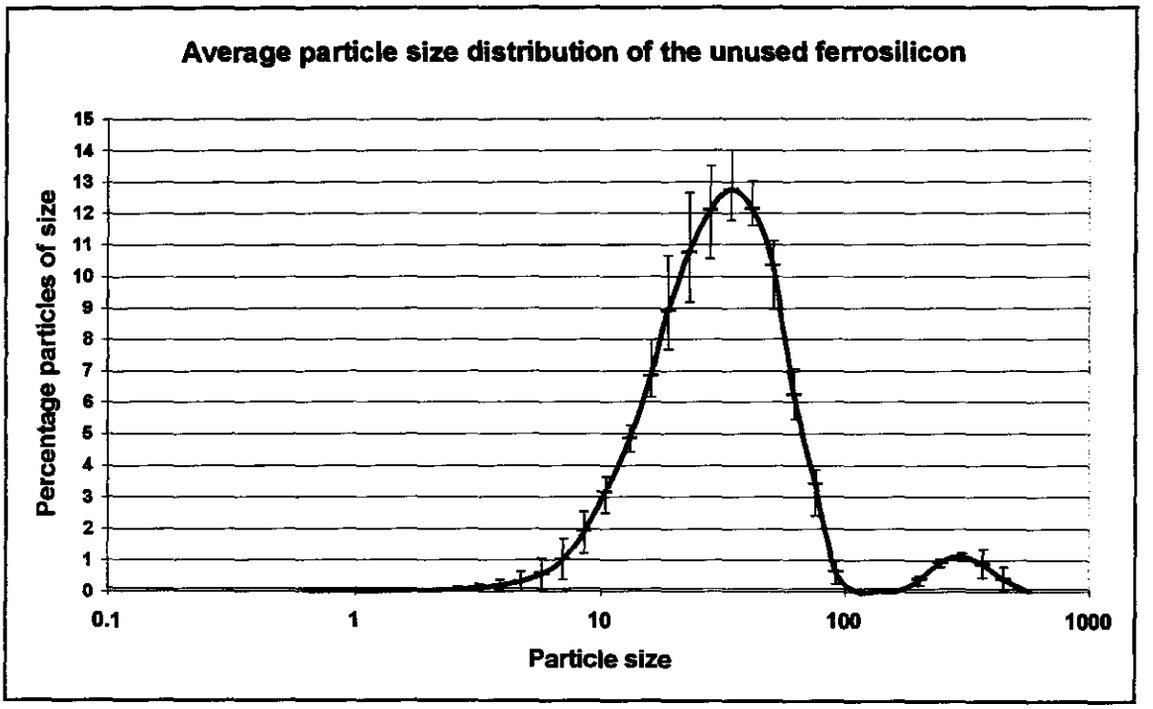

Figure 4.1: The average particle size distribution as determined with the Malvern Mastersizer.

The amount of bigger particles, seen on the right hand side of **Figure 4.1** (the smaller "bump" on the right hand side), could be due to the fact that some bigger particle have protrusions and some of the finer particles form agglomerations, with both of these registering as bigger particles during particle size analysis.

4.2.2 SEM analysis of the unused ferrosilicon

The SEM analysis showed that the ferrosilicon had 14.11 ± 0.7 wt% silicon and traces of aluminium, potassium and calcium (total of 4.61 ● 0.32 wt%), the balance being iron.

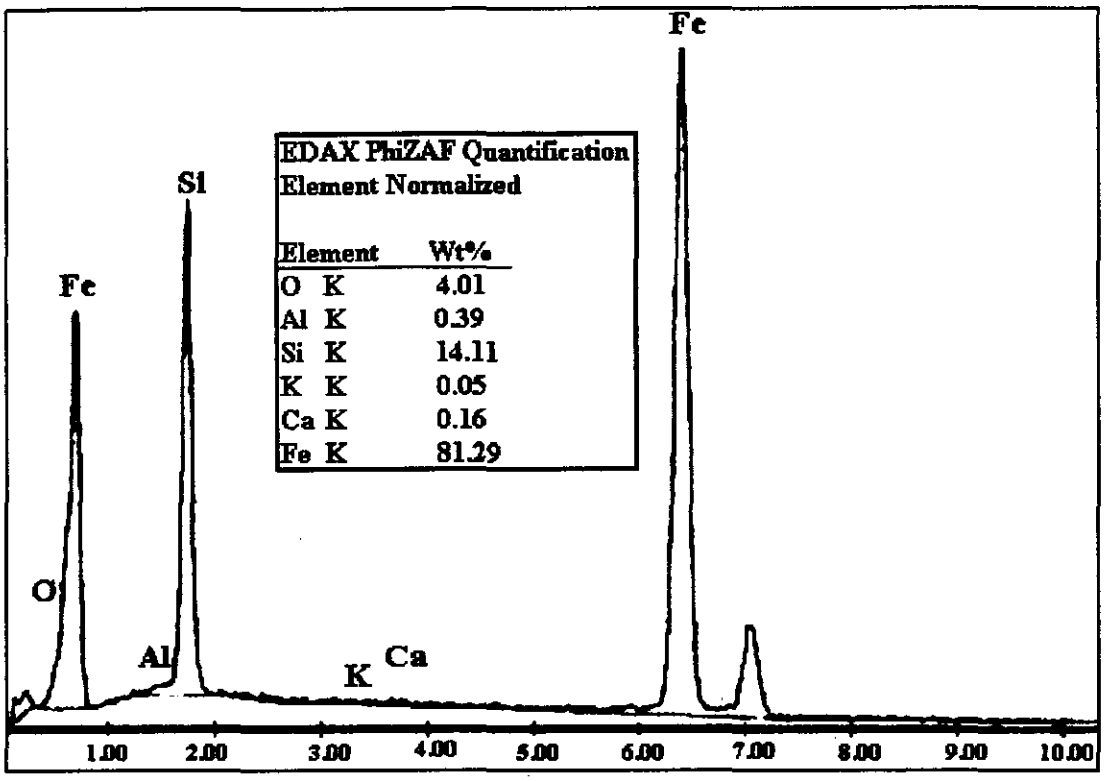

Figure 4.2: SEM analysis of the unused ferrosilicon

Microphotographs of the ferrosilicon (**Figure 4.3**) showed the characteristic spheroid particles as well as particles with protrusions. A limited amount of broken particles (< 5%) were also observed, and this phenomenon can be attributed to the breaking-up of bigger particles during handling, where a high degree of cavitation in these particles was present. Agglomeration of finer particles (**Figure 4.3(b)**) is also evident and these agglomerations can have a big effect on the actual particle size distribution of the unused ferrosilicon, because the strength (or stability) of these agglomerations is unknown.

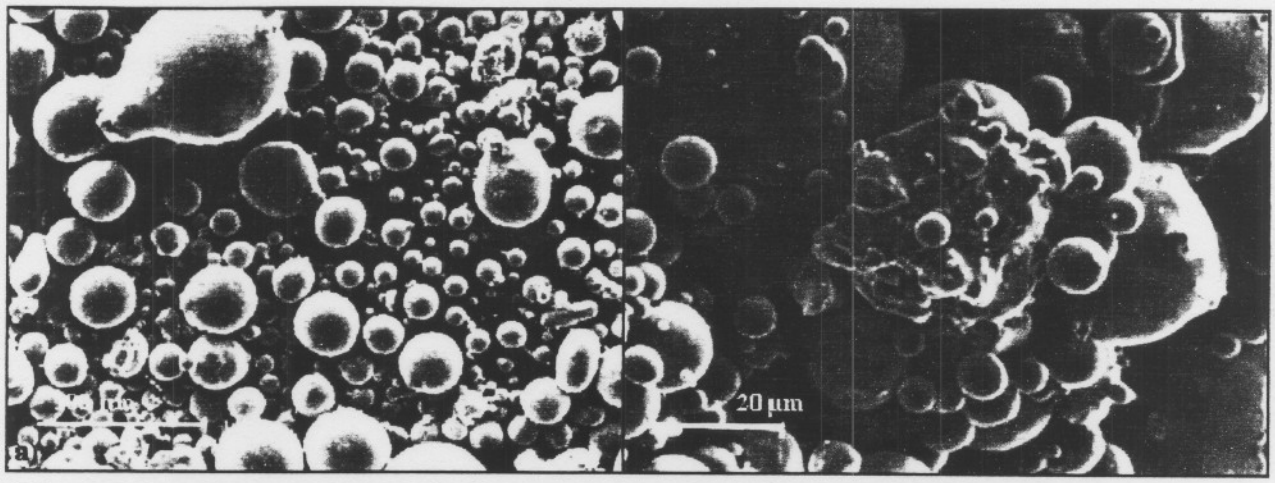

Figure 4.3(a) and (b): SEM microphotographs of the unused ferrosilicon, showing spheres, spheres with protrusions and agglomerates.

4.2.3 Mössbauer spectrometric analysis

Mössbauer spectroscopy revealed a spectrum with two sextets with a hyperfine magnetic field strengths of A = 19.9 ± 0.3T and B = 30.7 ± 0.3T respectively. This corresponds to the values obtained by Stearns [5] of A = 19.9T and B = 30.2T, and Nkosibomvu *et al.* [4] of A = 19.7 ± 0.5T and B = 31.3 ± 0.5T. The Mössbauer spectrum of the unused ferrosilicon is shown in **Figure 4.4**.

Furthermore, the intensity ratio for the two sextets was seen to be about 3/2 which corresponds to a Satmagan value (according to Nkosibomvu *et al.* [4]) of≈ 59% which indicates a high ordered system (a Fe_3Al type system).

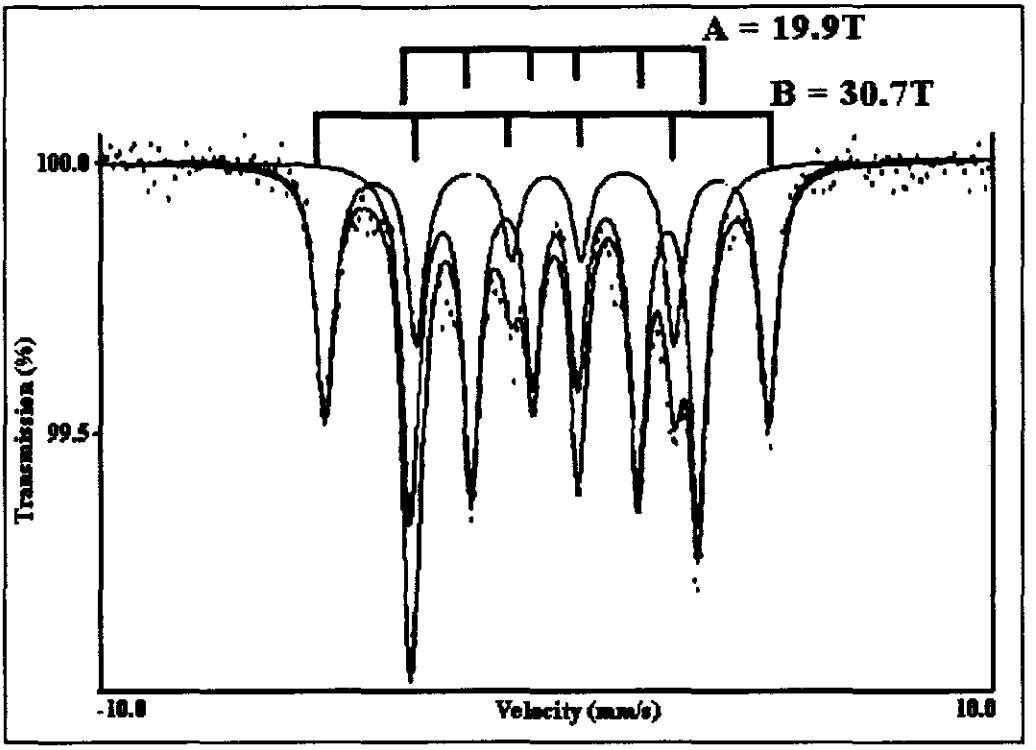

Figure 4.4: The Mössbauer spectrum of the unused ferrosilicon.

4.3 Characteristics of the ferrosilicon used in the attrition system

An attrition system was designed to investigate the effect pumping of the ferrosilicon slurry will have on the ferrosilicon particles themselves.

4.3.1 Density and particle size distribution of the ferrosilicon used in the attrition system

The density of the used ferrosilicon was determined, using the stereopicnometer and a density of 6.966 g/cm^3 was obtained This shows a reduction in density of 2.3% from the initial value of 7.177 g/cm^3, which could be due to the drying process applied before the density was determined, or due to oxides, with lower density, adhering to the ferrosilicon. No measurement of the density of different size fractions were done.

The size distribution was determined using the wet sieve technique with the effluent passing a magnetic separator. The size distribution measurements yielded values of 100% of the particles smaller than 300 μm and 85% smaller than 54 μm, while the values for the unused ferrosilicon was 98.08 ± 1% and 83.79 ± 2.66% respectively. Thus, a particle size distribution similar to the initial distribution was found, although the biggest particles (of size bigger than 300 μm) were not present.

4.3.2 SEM analysis of the samples obtained from the attrition system

The SEM elemental analysis of the used ferrosilicon did not change with respect to the unused ferrosilicon. An inspection of the SEM microphotographs of the used ferrosilicon showed that the irregularities and protrusions on the bigger particles were mostly abraded away.

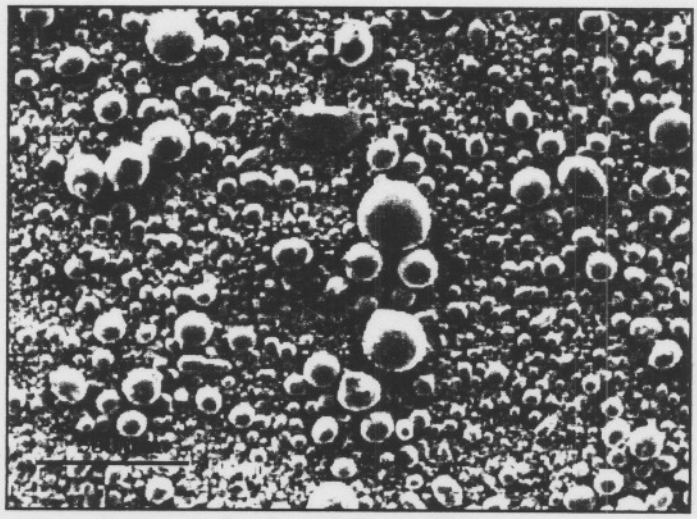

Figure 4.5: SEM microphotograph of used ferrosilicon.

The distinct absence of the agglomerations of small particles indicates that definite particle break-up does occur. The microphotograph (**Figure 4.3**) of the unused ferrosilicon clearly shows the agglomerated particles, which could probably be the source for smaller particles after some abrasion takes place. A microphotograph of the used

ferrosilicon can be seen in **Figure 4.5**, where a reduction in the amount of irregularities and agglomerations can be clearly seen.

4.3.3 Mössbauer spectroscopic results of the samples obtained from the attrition system.

The Mössbauer spectrum showed the two expected sextets with hyperfine magnetic field strengths of A = 20.1 ± 0.3 T and B = 31.2 ± 0.3 T respectively, but an additional sextet with a hyperfine magnetic field strength of C = 25.4 ± 0.3 T was also observed. Stearns [5] also observed a possible additional third sextet, which might be an indication of a change in magnetic properties of the alloy or an indication of the ordering in the alloy. The relative peak intensity (A:B) indicates a saturation magnetization of about 59% in accordance with the results obtained for the unused ferrosilicon and also as observed by Nkosibomvu *et al.* [4]. A typical spectrum of the used ferrosilicon is shown in **Figure 4.6**.

A greenish colored froth was observed at the beginning stages of the attrition process. When the froth (typical of Fe^{2+}-ions in water) was collected it rapidly turned to a yellow-brown Fe^{3+}-oxide when exposed to oxygen. The yellow-brown froth was subjected to Mössbauer analysis and was found to be an oxyhidroxide, FeOOH, but the isomer shift was lower and the quadrupole shift larger than expected. The Mössbauer parameters however still fall within the experimental range for FeOOH. The Mössbauer spectrum of the froth is shown in **Figure 4.7**, which shows two doublets from the possible 2 oxyhidroxides present. A detailed Mössbauer analysis of the oxyhidroxide can be conducted at liquid nitrogen temperatures to determine the type of FeOOH that formed, but this falls beyond the scope of this experiment, where the ferrosilicon was to be characterized.

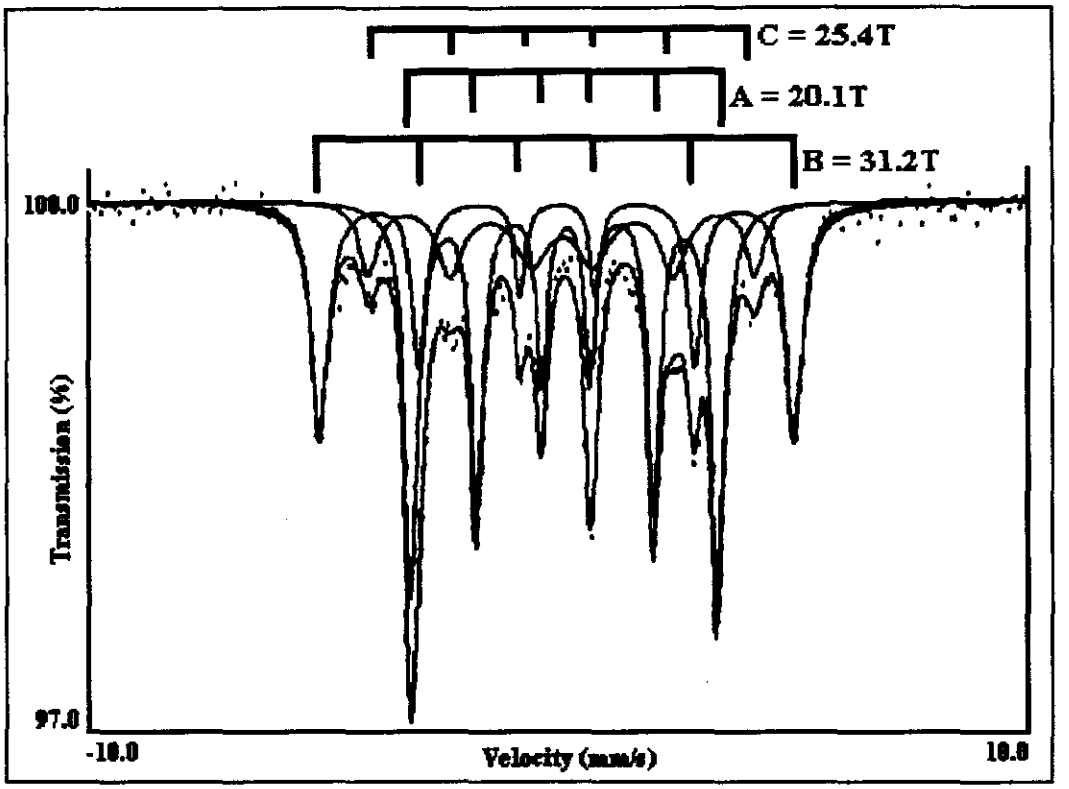

Figure 4.6: Mössbauer spectrum of the used ferrosilicon.

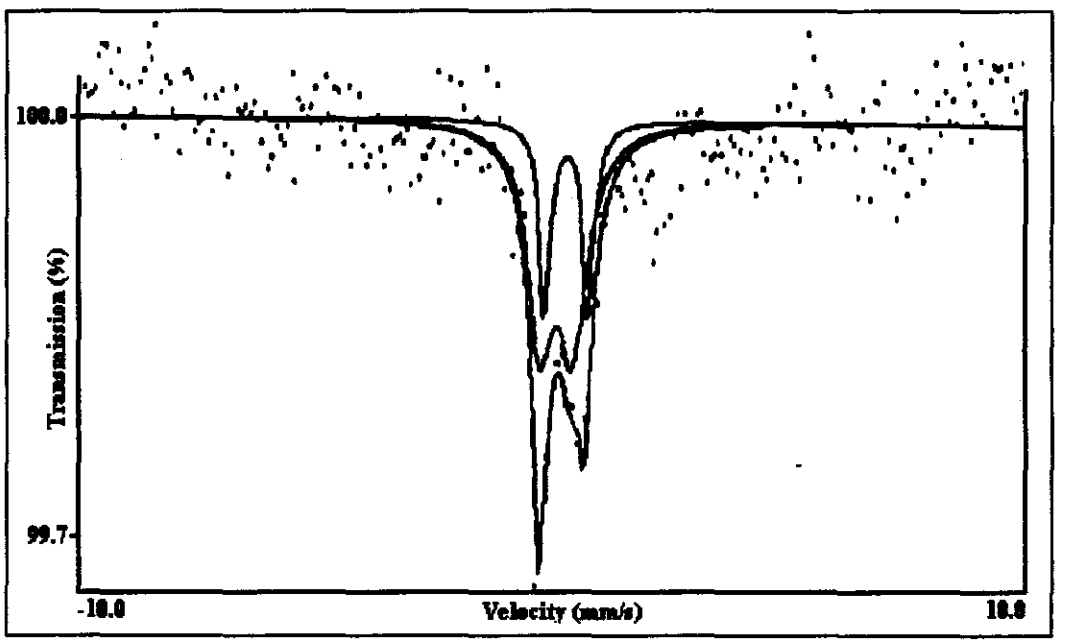

Figure 4.7: Mössbauer spectrum of the collected froth.

4.3.4 Mössbauer results from the non-magnetic material and the ferrosilicon stored under a lime solution

An analysis of the non-magnetic material (solids not recovered with the magnetic separator) showed the two sextets (with hyperfine magnetic field strengths of A = 19.7 ± 0.3 T and B = 29.5 ± 0.3 T respectively) associated with the ferrosilicon powders, as well as the doublet associated with the froth, with quadropole splitting (QS) of 0.72 ± 0.02 $mm.s^{-1}$ and Isomer shift (IS) of 0.31 ± 0.02 $mm.s^{-1}$. Loss of the ferrosilicon in the effluent stream was however negligible as it was far less than 1%.

Storage of the samples (for up to 3 months) seemed to have no effect on the properties of the ferrosilicon. It was expected [1] that the samples stored with the added lime (which is used in the Sishen plant to prevent hardening of the ferrosilicon medium during storage) would show less or no corrosion with respect to the sample stored without lime. There was however no difference in these sample. The samples for both the medium stored with the addition of lime and those stored without the added lime, gave rise to Mössbauer spectra with the sextets with hyperfine magnetic fields of A = 19.7 ± 0.3 T and B = 30.4 ± 0.3 T.

In **Table 4.1**, the relevant Mössbauer parameters, obtained from the Mössbauer spectra for the unused ferrosilicon, used ferrosilicon as well as the froth that formed during the attrition experiments, are shown.

Table 4.1: Mössbauer parameters of iron-components in fresh ferrosilicon, used ferrosilicon and the observed froth.

Sample	IS (mms^{-1}) (±0.02)	QS (mms^{-1}) (±0.02)	H (T) (±0.3)	Relative intensity (%)
ferrosilicon (unused)				
Sextet 1	0.04	0.04	30.7	42 (40)
Sextet 2	0.23	0.00	19.9	58 (60)
ferrosilicon (used)				
Sextet 1	0.05	0.01	31.2	31 (40)*
Sextet 2	0.23	-0.01	20.1	47 (60)*
Sextet 3	0.15	0.00	25.4	22
Froth	0.17	0.69		71
	0.35	0.92		29

Note: IS = Isomer shift relative to α-iron, QS = Quadrupole splitting and H = Hyperfine magnetic field strength

* In the used ferrosilicon, the ratio between the strengths of the first two sextets (figures in brackets) stayed the same, even with the addition of the third sextet.

4.4 Mössbauer spectroscopic results of the ferrosilicon samples taken at the Sishen mine

Samples were taken at the Sishen dense medium separation plant to be able to make a comparison of the results obtained in the laboratory to samples from the plant. These samples included samples of the sink and float products (ore and waste streams), as well as samples from the feed, concentrate and discard streams of the magnetic separators. A

sample of the dense medium in use was also taken for a particle size distribution, using the Malvern Mastersizer.

4.4.1 Particle size distribution of the ferrosilicon in use at the Sishen plant

The size distribution was determined using the Malvern Mastersizer. The size distribution measurements yielded values of 94.43 ± 0.08% of the particles smaller than 300 μm and 58 ± 4.6% smaller than 54 μm, while the values for the unused ferrosilicon was 98.08 ± 1% and 83.79 ± 2.66% respectively. The average particle size was determined to be 47 μm, while the average particle size of the unused ferrosilicon was 30 μm. A graphic representation of the particle size distribution results is shown in **Figure 4.8**.

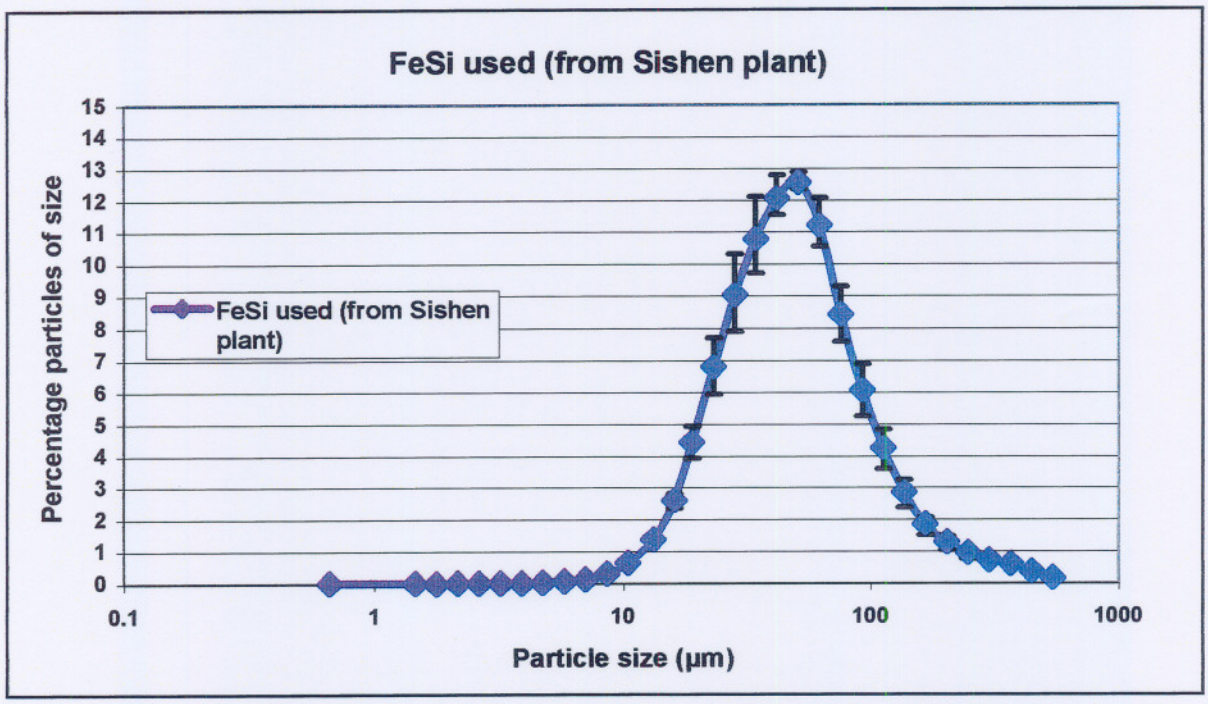

Figure 4.8: The average particle size distribution as determined with the Malvern Mastersizer for the ferrosilicon as used in the Sishen plant.

4.4.2 The characteristics of the ferrosilicon that adhered to the sink and float product samples

Three sets of samples were taken for each of the two sink product (ore) streams and the one float product (waste) stream. The Mössbauer spectra of these samples showed the two expected sextets with hyperfine magnetic field strengths of A = 19.5 ± 0.3 T and B = 28.6 ± 0.3 T respectively. The relevant values obtained from the Mössbauer spectra are shown in **Table 4.2**.

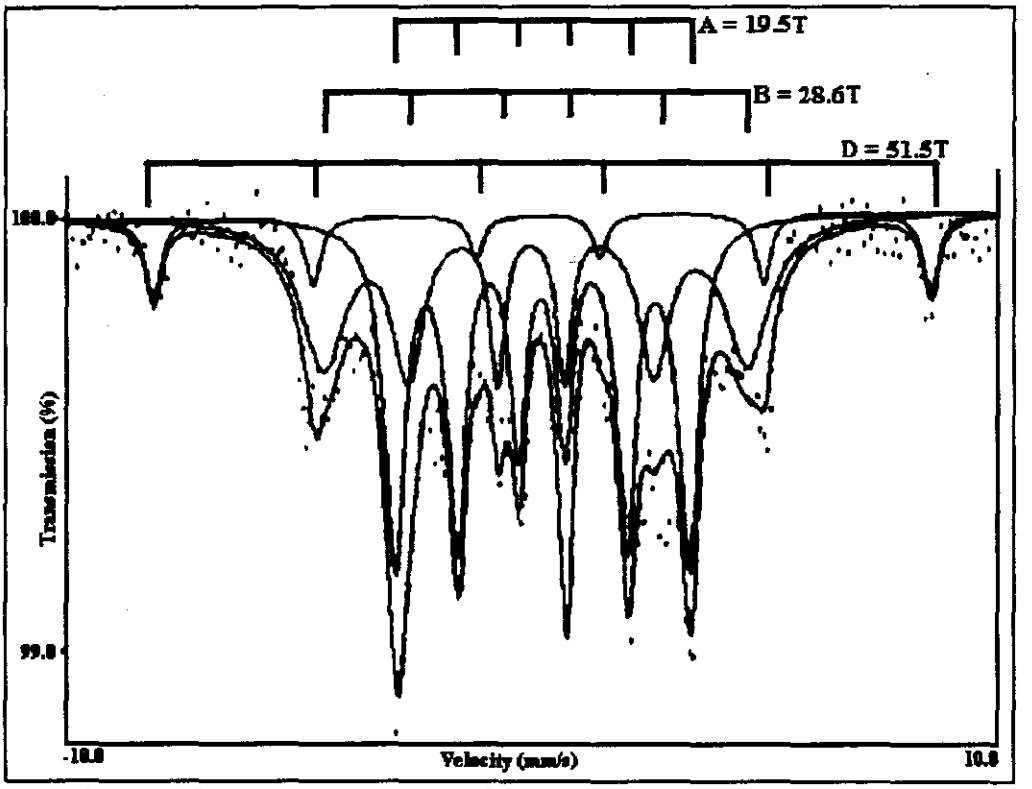

Figure 4.9: The Mössbauer spectrum of the ferrosilicon adhering to the ore samples clearly showing the additional Mössbauer peaks due to the presence of hematite.

An additional sextet with a hyperfine magnetic field strength of D = 51.5 ± 0.3 T was also observed in the Mössbauer spectrum (see **Figure 4.9**) of the ferrosilicon adhering to the samples taken from the two product (iron ore) streams, while the ferrosilicon adhering to the waste product did not show a third sextet. The hyperfine magnetic field strength of

this third sextet was not the same as the one observed in the attrition system samples, which had a field strength of C = 25.4 ± 0.3 T. A hyperfine magnetic field strength of ≈ 52 T typical for hematite was found, which thus indicates the adhesion of hematite (<10%) to the ferrosilicon. The presence of hematite in the dense medium separation system is not abnormal, as iron ore is being benificiated but could influence the density of the dense medium material. The relative peak intensity ratio for all three ferrosilicon samples, shown in **Table 4.2**, indicate a saturation magnetization of about 58% in accordance with the results obtained for the unused and attrition system ferrosilicon samples, as well as those found by Nkosibomvu *et al.* [4].

Table 4.2: Mössbauer parameters of the iron-components in the ferrosilicon adhering to the ore and waste samples from the Sishen plant

Sample	IS (mms^{-1}) (±0.02)	QS (mms^{-1}) (±0.02)	H (T) (±0.3)	Relative intensity (%)
Ore sample 1				
Sextet 1	0.24	0.09	51.9	9
Sextet 2	0.07	0.10	28.3	41(45)*
Sextet 3	0.23	0.00	19.6	50(55)*
Ore sample 2				
Sextet 1	0.26	-0.08	51.5	9
Sextet 2	0.03	0.05	28.6	41(45)*
Sextet 3	0.23	0.01	19.5	50(55)*
Discard				
Sextet 1	0.04	0.03	29.7	47(47)
Sextet 2	0.23	0.01	19.7	53(53)

Note: IS = Isomer shift relative to α-iron, QS = Quadrupole splitting and H = Hyperfine magnetic field strength

*The ratio between the strengths of the first two sextets (figures in brackets) stayed the same, even with the addition of the third sextet.

4.4.2 Samples obtained from the magnetic separator

As in the preceding Mössbauer spectroscopic results, the same two sextets were observed in the feed, the discard and the product (concentrate), obtained from the samples taken at the magnetic separator in the Sishen plant. The sextets have hyperfine magnetic field strengths of A = 19.6 ● 0.3 T and B = 29.4 ± 0.3 T respectively, which corresponds well with the results for the ferrosilicon under investigation. A third sextet was also observed in the discard sample with hyperfine magnetic field strengths of about D = 51 ± 0.3 T which again corresponds to the hematite observed in the ferrosilicon adhering to the ore samples. The parameters obtained from the Mössbauer spectra for each sample are shown in **Table 4.3**.

Table 4.3: Mössbauer parameters of iron-components present in the magnetic separator samples

Sample	IS (mms^{-1}) (±0.02)	QS (mms^{-1}) (±0.02)	H (T) (±0.3)	Relative intensity (%)
Feed				
Sextet 1	0.05	0.03	29.4	49(49)
Sextet 2	0.24	0.00	19.6	51(51)
Discard				
Sextet 1	0.30	-0.26	51.0	22
Sextet 2	0.03	0.04	29.4	41(53)
Sextet 3	0.24	-0.00	19.6	37(47)
Concentrate				
Sextet 1	0.05	0.03	29.6	46(46)
Sextet 2	0.24	0.00	19.7	54(54)

Note: IS = Isomer shift relative to α-iron, QS = Quadrupole splitting and H = Hyperfine magnetic field strength

It should be noted that a difference in the relative peak intensity ratio (A:B) for the two sextets A and B for all three samples was observed. According to the Satmagan curve produced by Nkosibomvu *et al.* [4], the discard sample has a saturation magnetization (Satmagan) value ($\approx 57\%$) slightly lower than the values ($\approx 58\%$) for the feed and concentrate samples. The lower discard Satmagan value corresponds to the work of Hunt *et al.* [3] where their discard samples also had lower Satmagan values than the feed samples.

Again, the additional sextet with hyperfine magnetic field strength of 51 ± 0.3T was observed which indicates the adhesion of hematite to the ferrosilicon, even after magnetic separation has been performed. Mössbauer spectra for the magnetic separator feed and discard samples are shown in **Figures 4.10** and **Figure 4.11** respectively.

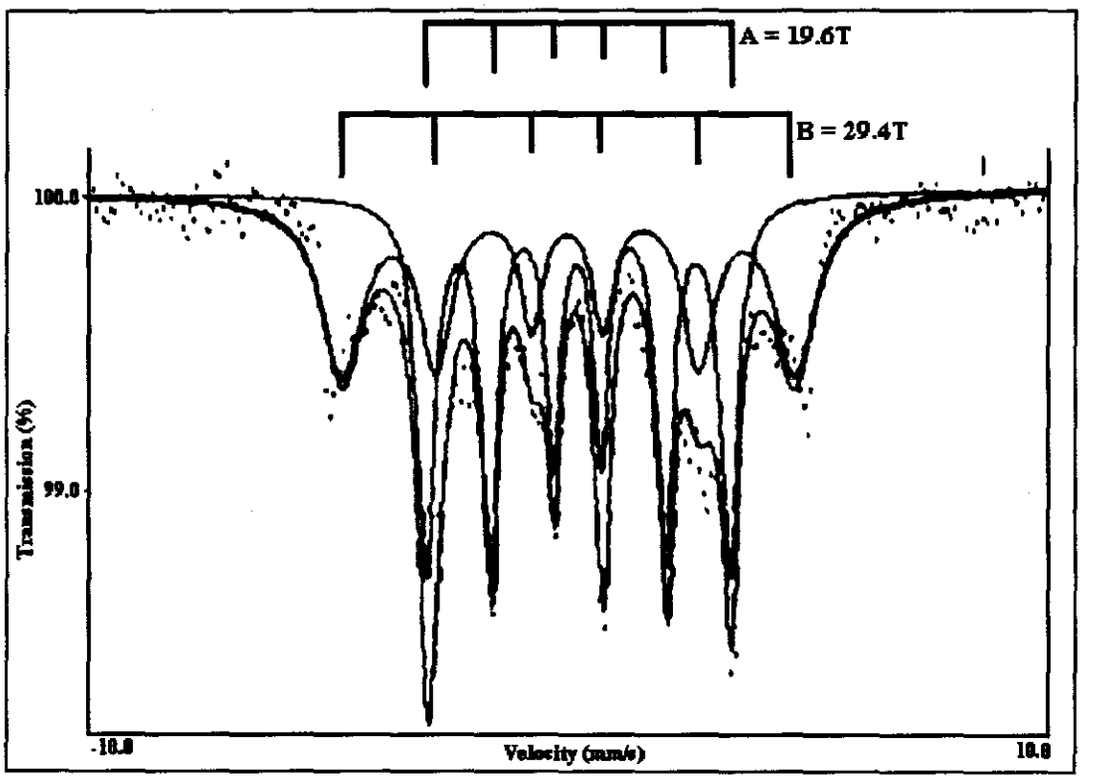

Figures 4.10: The Mössbauer spectrum of the magnetic separator feed sample.

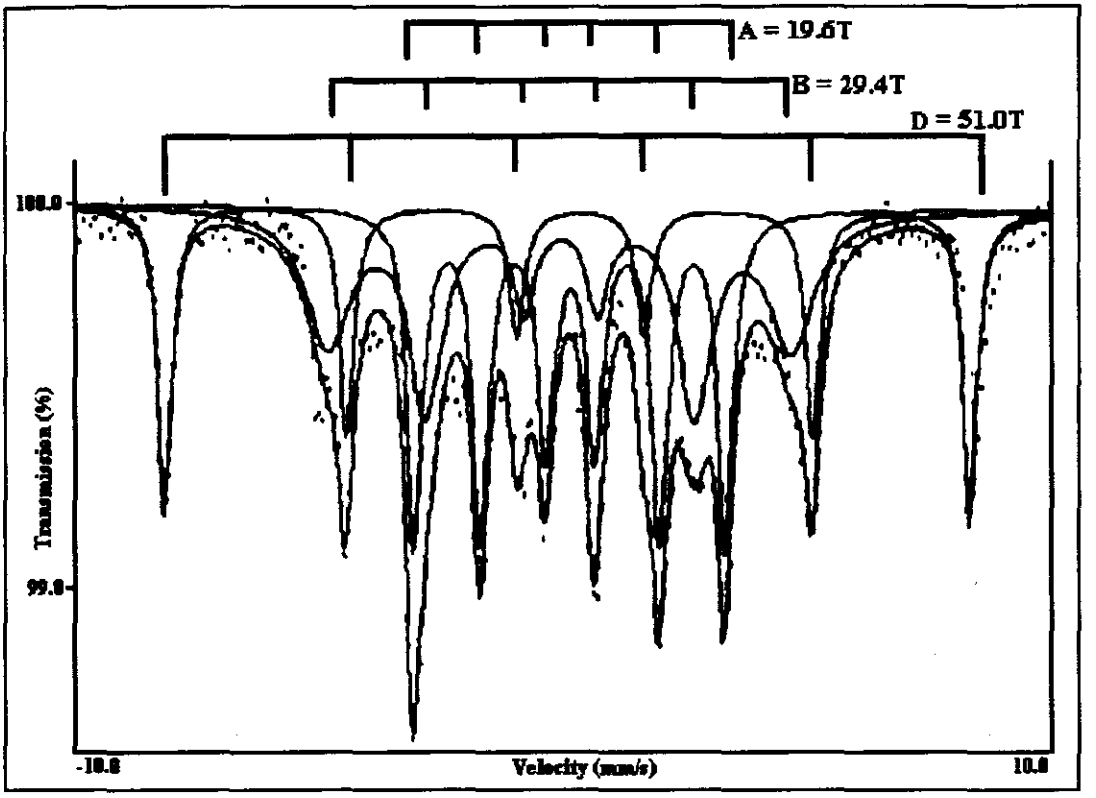

Figure 4.11: The Mössbauer spectrum of the magnetic separator discard sample.

4.5 Discussion of the results obtained

The discussion of the results obtained will be divided under the following two points:

- Used vs. unused ferrosilicon results (from the laboratory)
- Laboratory results vs. Sishen plant results

4.5.1 Used vs. unused ferrosilicon

Density

A change in density was observed between the used and unused ferrosilicon, with the used ferrosilicon having a density of 6.966 g/cm^3, which is 2.3% lower than the unused ferrosilicon density of 7.177 g/cm^3. The change in density could be assigned to a change

that occurs in the passive layer, where the initial passive layer was removed, and the new passive layer formed with a higher oxygen content. Geurney [13] also reported a change in the passive layer from unused to used atomised ferrosilicon, but no indication could be found if a reduction in density was the result. The possible formation of oxides on the outer surface of the ferrosilicon particles could also explain the reduction in density.

Particle size distribution

The particle size distribution of the ferrosilicon used in the laboratory experiments and unused ferrosilicon is similar for the particles smaller than 300 μm. This may indicate that little or no abrasion took place in the laboratory experiments, with only the biggest particles with protrusions, particles with cavitation or the agglomerated fine particles breaking up, which is indicated by the distinct absence of particles with protrusions and agglomerations after use, although the absence of cavitated particles can not be confirmed. The fact that the amount of smaller particles did not increase due to this break-up of larger particles, might suggest that some loss of the finer particles takes place, possibly through magnetic recovery or abrasion.

When also considering the particle size distribution of the ferrosilicon that was used in the Sishen plant, a definite shift in the particle size distribution can be seen in **Figure 4.12** with respect to the unused ferrosilicon particle size distribution. The rightwards shift of this particle size distribution curve indicates that a large amount of the finer particles are lost, because no abundance of finer particles were found. This particle size distribution curve also indicates that some of the finer particles that were lost, were replaced, possibly due to the abrasion of the larger particles. The loss of the finer particles may be due to the inefficient recovery of the ferrosilicon by the magnetic separators.

The abrasion process seems to be a slow process, when the particle size distribution of the laboratory used ferrosilicon is compared with that of the ferrosilicon used in the Sishen plant. The laboratory experiments took five days each, with no significant change in the particle size distribution, which indicates that the degree of abrasion was low.

It must be remembered that during the wet sieve technique employed to determine the particle size distribution, in the laboratory experiments, a bench scale magnetic separator was used. This caused any fine material not recovered by the magnetic separator to be lost, which might explain the lack of increase of the finer ferrosilicon particles. This also corresponds to the personal experience of Myburgh [1], who suspects that the ultra fine material is lost, otherwise an abundance of finer particles could be expected, and the pathway of loss is possibly through the process of magnetic recovery.

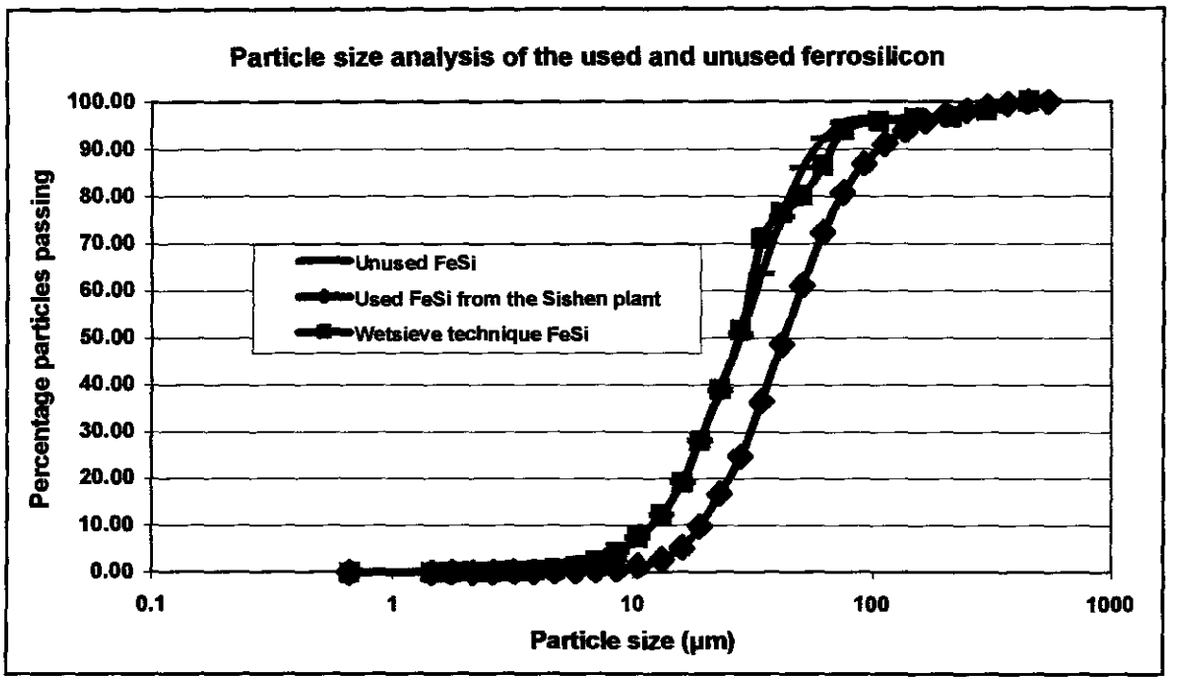

Figure 4.12: The average particle size distribution (cumulative) as determined with the Malvern Mastersizer.

Chemical analysis (SEM results)

The chemical analysis of the used and unused ferrosilicon remained the same, as was expected.

Mössbauer parameters

The two sextets observed (with hyperfine magnetic field strengths of A $\approx$ 20 T and B $\approx$ 30 T) in both the used and unused ferrosilicon, corresponds to the parameters

obtained by Steams [5] and Nkosibomvu *et al.* [4]. With the intensity ratio for the two sextets of about 3/2, the ferrosilicon has a Satmagan value of about 59 %. According to Nkosibomvu [4] this indicates a high ordered Fe_3Al type system. Steams [5] also described the ferrosilicon system becoming more ordered as the silicon content increases (for annealed alloys), with a 14.7 wt% silicon alloy being "best ordered" with respect to the Fe_3Al system. Thus, for the presently used ferrosilicon, some degree of ordering into the Fe_3Al type system can be seen. The additional third sextet observed in the Mössbauer spectrum of the used ferrosilicon was similar to the third sextet observed by Steams [5], where it was reported that the additional third sextet indicates that some degree of ordering into the Fe_3Al type system exists.

The froth that formed in the attrition system was also observed by Hunt *et al.* [3], which was reported as being typical in a system where active oxidation takes place. The Mössbauer spectrum, with the two doublets due to the froth, pointed to an oxyhidroxide, FeOOH, but the isomer shift was lower and the quadrupole shift larger than expected, which could indicated the presence of a second oxyhidroxide as was found by Waanders and Vorster [19]. Only by means of liquid nitrogen Mössbauer spectroscopy can the identities of the oxyhidroxides be determined.

An analysis of the non-magnetic material showed the two expected sextets associated with ferrosilicon, but also an additional doublet associated with the froth. The relative peak intensity ratio of the two sextets indicated a Satmagan value of about 57 %. This is a bit lower than the value of 59 % for the ferrosilicon itself (Nkosibomvu *et al.* [4]). Hunt *et al.* [3] observed the same phenomenon, with the reason reported to be that the bulk chemical analysis (and thus the Satmagan value) may differ from the chemical analysis of different size fractions, where the average particle size of the unrecovered ferrosilicon was also found to be significantly smaller than the feed [3]. This may also further explain the absence of a greater amount of finer particles as would be suspected when abrasion takes place. Thus, the loss of some of the finer particles might occur due to its lower Satmagan value.

The chemical analysis of the finer particles were obtained and compared with that of the bulk chemical analysis of the ferrosilicon. There was no significant difference between the chemical analysis of the finer particles and that of the bulk chemical analysis. This then indicates that the Satmagan value should be the same for the finer particles as for the ferrosilicon bulk samples, which was not the case. A possible explanation for this contradiction is that the Satmagan test is influenced by the particle size distribution of the material. If a characteristic like bulk density (which depends on the size distribution) plays a role in the Satmagan test, then a smaller particle size distribution may account for the loss in Satmagan value.

Another possible explanation is the effect of corrosion on the particles, since corrosion has an impact on the Satmagan value. Smaller particles with a higher specific surface area are more prone to corrosion and thus to a reduction in Satmagan value.

4.5.2 Laboratory results vs. results obtained from the Sishen plant samples

Ferrosilicon adhering to the ore and waste samples

The Mössbauer results produced the two expected sextets associated with the unused ferrosilicon, but an additional sextet was also observed with hyperfine magnetic field strength of D = 51.5 ● 0.3 T. The hyperfine magnetic field strength of this third sextet, indicates the presence and thus adhesion of hematite to the ferrosilicon particles. The origin of the hematite can be ascribed to the process of iron ore beneficiation being used, where hematite is present. The absence of the third sextet in the Mössbauer spectrum of the ferrosilicon adhered to the waste product, could be due to the fact that the observed third peak in this case could have had a relative intensity of less than 5%, which would then not show up on the results.

The magnetic separator samples

Both the sextets associated with the ferrosilicon samples used in the laboratory were observed in the samples from the Sishen plant, with the Satmagan value of 58 % for the

feed and concentrated ferrosilicon samples, and a Satmagan value of 57 % for the discard ferrosilicon sample. It is clear that the Satmagan value for the discard sample is slightly lower than that of the feed, which corresponds to the results obtained for the laboratory samples. Hunt *et al.* [3] also observed the lower Satmagan value for the ferrosilicon that could not be recovered by the magnetic separator. The lower Satmagan value may be due to a different chemical composition of these ferrosilicon particles, with respect to the bulk chemical analysis, according to Hunt *et al.* [3]. This could however not be proven, and the conclusion was made that the lower Satmagan value may rather be attributed to the corrosion of these finer particles. The third sextet observed in the discard stream ferrosilicon, which indicates the adherence of hematite, was the same sextet observed in the ferrosilicon adhering to the ore. The reason for the adherence of the hematite to the ferrosilicon not recovered by the magnetic separator could be due to the corrosion of these ferrosilicon particles. It could also be reasoned that the adhesion of the hematite to a ferrosilicon particle could lower its Satmagan value, which then influences the recoverability of the particle.

Thus, some of the losses of ferrosilicon experienced in the dense medium separation plant could be linked directly and indirectly with the abrasion process of the ferrosilicon used in the dense medium separation plant. During the abrasion process, particles are formed which are either too fine to be sufficiently recovered, or has changed sufficiently due to corrosion to adversely affect its magnetic recoverability.

CHAPTER 5: CONCLUSIONS AND RECOMMENDATIONS

5.1 Conclusions

From the results obtained the following conclusions can be made:

- Losses that occur due to the abrasion of the ferrosilicon particles are unavoidable. However, ferrosilicon losses do also occur due to insufficient product washing (ore and discard washing) and inefficient magnetic recovery. The efficiency of the magnetic separators is indirectly influenced by the chemical composition of the ferrosilicon particles to be recovered. By ensuring that the chemical composition of the smaller ferrosilicon particles to be the same or closer to the bulk chemical composition, the loss of finer particles through inefficient magnetic recovery could be significantly lowered.
- The explanation that the manufacturing process caused the difference in chemical composition of the finer particles with respect to the bulk chemical composition, was disproved by Grobler [20], where chemical analysis of the finer particles showed no significant difference in chemical composition from the bulk chemical composition. The difference in the chemical composition of the finer particles could thus rather be ascribed to the influence of corrosion on the particles.
- No definite change in magnetic properties can be seen, while the ferrosilicon is used as a dense medium separation material, especially when comparing the results of the magnetic separator samples with the ferrosilicon samples of the laboratory experiments. A difference in magnetic property (or magnetic recoverability) was however observed between individual particles.
- The adhesion of hematite to the ferrosilicon particles does occur. Adhesion of hematite was observed in the discard stream ferrosilicon, and could be due to the effect of corrosion on certain ferrosilicon particles.
- The addition of lime seems to have no effect on the used and stored ferrosilicon. Both the ferrosilicon slurry stored with and without the lime did not change

according to the results obtained from the SEM analyses and Mössbauer spectroscopy.

- Some extent of ordering does exist in the ferrosilicon powder, with the saturation magnetization value (Satmagan) being an indication of the degree of ordering.

Returning to the initial hypotheses the following commentary can be given:

1. A particle size distribution change did take place, which proves hypothesis 1. The similar particle size distribution (with respect to the smaller particles) indicates the production of finer particles during use due to abrasion. These particles may then be either lost due to their small size or due to their chemical composition (when this is different from the bulk chemical composition), which influences the efficiency of magnetic recovery.
2. No dramatic change could be determined in the density of the bulk ferrosilicon material, although adhesion of a small amount of hematite does occur, and the possible change in density may be neglected. Thus, hypothesis 2 is disproved.
3. No definite magnetic property change could be shown to occur in the ferrosilicon particles. A difference in magnetic recoverability can however be seen for some particles. The inefficiency of the magnetic separator to recover all the ferrosilicon should rather be ascribed to the effect of corrosion on certain ferrosilicon particles and/or the addition of hematite to the ferrosilicon particle, which influences the Satmagan value and thus its recoverability. Therefor, hypothesis 3 was disproven.
4. The last hypothesis, hypothesis 4, was also disproven. The absence or addition of lime in the samples that were stored for up to 3 months had no discernable effect on the ferrosilicon, both the samples with and without the lime addition stayed exactly the same as before storage took place. Literature does however show that the practice of the addition of an oxidizer to stagnant ferrosilicon medium volumes do exist, which ensures passivation of the medium (ferrosilicon).

5.2 Recommendations

The following recommendations can be made concerning the work done:

- Much more work should be done to give a better overview of the influence that abrasion has on the recovery of ferrosilicon, specifically in the ferrosilicon used by Sishen, during its use as dense medium separation material.
- Special attention should be given to the study of the corrosion characteristics of the medium, in storage, during plant down time, and the effect of adding the lime solution.
- Manufacturers should ensure that the ferrosilicon they produce are within the accepted chemical composition specifications, with regard to bulk as well as the different size fraction compositions.
- More work should also be done on the effect of corrosion on the magnetic recoverability of the ferrosilicon particle.

References

1. Myburgh, H. (2001). Plant superintendent Sishen mine, Kumba Resources, private communication.

2. Napier-munn, T.J., Kojovic, T., Scott, I.A., Shi, F., Masinja, J.H. & Baguley, P.J. (1995). Some causes of medium loss in dense medium plants. Minerals Engineering Vol. 8 No. 6. pp. 659–678.

3. Hunt, S.M., Hansen, J.O. & Davy, A.T. (1986) The influence of ferrosilicon properties on dense medium separation plant consumption. AIMM bulletin and proceedings (Australasian Institute of Mining and Metallurgy) Vol. 291 No 7. pp. 73–82.

4. Nkosibomvu, Z.L., Witcomb, M.J., Cornish, L.A. & Pollak, H. (1998) Mössbauer spectroscopy and SEM characterisation of commercial ferrosilicon powders. Hyperfine Interactions Vol. 112 No. 1/4. pp 261–265.

5. Stearns, M.B. (1963) Internal magnetic, isomer shifts, and relative abundances of the various Fe sites in FeSi alloys. Physical Review Vol. 129 No. 3. pp. 1136–1144.

6. Kelsall, G.H., & Williams, R.A. (1991). Electrochemical behavior of ferrosilicides (Fe_xSi) in neutral and alkaline aqueous electrolytes I. Journal of the Electrochemical Society Vol. 138 No. 4. pp. 931–940.

7. Kelsall, G.H., & Williams, R.A. (1991). Electrochemical behavior of ferrosilicides (Fe_xSi) in neutral and alkaline aqueous electrolytes II. Journal of the Electrochemical Society Vol. 138 No. 4. pp. 941–951.

8. Kelsall, G.H., & Williams, R.A. (1991). Electrochemical behavior of ferrosilicides (Fe_xSi) in neutral and alkaline aqueous electrolytes III. Journal of the Electrochemical Society Vol. 138 No. 4. pp. 951–957.

9. Williams, R.A. & Kelsall, G.H. (1989). An investigation of the surface properties of atomized Fe_xSi powders. Journal of Colloid and Interface Science Vol. 132 No. 1. pp. 210–219.

10. Wiliams, R.A. & Kelsall, G.H. (1992) Degradation of ferrosilicon media in dense medium separation circuits. Minerals Engineering Vol. 5 No. 1. pp. 57–77.

11. Williams, R.A., Kelsall, G.H. & Gochin, R.J. (1986) Differences in physical properties of milled and atomized ferrosilicon powders. Transactions of the Institution of Mining & Metallurgy, Section C Vol. 95. pp. 215–221.

12. Ferrara, G. & Schena, G.D. (1986) Influence of contamination and type of ferrosilicon on viscosity and stability of dense media. Transactions of the Institution of Mining & Metallurgy, Section C Vol. 95. pp. 211–215.

13. Guerney, P.J. (1994) Testing for ferrosilicon corrosion suseptibility. Fifth Samancor Symposium on Dense Media Separation. South Africa.

14. ASM Handbook, Vol. 3, Alloy Phase Diagrams (1992), Materials Park, Ohio.

15. Skoog, D.A., Holler, F.J. & Nieman, T.A. (1998) Principles of instrumental analyses. Fifth edition. Harcourt Brace & Company. pp. 850.

16. Frauenfelder, H. (1962) The Mössbauer effect. W.A. Benjamin, Inc. pp. 336.

17. Parish, R.V. (1990) NMR, NQR, EPR, and Mössbauer spectroscopy in inorganic chemistry. Ellis Norwood Limited. pp. 128–164.

18. Tiedt, L.R. & Pretorius, W.E. (1998) An introduction to electron microscopy and X-ray microanalysis, Laboratory for electron microscopy Potchefstroom University for CHE

19. Waanders, F.B. & Vorster, S.W. (1994). A Mössbauer spectroscopy study of the corrosion of nodular cast iron in mine waters. Hyperfine Interactions Vol. 92. pp. 1027-1033

20. Grobler, P.J. (2003). Kumba Resources, private communication.

APPENDIX A

The relevant data collected as used in the dissertation will be given in this appendix.

A1 Raw data for the unused ferrosilicon

A1.1 Stereopycnometer data

Table A1: Measured density values of the unused ferrosilicon.

	Test 1	Test 2	Test 3
V_{out} (P_2)	16.898	16.916	16.905
V_{in} (P_3)	10.212	10.224	10.218

Note: Sample weight = 242.3 g

A1.2 Malvern Mastersizer data

Table A2: Particle size distribution values obtained from the Malvern Mastersizer (% mass passing), with the highlighted value being the average size (d_{50}).

Size passing (μm)	Sample 1	Sample 2	Sample 3	Sample 4
1.32	0	0	0	0
1.6	0.03	0.03	0	0
1.95	0.08	0.09	0	0
2.38	0.16	0.18	0	0
2.9	0.3	0.33	0	0
3.53	0.51	0.55	0	0
4.3	0.88	0.92	0	0
5.24	1.49	1.55	0	0.03
6.39	2.5	2.6	0.06	0.11
7.78	4.1	4.27	0.44	0.53

Size passing (μm)	Sample 1	Sample 2	Sample 3	Sample 4
9.48	6.52	6.81	1.93	1.75
11.55	9.99	10.44	4.9	4.24
15.08	14.74	15.37	10.15	8.66
17.15	20.89	21.68	18.12	15.52
20.9	28.57	29.4	28.77	25.02
25.46	37.87	38.57	41.41	36.89
31.01	48.68	49.12	54.9	50.36
37.79	60.67	60.87	68.04	64.35
46.03	72.65	72.75	79.64	77.37
56.09	83.37	83.85	88.6	87.92
68.33	90.42	90.71	94.16	93.36
83.26	94.18	94.57	96.58	96.91
101.44	95.09	95.54	96.99	97.17
123.59	95.1	95.54	96.99	97.17
150.57	95.1	95.54	96.99	97.17
183.44	95.14	95.54	97.02	97.18
223.51	95.6	95.75	97.53	97.64
272.31	96.65	96.54	98.51	98.53
331.77	97.9	97.78	99.52	99.51
404.21	99.11	99.12	99.98	99.98
492.47	99.9	99.9	100	100
600	100	100	100	100

Note: See attached raw data sheets for the Malvern Mastersizer Appendix C

A1.3 Chemical composition

Table A3: Chemical composition of the unused ferrosilicon as determined by SEM analysis.

	Sample 1	Sample 2	Average
Fe (wt %)	80.56	82.01	81.29
Si (wt %)	14.80	13.41	14.11
O (wt %)*	3.87	4.15	4.01
Al (wt %)	0.45	0.33	0.39
K (wt %)	0.10	0.00	0.05
Ca (wt %)	0.23	0.09	0.16

Note: See attached raw data sheet of the unused ferrosilicon SEM data in Appendix C

*The amount of O represents the amount of possible oxides in the sample

A1.4 Mössbauer spectroscopic parameters of the unused ferrosilicon

Table A4: Mössbauer parameters of the iron-components in the unused ferrosilicon.

	IS (mms^{-1}) (±0.02)	QS (mms^{-1}) (±0.02)	H (T) (±0.3)	Relative Intensity (%)
Sextet 1 (B)	0.04	0.04	30.7	42
Sextet 2 (A)	0.23	0.00	19.9	58

Note: IS = Isomer shift relative to α-iron, QS = Quadropole splitting and H = Hyperfine magnetic field strength. See attached raw data sheet of the unused ferrosilicon Mössbauer spectra data.

A2 Data collected from the ferrosilicon used in the attrition system experiments

A2.1 Density measured for the used ferrosilicon

Table A5: Steropynometer results for the used ferrosilicon

	Test 1	Test 2	Test 3
V_{out} (P_2)	17.056	17.080	17.022
V_{in} (P_3)	10.201	10.215	10.179
Calculated Density	6.969	6.967	6.961

Note: Sample weight = 257.3 g.

A2.2 Particle size distribution using the wet sieve technique

Table A6: Cumulative mass % of particles passing sieve.

Sieve size (μm)	Day 2	Day 3	Day 4	Day 5
+450	0	0	0	0
+300 –450	13.5	17.1	7.4	5.1
+212 –300	4.8	5.4	6.5	11.8
+150 -212	1.2	2	2	2.7
+106 –150	2.7	2.7	4.9	3.3
+75 –106	24.3	7.4	6.2	7.3
+53 -75	65.6	55	60.7	44.9
+37.5 -53	47.4	46.7	36.4	54.9
-37.5	452.9	449.6	372	424.5
Sample weight	612.4	585.9	496.1	554.5

A2.3 Mössbauer parameters of the attrition system ferrosilicon

Table A7: Mössbauer parameters of the iron-components in attrition system ferrosilicon, the observed froth and the non-magnetic material.

	IS (mms^{-1}) (±0.02)	QS (mms^{-1}) (±0.02)	H (T) (±0.3)	Relative Intensity (%)
Ferro. Sextet 1 (B)	0.05	0.01	31.2	31
Ferro. Sextet 2 (A)	0.23	-0.01	20.1	47
Ferro. Sextet 3 (C)	0.15	0.00	25.4	22
Froth doublet 1	0.17	0.69		71
Froth doublet 2	0.35	0.92		29
Non-mag. material Sextet 1 (B)	0.06	-0.03	19.7	24
Non-mag. material Sextet 2 (A)	0.23	-0.02	29.5	25
Non-mag. material doublet	0.31	0.72		51

Note: IS = Isomer shift relative to α-iron, QS = Quadropole splitting and H = Hyperfine magnetic field strength. See attached raw data sheet of the attrition system ferrosilicon Mössbauer spectra data.

A3 Data collected from the samples taken at the Sishen plant

A3.1 Malvern Mastersizer data

Table A8: Particle size distribution values obtained from the Malvern Mastersizer (% mass passing) for the unused ferrosilicon.

Size passing (μm)	Sample 1	Sample 2	Sample 3
1.32	0.00	0.00	0.04
1.6	0.00	0.00	0.07
1.95	0.00	0.00	0.09
2.38	0.00	0.00	0.13
2.9	0.01	0.00	0.16
3.53	0.02	0.01	0.20
4.3	0.04	0.02	0.25
5.24	0.08	0.05	0.32
6.39	0.14	0.11	0.43
7.78	0.28	0.22	0.61
9.48	0.57	0.50	0.95
11.55	1.19	1.14	1.66
15.08	2.49	2.56	3.11
17.15	4.86	5.37	5.77
20.9	8.79	10.31	10.23
25.46	14.72	18.03	17.00
31.01	22.62	28.35	25.90
37.79	32.34	40.45	36.47
46.03	43.89	53.23	48.33
56.09	56.77	65.69	60.69
68.33	68.84	76.24	71.75
83.26	78.16	83.82	80.19
101.44	85.07	89.06	86.26
123.59	89.90	92.64	90.63
150.57	93.16	95.03	93.62
183.44	95.23	96.54	95.66

Size passing (μm)	Sample 1	Sample 2	Sample 3
223.51	96.66	97.58	97.13
272.31	97.73	98.35	98.19
331.77	98.59	98.95	98.94
404.21	99.37	99.47	99.51
492.47	99.84	99.82	99.84
600	100.00	100.00	100.00

Note: See attached raw data sheets for the Malvern Mastersizer Appendix C

A3.2 Mössbauer parameters obtained for the ferrosilicon adhered to the sink and float product samples

Table A9: Mössbauer parameters of the iron-components in the ferrosilicon adhered to the sink and float product samples from the Sishen plant.

	IS (mms^{-1}) (±0.02)	QS (mms^{-1}) (±0.02)	H (T) (±0.3)	Relative Intensity (%)
Ore sample 1				
Sextet 1 (D)	0.24	0.09	51.9	9
Sextet 2 (B)	0.07	0.10	28.3	41
Sextet 3 (A)	0.23	0.00	19.6	50
Ore sample 2				
Sextet 1 (D)	0.26	-0.08	51.5	9
Sextet 2 (B)	0.03	0.05	28.6	41
Sextet 3 (A)	0.23	0.01	19.5	50
Discard sample				
Sextet 1 (B)	0.04	0.03	29.7	47
Sextet 2 (A)	0.23	0.01	19.7	53

Note: IS = Isomer shift relative to α-iron, QS = Quadropole splitting and H = Hyperfine magnetic field strength. See attached raw data sheet of the unused ferrosilicon Mössbauer spectra data.

A3.3 Mössbauer parameters obtained for the ferrosilicon present in the magnetic separator samples.

Table A10: Mössbauer parameters of the iron-components in the ferrosilicon samples from the magnetic separator at the Sishen plant.

	IS (mms^{-1}) (±0.02)	QS (mms^{-1}) (±0.02)	H (T) (±0.3)	Relative Intensity (%)
Feed				
Sextet 2 (B)	0.05	0.03	29.4	49
Sextet 3 (A)	0.24	0.00	19.6	51
Discard				
Sextet 1 (D)	0.30	-0.26	51.0	22
Sextet 2 (B)	0.03	0.04	29.4	41
Sextet 3 (A)	0.24	-0.00	19.6	37
Concentrate				
Sextet 1 (B)	0.05	0.03	29.6	46
Sextet 2 (A)	0.24	0.00	19.7	54

Note: IS = Isomer shift relative to α-iron, QS = Quadropole splitting and H = Hyperfine magnetic field strength. See attached raw data sheet of the unused ferrosilicon Mössbauer spectra data.

APPENDIX B

B1 Data collected for the unused ferrosilicon

B1.1: Density measurements using the stereopycnometer

Density measurements were done using the stereopycnometer, with each sample being measured 3 times to enable a better average value. The values obtained from the sample of the unused ferrosilicon is shown in **Table B1**, with the relevant densities calculated for each set of values.

Table B1: Measured and calculated values of the density measurements of the unused ferrosilicon.

	Test 1	Test 2	Test 3
V_{out} (P_2)	16.898	16.916	16.905
V_{in} (P_3)	10.212	10.224	10.218
Calculated Density	7.171	7.178	7.181

Sample calculation of the ferrosilicon density (Test 1):

$V_p = V_c + V_A/(1 - P_2/P_3)$

Where V_p = Sample volume

V_c = Sample cell volume (155.37 cm^3)

V_A = Added volume (79.60 cm^3)

P_2 = Pressure measured in system before added volume (16.898 Psi)

P_3 = Pressure measured in system after added volume (10.212 Psi)

Thus: $V_p = 33.79$ cm^3

Density = Sample mass/V_p

Sample mass = 242.3 g

Thus: Density = 7.171 g/cm^3

B1.2: Particle size distribution of the unused ferrosilicon

The particle size distribution was done using the Malvern Mastersizer, and the following values were obtained:

Table B2: Particle size distribution values obtained from the Malvern Mastersizer (% particles of size).

Particle size (μm)	Sample 1	Sample 2	Sample 3	Sample 4	Average
0.66	0	0	0	0	0
1.45	0.03	0.03	0.00	0.00	0.02
1.77	0.05	0.06	0.00	0.00	0.03
2.15	0.08	0.09	0.00	0.00	0.04
2.63	0.14	0.15	0.00	0.00	0.07
3.20	0.21	0.22	0.00	0.00	0.11
3.90	0.37	0.37	0.00	0.00	0.19
4.75	0.61	0.63	0.00	0.03	0.32
5.79	1.01	1.05	0.06	0.08	0.55
7.05	1.60	1.67	0.38	0.42	1.02
8.59	2.42	2.54	1.49	1.22	1.92
10.46	3.47	3.63	2.97	2.49	3.14
13.20	4.75	4.93	5.25	4.42	4.84
16.08	6.15	6.31	7.97	6.86	6.82
18.93	7.68	7.72	10.65	9.50	8.89
23.07	9.30	9.17	12.64	11.87	10.75
28.10	10.81	10.55	13.49	13.47	12.08
34.23	11.99	11.75	13.14	13.99	12.72
41.71	11.98	11.88	11.60	13.02	12.12
50.81	10.72	11.10	8.96	10.55	10.33
61.91	7.05	6.86	5.56	5.44	6.23
75.43	3.76	3.86	2.42	3.55	3.40
91.90	0.91	0.97	0.41	0.26	0.64
111.97	0.01	0.00	0.00	0.00	0.00
136.41	0.00	0.00	0.00	0.00	0.00
166.19	0.04	0.00	0.03	0.01	0.02

202.49	0.46	0.21	0.51	0.46	0.41
246.71	1.05	0.79	0.98	0.89	0.93
300.57	1.25	1.24	1.01	0.98	1.12
366.20	1.21	1.34	0.46	0.47	0.87
446.16	0.79	0.78	0.02	0.02	0.40
543.58	0.10	0.10	0.00	0.00	0.05

A graphical representation of the discreet particle size distribution can be seen in **Figure B1**.

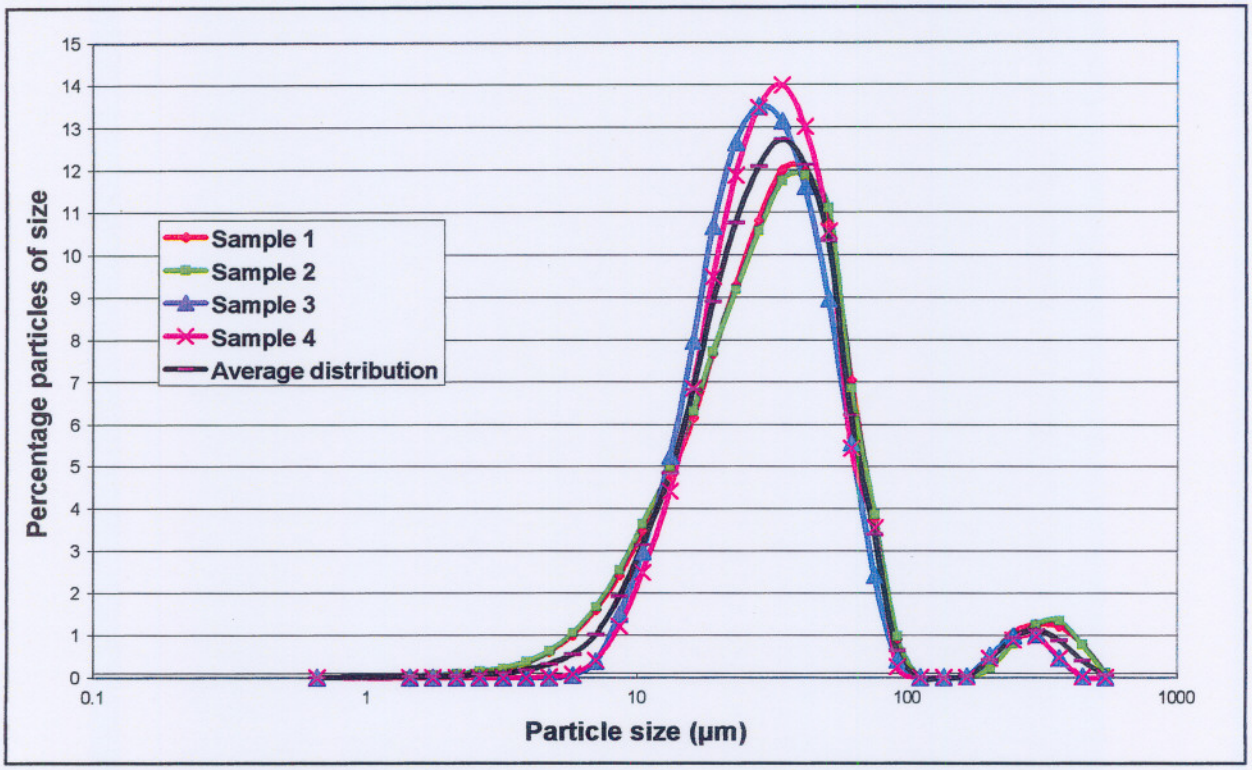

Figure B1: Discrete particle size distribution of the unused ferrosilicon (as obtained from the Malvern Mastersizer results).

B1.3: Chemical composition

The chemical composition of the unused ferrosilicon was done using SEM analysis. The following initial chemical composition were obtained:

Table B3: Chemical composition of the unused ferrosilicon as determined by SEM analysis.

	Sample 1	Sample 2	Average
Fe (wt %)	80.56	82.01	81.29
Si (wt %)	14.80	13.41	14.11
O (wt %)	3.87	4.15	4.01
Al (wt %)	0.45	0.33	0.39
K (wt %)	0.10	0.00	0.05
Ca (wt %)	0.23	0.09	0.16

B1.4: Mössbauer spectroscopic parameters of the unused ferrosilicon

Each sample analyses in the Mössbauer spectrometer took up to 3 days, to ensure that an adequate amount of data was collected, which would ensure a better analysis of the sample. The Mössbauer spectroscopic parameters were found to be the following:

Table B4: Mössbauer parameters of the iron-components in unused ferrosilicon.

	IS (mms^{-1}) (±0.02)	QS (mms^{-1}) (±0.02)	H (T) (±0.3)	Relative Intensity (%)
Sextet 1 (B)	0.04	0.04	30.7	42
Sextet 2 (A)	0.23	0.00	19.9	58

Note: IS = Isomer shift relative to α-iron, QS = Quadropole splitting and H = Hyperfine magnetic field strength.

B2 Data collected from the ferrosilicon used in the attrition system experiments

B2.1 Density measured for the used ferrosilicon

The values obtained from the stereopycnometer, for the used ferrosilicon, are shown in **Table B5**, with the relevant densities.

Table B5: Stereopynometer results for the used ferrosilicon

	Test 1	Test 2	Test 3
V_{out} (P_2)	17.056	17.080	17.022
V_{in} (P_3)	10.201	10.215	10.179
Calculated Density	6.969	6.967	6.961

Note: Sample weight = 257.3 g

B2.2 Particle size distribution using the wet sieve technique

The particle size distribution was done with a sieve series with top size of 450 μm and a bottom size of 37.5 μm, with an aperture size reduction factor of $\sqrt{2}$.

Table B6: Cumulative mass % of particles passing sieve.

Sieve size (μm)	Day 2	Day 3	Day 4	Day 5
450	100.00	100.00	100.00	100.00
300	97.80	97.08	98.51	99.08
212	97.01	96.16	97.20	96.95
150	96.82	95.82	96.80	96.47
106	96.37	95.36	95.81	95.87
75	92.41	94.09	94.56	94.55
53	81.69	84.71	82.32	86.46
37.5	73.95	76.74	74.98	76.56

B2.3 Mössbauer parameters of the attrition system ferrosilicon

The Mössbauer spectroscopic parameters were found to be the following:

Table B7: Mössbauer parameters of the iron-components in attrition system ferrosilicon and the observed froth.

	IS (mms^{-1}) (±0.02)	QS (mms^{-1}) (±0.02)	H (T) (±0.3)	Relative Intensity (%)
Ferro. Sextet 1 (B)	0.05	0.01	31.2	31
Ferro. Sextet 2 (A)	0.23	-0.01	20.1	47
Ferro. Sextet 3 (C)	0.15	0.00	25.4	22
Froth doublet 1	0.17	0.69		71
Froth doublet 2	0.35	0.92		29
Non-mag. material Sextet 1 (B)	0.06	-0.03	19.7	24
Non-mag. material Sextet 2 (A)	0.23	-0.02	29.5	25
Non-mag. material doublet	0.31	0.72		51

Note: IS = Isomer shift relative to α-iron, QS = Quadropole splitting and H = Hyperfine magnetic field strength.

B3 Data collected from the samples taken at the Sishen plant

B3.1 Particle size distribution from the samples taken at the Sishen plant

The particle size distribution was doen using the Malvern Mastersizer, and the following values were obtained:

Table B8: Particle size distribution values obtained from the Malvern Mastersizer for the ferrosilicon used at the Sishen plant (% particles of size).

Particle size (µm)	Sample 1	Sample 2	Sample 3	Average
0.66	0.00	0.00	0.04	0.01
1.45	0.00	0.00	0.03	0.01
1.77	0.00	0.00	0.02	0.01
2.15	0.00	0.00	0.04	0.01
2.63	0.01	0.00	0.03	0.01
3.20	0.01	0.01	0.04	0.02
3.90	0.02	0.01	0.05	0.03
4.75	0.04	0.03	0.07	0.05
5.79	0.06	0.06	0.11	0.08
7.05	0.14	0.11	0.18	0.14
8.59	0.29	0.28	0.34	0.30
10.46	0.62	0.64	0.71	0.66
13.20	1.30	1.42	1.45	1.39
16.08	2.37	2.81	2.66	2.61
18.93	3.93	4.94	4.46	4.44
23.07	5.93	7.72	6.77	6.81
28.10	7.90	10.32	8.90	9.04
34.23	9.72	12.10	10.57	10.80
41.71	11.55	12.78	11.86	12.06
50.81	12.88	12.46	12.36	12.57
61.91	12.07	10.55	11.06	11.23
75.43	9.32	7.58	8.44	8.45
91.90	6.91	5.24	6.07	6.07
111.97	4.83	3.58	4.37	4.26
136.41	3.26	2.39	2.99	2.88

Particle size (µm)	Sample 1	Sample 2	Sample 3	Average
166.19	2.07	1.51	2.04	1.87
202.49	1.43	1.04	1.47	1.31
246.71	1.01	0.77	1.06	0.97
300.57	0.86	0.60	0.75	0.74
366.20	0.78	0.52	0.57	0.62
446.16	0.47	0.35	0.33	0.38
543.58	0.16	0.18	0.16	0.17

A graphical representation of the discreet particle size distribution can be seen in **Figure B2.**

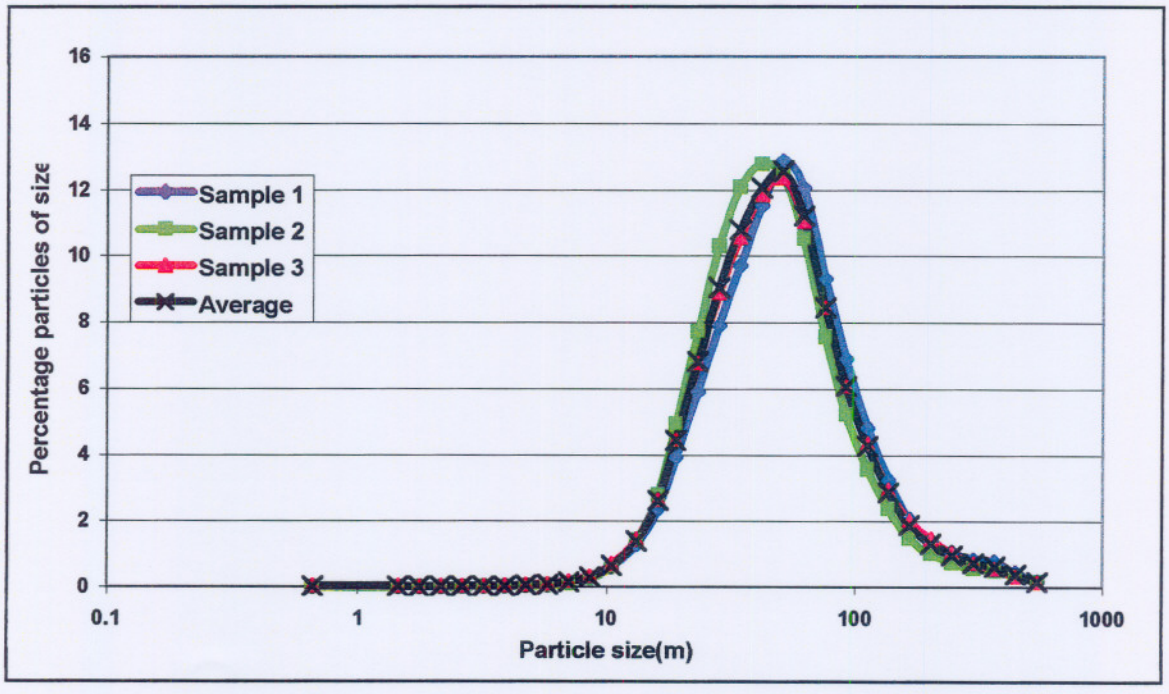

Figure B2: Discrete particle size distribution of the ferrosilicon used in the Sishen plant (as obtained from the Malvern Mastersizer results).

B3.2 Mössbauer parameters obtained for the ferrosilicon adhered to the sink and float product samples

The following parameters were obtained:

Table B9: Mössbauer parameters of the iron-components in the ferrosilicon adhered to the sink and float product samples from the Sishen plant.

	IS (mms^{-1}) (±0.02)	QS (mms^{-1}) (±0.02)	H (T) (±0.3)	Relative Intensity (%)
Ore sample 1				
Sextet 1 (D)	0.24	0.09	51.9	9
Sextet 2 (B)	0.07	0.10	28.3	41
Sextet 3 (A)	0.23	0.00	19.6	50
Ore sample 2				
Sextet 1 (D)	0.26	-0.08	51.5	9
Sextet 2 (B)	0.03	0.05	28.6	41
Sextet 3 (A)	0.23	0.01	19.5	50
Discard sample				
Sextet 1 (B)	0.04	0.03	29.7	47
Sextet 2 (A)	0.23	0.01	19.7	53

Note: IS = Isomer shift relative to α-iron, QS = Quadropole splitting and H = Hyperfine magnetic field strength.

B3.3 Mössbauer parameters obtained for the ferrosilicon present in the magnetic separator samples.

The following parameters were obtained:

Table B10: Mössbauer parameters of the iron-components in the ferrosilicon samples from the magnetic separator at the Sishen plant.

	IS (mms^{-1}) (±0.02)	QS (mms^{-1}) (±0.02)	H (T) (±0.3)	Relative Intensity (%)
Feed				
Sextet 2 (B)	0.05	0.03	29.4	49
Sextet 3 (A)	0.24	0.00	19.6	51
Discard				
Sextet 1 (D)	0.30	-0.26	51.0	22
Sextet 2 (B)	0.03	0.04	29.4	41
Sextet 3 (A)	0.24	-0.00	19.6	37
Concentrate				
Sextet 1 (B)	0.05	0.03	29.6	46
Sextet 2 (A)	0.24	0.00	19.7	54

Note: IS = Isomer shift relative to α-iron, QS = Quadropole splitting and H = Hyperfine magnetic field strength.

APPENDIX C

Raw data sheets of:

- Malvern Mastersizer Unused ferrosilicon Sample 1
- Malvern Mastersizer Unused ferrosilicon Sample 2
- Malvern Mastersizer Unused ferrosilicon Sample 3
- Malvern Mastersizer Unused ferrosilicon Sample 4
- Malvern Mastersizer Used ferrosilicon from Sishen plant Sample 1
- Malvern Mastersizer Used ferrosilicon from Sishen plant Sample 2
- Malvern Mastersizer Used ferrosilicon from Sishen plant Sample 3
- Malvern Mastersizer Unused finer ferrosilicon particles analyzed
- Analytical report Unused finer ferrosilicon particles analyzed
- Unused ferrosilicon SEM data sheet Sample 1
- Unused ferrosilicon SEM data sheet Sample 2
- Mössbauer spectrum data sheet Unused ferrosilicon
- Mössbauer spectrum data sheet Used ferrosilicon Magnetic fraction
- Mössbauer spectrum data sheet Used ferrosilicon Non-Magnetic fraction
- Mössbauer spectrum data sheet Froth
- Mössbauer spectrum data sheet Ore Sample 1
- Mössbauer spectrum data sheet Ore Sample 2
- Mössbauer spectrum data sheet Discard
- Mössbauer spectrum data sheet Magnetic separator sample Feed
- Mössbauer spectrum data sheet Magnetic separator sample Discard
- Mössbauer spectrum data sheet Magnetic separator sample Concentrate

MALVERN INSTRUMENTS

MASTERSIZER X

Version 1.2a

Tue, Feb 12, 2002 11:44AM

Ferrosilicon

Monster: **Sample 1**

Dispersant: Milli RO water in MSX14
Sample 2
Sample File Name: FERRO_01, Record: 3 Source: Analysed
Measured on: Fri, Jan 04, 1980 8:54PM Last saved on: Fri, Jan 04, 1980 8:54PM

Presentation: 2THD
Polydisperse model Volume Result Focus = 300 mm.

Residual = 0.791 % Concentration = 0.010 % Obscuration = 19.22 %
d (0.5) = 31.72 µm d (0.1) = 11.55 µm d (0.9) = 67.16 µm
D [4, 3] = 47.42 µm Span = 1.75
Sauter Mean (D[3,2]) = 22.49 µm Mode = 37.84 µm
Specific Surface Area = 0.2667 sq. m. / gm Density = 1.00 gm. / c.c.

Size (Lo) µm	Result In %	Size (Hi) µm	Result Below %	Size (Lo) µm	Result In %	Size (Hi) µm	Result Below %
0.50	0.00	1.32	0.00	25.46	10.81	31.01	48.68
1.32	0.02	1.60	0.03	31.01	12.00	37.79	60.67
1.60	0.05	1.95	0.08	37.79	11.98	46.03	72.65
1.95	0.08	2.38	0.16	46.03	10.72	56.09	83.37
2.38	0.13	2.90	0.30	56.09	7.06	68.33	90.42
2.90	0.22	3.53	0.51	68.33	3.76	83.26	94.18
3.53	0.36	4.30	0.88	83.26	0.91	101.44	95.09
4.30	0.61	5.24	1.49	101.44	0.00	123.59	95.10
5.24	1.01	6.39	2.50	123.59	0.00	150.57	95.10
6.39	1.60	7.78	4.10	150.57	0.04	183.44	95.14
7.78	2.42	9.48	6.52	183.44	0.46	223.51	95.60
9.48	3.47	11.55	9.99	223.51	1.04	272.31	96.65
11.55	4.75	14.08	14.74	272.31	1.26	331.77	97.90
14.08	6.15	17.15	20.89	331.77	1.21	404.21	99.11
17.15	7.68	20.90	28.57	404.21	0.78	492.47	99.90
20.90	9.29	25.46	37.87	492.47	0.10	600.00	100.00

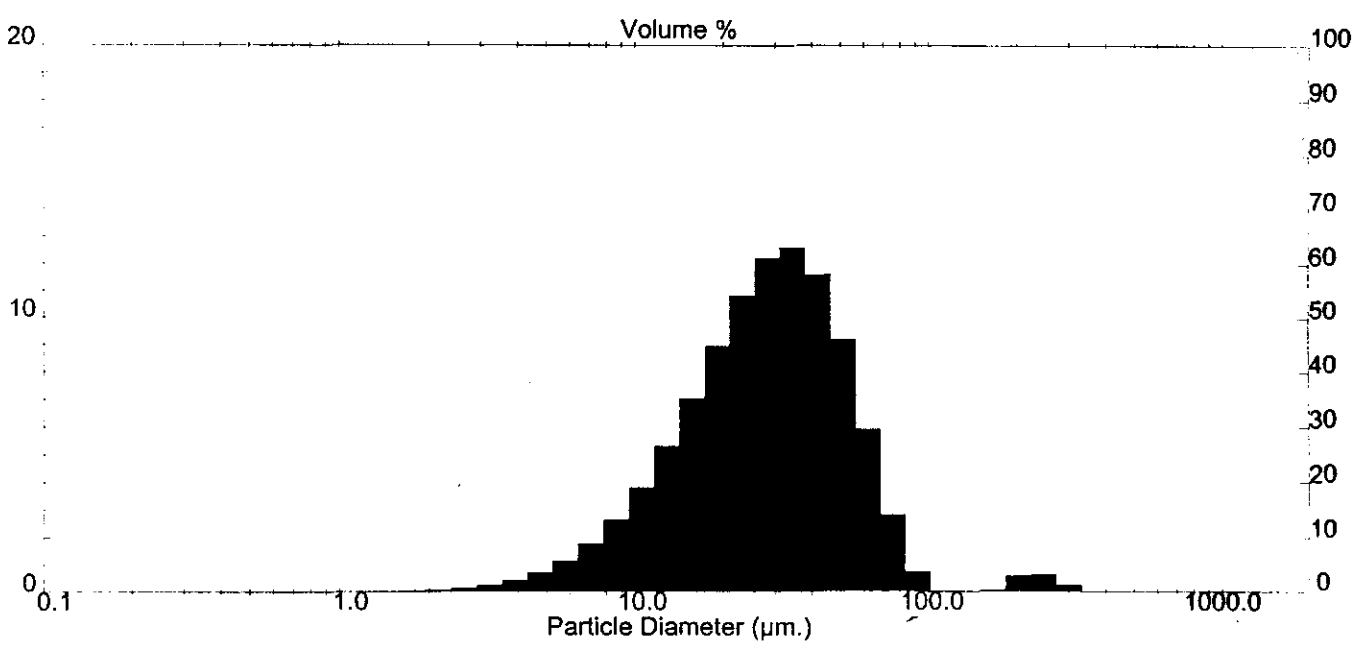

MALVERN INSTRUMENTS **MASTERSIZER X**

Version 1.2a

Tue, Feb 12, 2002 11:44AM

Ferrosilicon :

Monster: **Sample 2**

Dispersant: Milli RO water in MSX14
Sample 3
Sample File Name: FERRO_01, Record: 5 Source: Analysed
Measured on: Fri, Jan 04, 1980 8:59PM Last saved on: Fri, Jan 04, 1980 8:59PM

Presentation: 2THD
Polydisperse model

Volume Result

Focus = 300 mm.

Residual = 0.976 %
d (0 .5) = 31.49 µm
D [4, 3] = 46.71 µm
Sauter Mean (D[3,2]) = 22.13 µm
Specific Surface Area = 0.2711 sq. m. / gm

Concentration = 0.010 %
d (0.1) = 11.31 µm
Span = 1.75

Obscuration = 19.87 %
d (0.9) = 66.41 µm

Mode = 38.57 µm
Density = 1.00 gm. / c.c.

Size (Lo) µm	Result In %	Size (Hi) µm	Result Below %
0.50	0.00	1.32	0.00
1.32	0.03	1.60	0.03
1.60	0.06	1.95	0.09
1.95	0.09	2.38	0.18
2.38	0.14	2.90	0.33
2.90	0.22	3.53	0.55
3.53	0.37	4.30	0.92
4.30	0.63	5.24	1.55
5.24	1.05	6.39	2.60
6.39	1.67	7.78	4.27
7.78	2.54	9.48	6.81
9.48	3.63	11.55	10.44
11.55	4.94	14.08	15.37
14.08	6.31	17.15	21.68
17.15	7.72	20.90	29.40
20.90	9.17	25.46	38.57
25.46	10.55	31.01	49.12
31.01	11.75	37.79	60.87
37.79	11.88	46.03	72.75
46.03	10.78	56.09	83.54
56.09	7.18	68.33	90.71
68.33	3.86	83.26	94.57
83.26	0.97	101.44	95.54
101.44	0.00	123.59	95.54
123.59	0.00	150.57	95.54
150.57	0.00	183.44	95.54
183.44	0.20	223.51	95.75
223.51	0.79	272.31	96.54
272.31	1.24	331.77	97.78
331.77	1.33	404.21	99.12
404.21	0.78	492.47	99.90
492.47	0.10	600.00	100.00

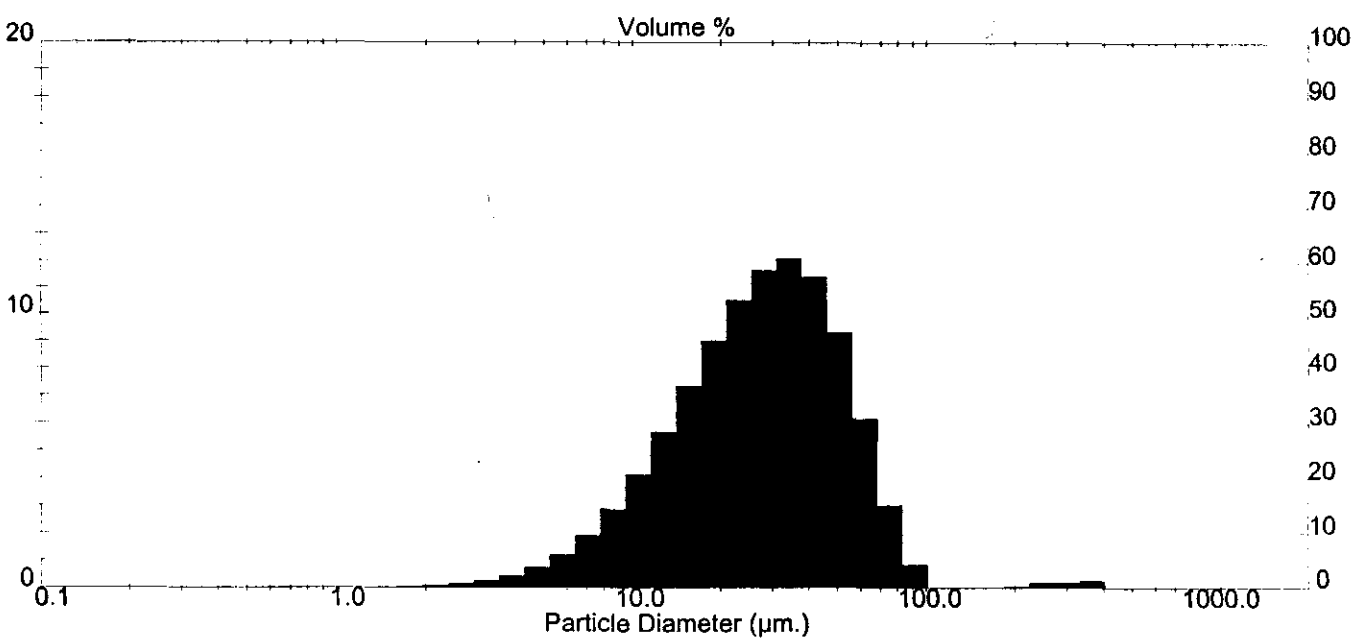

MALVERN INSTRUMENTS

MASTERSIZER X

Version 1.2a

Tue, Feb 12, 2002 11:45AM

Ferrosilicon :

Monster: **Sample 3**

Dispersant: Milli RO water in MSX14
Sample 1
Sample File Name: FERRO_02, Record: 1 Source: Analysed
Measured on: Fri, Jan 04, 1980 9:05PM Last saved on: Fri, Jan 04, 1980 9:06PM

Presentation: 2THD
Polydisperse model

Volume Result

Focus = 300 mm.

Residual = 0.954 %
d (0 .5) = 28.88 µm
D [4, 3] = 38.95 µm
Sauter Mean (D[3,2]) = 24.92 µm
Specific Surface Area = 0.2408 sq. m. / gm

Concentration = 0.010 %
d (0.1) = 14.02 µm
Span = 1.54

Obscuration = 16.96 %
d (0.9) = 58.37 µm

Mode = 29.16 µm
Density = 1.00 gm. / c.c.

Size (Lo) µm	Result In %	Size (Hi) µm	Result Below %
0.50	0.00	1.32	0.00
1.32	0.00	1.60	0.00
1.60	0.00	1.95	0.00
1.95	0.00	2.38	0.00
2.38	0.00	2.90	0.00
2.90	0.00	3.53	0.00
3.53	0.00	4.30	0.00
4.30	0.00	5.24	0.00
5.24	0.06	6.39	0.06
6.39	0.38	7.78	0.44
7.78	1.49	9.48	1.93
9.48	2.97	11.55	4.90
11.55	5.25	14.08	10.15
14.08	7.97	17.15	18.12
17.15	10.65	20.90	28.77
20.90	12.64	25.46	41.41
25.46	13.48	31.01	54.90
31.01	13.15	37.79	68.04
37.79	11.59	46.03	79.64
46.03	8.96	56.09	88.60
56.09	5.56	68.33	94.16
68.33	2.42	83.26	96.58
83.26	0.41	101.44	96.99
101.44	0.00	123.59	96.99
123.59	0.00	150.57	96.99
150.57	0.03	183.44	97.02
183.44	0.51	223.51	97.53
223.51	0.98	272.31	98.51
272.31	1.01	331.77	99.52
331.77	0.46	404.21	99.98
404.21	0.02	492.47	100.00
492.47	0.00	600.00	100.00

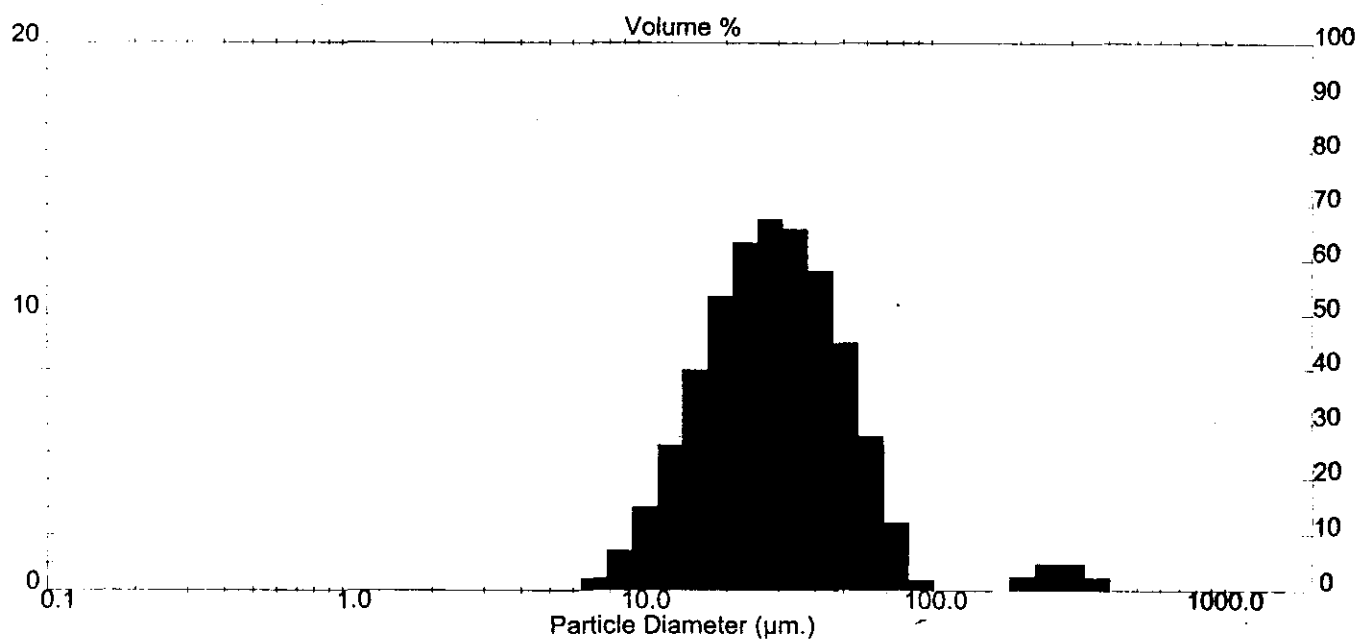

MALVERN INSTRUMENTS **MASTERSIZER X**

Version 1.2a

Tue, Feb 12, 2002 11:45AM

Ferrosilicon :

Monster: **Sample 4**

Dispersant: Milli RO water in MSX14
Sample 2
Sample File Name: FERRO_02, Record: 3 Source: Analysed
Measured on: Fri, Jan 04, 1980 9:11PM Last saved on: Fri, Jan 04, 1980 9:11PM

Presentation: 2THD
Polydisperse model

Volume Result

Focus = 300 mm.

Residual = 0.710 %
d (0 .5) = 30.85 µm
D [4, 3] = 40.02 µm
Sauter Mean (D[3,2]) = 26.15 µm
Specific Surface Area = 0.2294 sq. m. / gm

Concentration = 0.011 %
d (0.1) = 14.73 µm
Span = 1.44

Obscuration = 16.34 %
d (0.9) = 59.02 µm

Mode = 33.38 µm
Density = 1.00 gm. / c.c.

Size (Lo) µm	Result In %	Size (Hi) µm	Result Below %
0.50	0.00	1.32	0.00
1.32	0.00	1.60	0.00
1.60	0.00	1.95	0.00
1.95	0.00	2.38	0.00
2.38	0.00	2.90	0.00
2.90	0.00	3.53	0.00
3.53	0.00	4.30	0.00
4.30	0.03	5.24	0.03
5.24	0.08	6.39	0.11
6.39	0.42	7.78	0.53
7.78	1.22	9.48	1.75
9.48	2.49	11.55	4.24
11.55	4.43	14.08	8.66
14.08	6.86	17.15	15.52
17.15	9.50	20.90	25.02
20.90	11.87	25.46	36.89
25.46	13.47	31.01	50.36
31.01	13.99	37.79	64.35
37.79	13.02	46.03	77.37
46.03	10.55	56.09	87.92
56.09	6.04	68.33	93.96
68.33	2.94	83.26	96.91
83.26	0.26	101.44	97.17
101.44	0.00	123.59	97.17
123.59	0.00	150.57	97.17
150.57	0.02	183.44	97.18
183.44	0.46	223.51	97.64
223.51	0.89	272.31	98.53
272.31	0.98	331.77	99.51
331.77	0.47	404.21	99.98
404.21	0.02	492.47	100.00
492.47	0.00	600.00	100.00

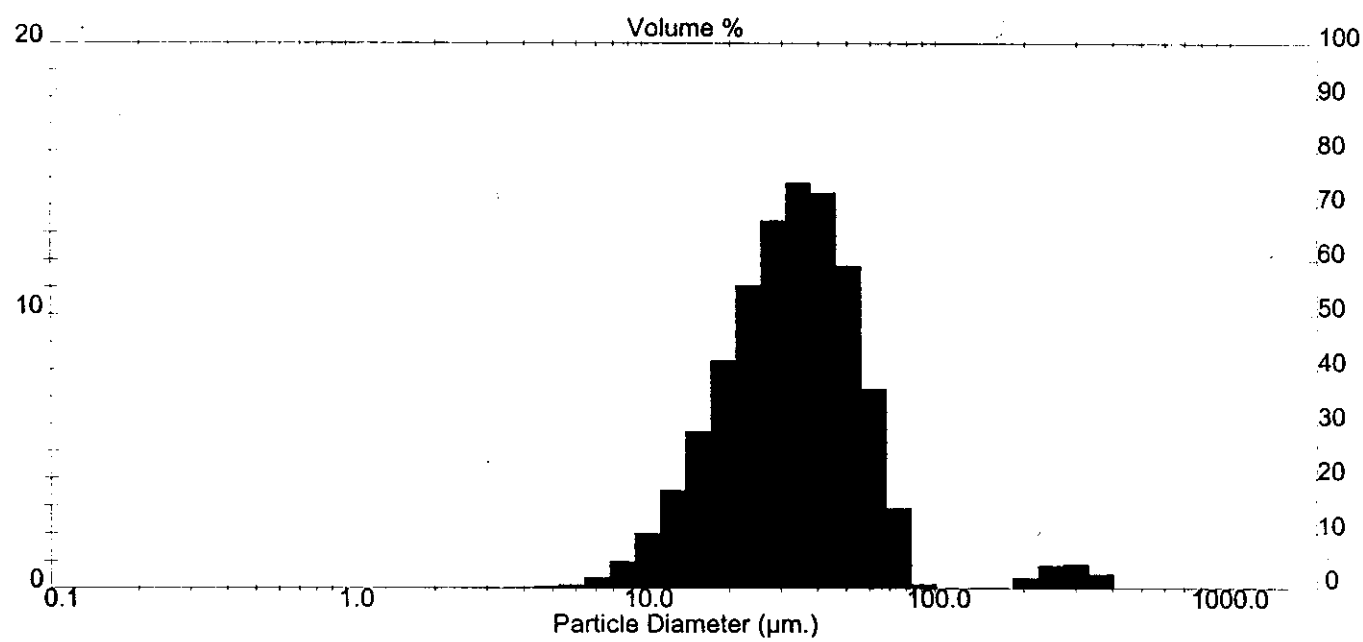

MALVERN INSTRUMENTS **MASTERSIZER X**

Version 1.2a — Fri. Oct 10, 2003 11:08AM

Sishen FeSi 1 :Run Number 1

Dispersant: Milli RO water in MSX14

Sample 1
Sample File Name: FERRO_01, Record: 1 — Source: Analysed
Measured on: Fri. Jan 04, 1980 8.14PM — Last saved on: Fri. Jan 04, 1980 8.15PM

Presentation: 2OHD
Very Polydisperse model

Volume Result

Focus = 300 mm

Residual = 2.084 %
d (0.5) = 50.62 µm
D [4, 3] = 67.77 µm
Sauter Mean (D[3,2]) = 40.81 µm
Specific Surface Area = 0.1470 sq. m. / gm

Concentration = 0.016 %
d (0.1) = 21.89 µm
Span = 2.02

Obscuration = 15.57 %
d (0.9) = 124.22 µm

Mode = 53.65 µm
Density = 1.00 gm. / c.c.

Size (Lo) µm	Result In %	Size (Hi) µm	Result Below %	Size (Lo) µm	Result In %	Size (Hi) µm	Result Below %
0.50	0.00	1.32	0.00	25.46	7.90	31.01	22.62
1.32	0.00	1.60	0.00	31.01	9.72	37.79	32.34
1.60	0.00	1.95	0.00	37.79	11.55	46.03	43.89
1.95	0.00	2.38	0.00	46.03	12.88	56.09	56.77
2.38	0.00	2.90	0.01	56.09	12.07	68.33	68.84
2.90	0.01	3.53	0.02	68.33	9.32	83.26	78.16
3.53	0.02	4.30	0.04	83.26	6.91	101.44	85.07
4.30	0.04	5.24	0.08	101.44	4.83	123.59	89.90
5.24	0.07	6.39	0.14	123.59	3.26	150.57	93.16
6.39	0.14	7.78	0.28	150.57	2.07	183.44	95.23
7.78	0.29	9.48	0.57	183.44	1.43	223.51	96.66
9.48	0.62	11.55	1.19	223.51	1.07	272.31	97.73
11.55	1.29	14.08	2.49	272.31	0.86	331.77	98.59
14.08	2.38	17.15	4.86	331.77	0.79	404.21	99.37
17.15	3.93	20.90	8.79	404.21	0.47	492.47	99.84
20.90	5.93	25.46	14.72	492.47	0.16	600.00	100.00

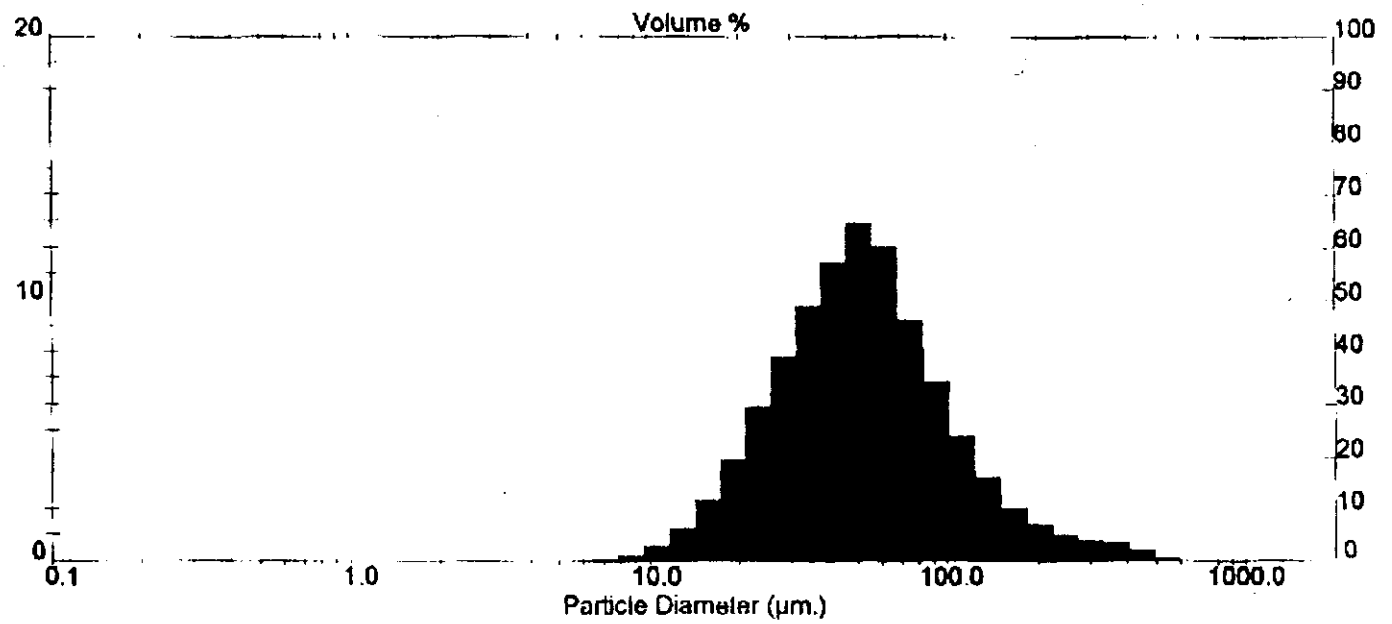

MALVERN INSTRUMENTS **MASTERSIZER X**

Version 1.2a

Fri, Oct 10, 2003 11:09AM

Sishen FeSi 2 :Run Number 3

Dispersant: Milli RO water in MSX14

Sample 2
Sample File Name: FERRO_01, Record: 3
Measured on: Fri, Jan 04, 1980 8:24PM Last saved on: Fri, Jan 04, 1980 8:24PM

Source: Analysed

Presentation: 20HD
Very Polydisperse model

Volume Result

Focus = 300 mm.

Residual = 0.953 %
d (0.5) = 43.80 µm
D [4, 3] = 59.26 µm
Sauter Mean (D[3,2]) = 37.14 µm
Specific Surface Area = 0.1616 sq. m. / gm

Concentration = 0.012 %
d (0.1) = 20.69 µm
Span = 1.95

Obscuration = 14.63 %
d (0.9) = 108.09 µm

Mode = 43.63 µm
Density = 1.00 gm. / c.c.

Size (Lo) µm	Result In %	Size (Hi) µm	Result Below %	Size (Lo) µm	Result In %	Size (Hi) µm	Result Below %
0.50	0.00	1.32	0.00	25.46	10.33	31.01	28.35
1.32	0.00	1.60	0.00	31.01	12.09	37.79	40.45
1.60	0.00	1.95	0.00	37.79	12.78	46.03	53.23
1.95	0.00	2.38	0.00	46.03	12.46	56.09	65.69
2.38	0.00	2.90	0.00	56.09	10.55	68.33	76.24
2.90	0.00	3.53	0.01	68.33	7.57	83.26	83.82
3.53	0.01	4.30	0.02	83.26	5.24	101.44	89.06
4.30	0.02	5.24	0.05	101.44	3.58	123.59	92.64
5.24	0.06	6.39	0.11	123.59	2.39	150.57	95.03
6.39	0.11	7.78	0.22	150.57	1.52	183.44	96.54
7.78	0.28	9.48	0.50	183.44	1.04	223.51	97.58
9.48	0.64	11.55	1.14	223.51	0.77	272.31	98.35
11.55	1.43	14.08	2.56	272.31	0.60	331.77	98.95
14.08	2.80	17.15	5.37	331.77	0.52	404.21	99.47
17.15	4.94	20.90	10.31	404.21	0.36	492.47	99.82
20.90	7.72	25.46	18.03	492.47	0.18	600.00	100.00

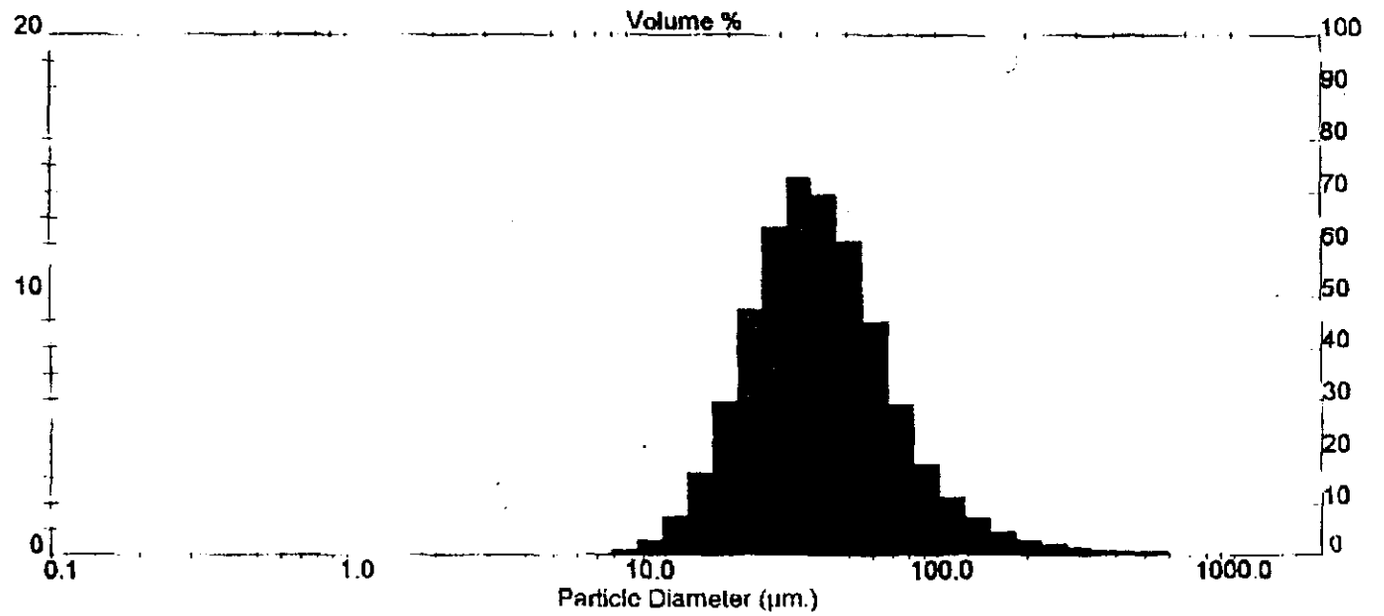

MALVERN INSTRUMENTS

MASTERSIZER X

Version 1.2a

Fri, Oct 10, 2003 11:09AM

Sishen FeSi 3 :Run Number 5

Dispersant: Milli RO water in MSX14

Sample 3
Sample File Name: FERRO_01, Record: 5
Measured on: Fri, Jan 04, 1980 8:35PM Last saved on: Fri, Jan 04, 1980 8:35PM

Source: Analysed

Presentation: 2OHD
Very Polydisperse model

Volume Result

Focus = 300 mm

Residual = 1.176 %
d (0.5) = 47.27 µm
D [4, 3] = 63.93 µm
Sauter Mean (D[3,2]) = 36.73 µm
Specific Surface Area = 0.1634 sq. m. / gm

Concentration = 0.012 %
d (0.1) = 20.72 µm
Span = 2.09

Obscuration = 15.14 %
d (0.9) = 119.57 µm

Mode = 49.05 µm
Density = 1.00 gm. / c.c.

Size (Lo) µm	Result In %	Size (Hi) µm	Result Below %	Size (Lo) µm	Result In %	Size (Hi) µm	Result Below %
0.50	0.04	1.32	0.04	25.46	8.90	31.01	25.90
1.32	0.03	1.60	0.07	31.01	10.57	37.79	36.47
1.60	0.03	1.95	0.09	37.79	11.86	46.03	48.33
1.95	0.03	2.38	0.13	46.03	12.36	56.09	60.69
2.38	0.04	2.90	0.16	56.09	11.06	68.33	71.75
2.90	0.04	3.53	0.20	68.33	8.44	83.26	80.19
3.53	0.05	4.30	0.25	83.26	6.08	101.44	86.26
4.30	0.07	5.24	0.32	101.44	4.36	123.59	90.63
5.24	0.11	6.39	0.43	123.59	2.99	150.57	93.62
6.39	0.18	7.78	0.61	150.57	2.04	183.44	95.66
7.78	0.34	9.48	0.95	183.44	1.48	223.51	97.13
9.48	0.71	11.55	1.66	223.51	1.06	272.31	98.19
11.55	1.45	14.06	3.11	272.31	0.75	331.77	98.94
14.06	2.67	17.15	5.77	331.77	0.56	404.21	99.51
17.15	4.46	20.90	10.23	404.21	0.33	492.47	99.84
20.90	6.77	25.46	17.00	492.47	0.16	600.00	100.00

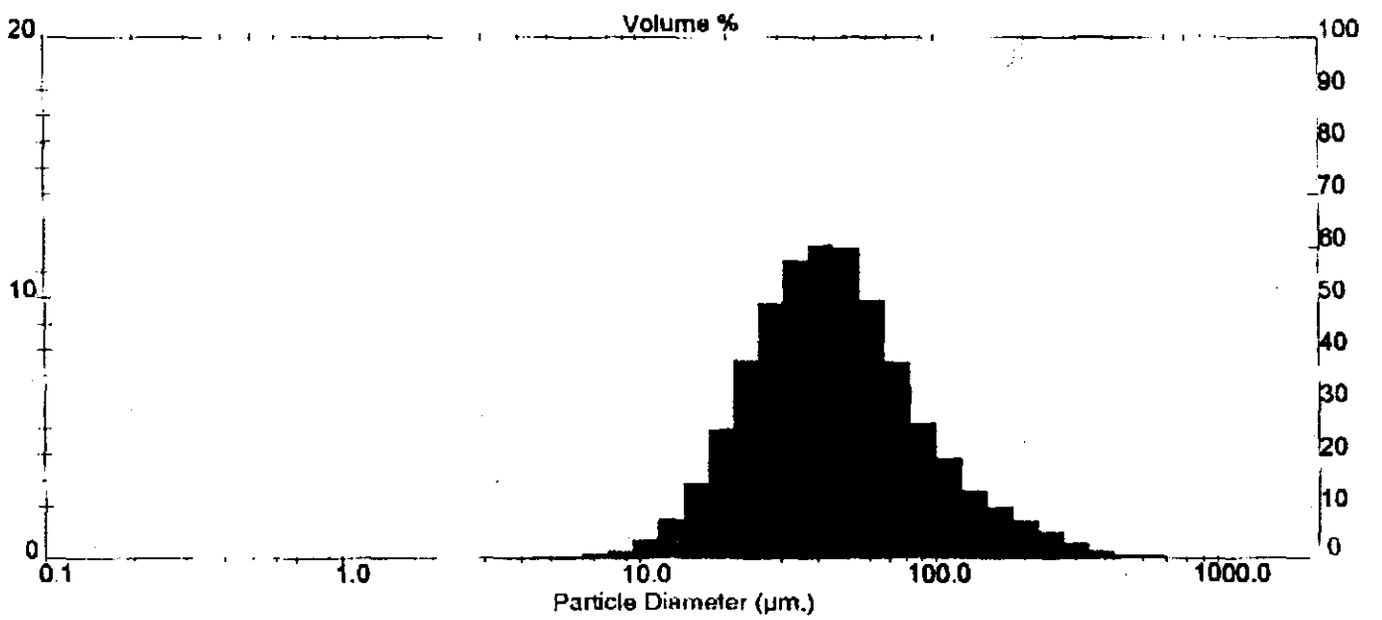

MALVERN INSTRUMENTS MASTERSIZER

Result: Analysis Report

Sample Details

Sample ID: FeSi (14)
Sample File: FESI
Sample Path: C:\SIZERS\DATA\
Sample Notes: Pump 8; Stirrer 8; Ultrasonoics 9
Sweeps 7.0 sek
Sample wet with Methanol
FeSi (14) Johan

Run Number: 3
Record Number: 4

Measured:
Analysed: Tue Nov 25 2003 8:33AM
Result Source: Averaged

System Details

Range Lens: 300RF mm
Presentation: 3OHD
Analysis Model: Polydisperse
Modifications: None

Beam Length: 2.40 mm
[Particle R.I. = (1.5295, 0.1000); Dispersant R.I. = 1.3300]

Sampler:

Obscuration: 13.1 %
Residual: 0.472 %

Result Statistics

Distribution Type: Volume
Mean Diameters:
D [4, 3] = 27.91 um

Concentration = 0.0226 %Vol
D (v, 0.1) = 7.00 um
D [3, 2] = 5.44 um

Density = 1.000 g / cub. cm
D (v, 0.5) = 21.35 um
Span = 2.043E+00

Specific S.A. = 1.1034 sq. m / g
D (v, 0.9) = 50.62 um
Uniformity = 7.367E-01

Size Low (um)	In %	Size High (um)	Under%
0.05	0.01	0.06	0.01
0.06	0.03	0.07	0.04
0.07	0.04	0.08	0.08
0.08	0.06	0.09	0.14
0.09	0.08	0.11	0.21
0.11	0.10	0.13	0.32
0.13	0.13	0.15	0.45
0.15	0.17	0.17	0.61
0.17	0.21	0.20	0.82
0.20	0.25	0.23	1.07
0.23	0.28	0.27	1.35
0.27	0.29	0.31	1.64
0.31	0.26	0.36	1.91
0.36	0.22	0.42	2.12
0.42	0.16	0.49	2.29
0.49	0.11	0.58	2.40
0.58	0.06	0.67	2.46
0.67	0.03	0.78	2.49
0.78	0.02	0.91	2.51
0.91	0.02	1.06	2.54
1.06	0.03	1.24	2.57
1.24	0.05	1.44	2.62
1.44	0.08	1.68	2.70
1.68	0.12	1.95	2.83
1.95	0.18	2.28	3.01
2.28	0.26	2.65	3.27
2.65	0.38	3.09	3.65
3.09	0.53	3.60	4.18
3.60	0.74	4.19	4.92
4.19	1.02	4.88	5.94
4.88	1.40	5.69	7.34
5.69	1.87	6.63	9.20

Size Low (um)	In %	Size High (um)	Under%
6.63	2.45	7.72	11.65
7.72	3.16	9.00	14.81
9.00	3.99	10.48	18.80
10.48	4.92	12.21	23.72
12.21	5.94	14.22	29.66
14.22	6.96	16.57	36.63
16.57	7.85	19.31	44.47
19.31	8.44	22.49	52.91
22.49	8.62	26.20	61.53
26.20	8.40	30.53	69.93
30.53	7.51	35.56	77.43
35.56	6.30	41.43	83.73
41.43	4.98	48.27	88.71
48.27	3.71	56.23	92.42
56.23	2.59	65.51	95.01
65.51	1.68	76.32	96.69
76.32	1.01	88.91	97.70
88.91	0.56	103.58	98.26
103.58	0.30	120.67	98.56
120.67	0.19	140.58	98.75
140.58	0.17	163.77	98.92
163.77	0.20	190.80	99.12
190.80	0.23	222.28	99.35
222.28	0.24	258.95	99.59
258.95	0.19	301.68	99.79
301.68	0.13	351.46	99.91
351.46	0.06	409.45	99.98
409.45	0.02	477.01	100.00
477.01	0.00	555.71	100.00
555.71	0.00	647.41	100.00
647.41	0.00	754.23	100.00
754.23	0.00	878.67	100.00

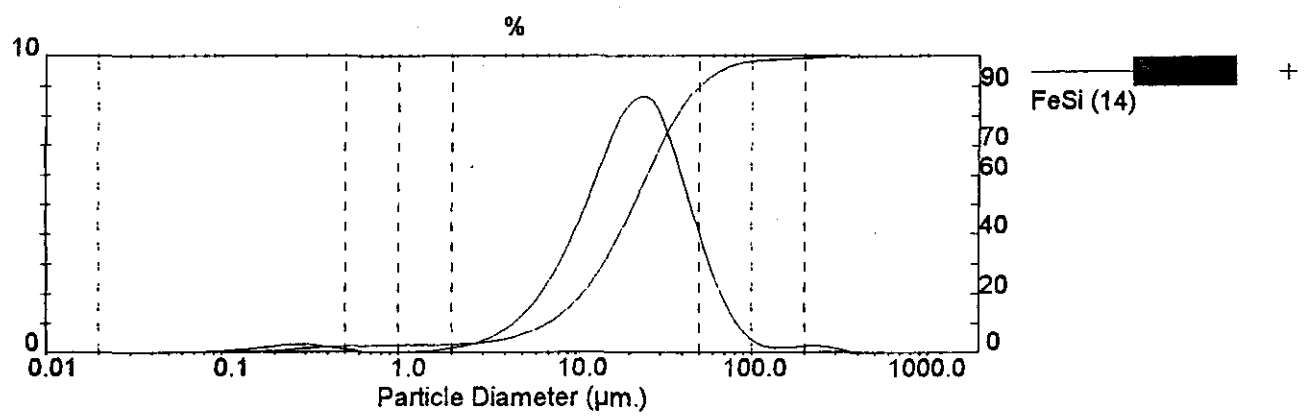

alvern Instruments Ltd.
alvern, UK
l:=+[44] (0)1684-892456 Fax:+[44] (0)1684-892789

ANALYTICAL REPORT FESI

No unauthorised copies may be made of this report.

JOHAN LIEBENBERG
NICO BOTES

Tel:

Fax:

Date of Request 2003/11/25

From : UIS Analytical Services
Analytical Chemistry
Laboratories D109, D120
Tel: (012) 307 -4783
Fax: (012) 307-3263
Fax: (012) 307-3263

Certificate of analysis: 1670

Sample Origen	Sample ID	Note: all results in percentage (%) unless specified otherwise						
		Si	Al	Fe	Mn	Cu	Cr	Ni
	FESI	14.4	0.15	84.9	0.26	0.02	0.04	0.01

Comments / additional information: Please note that where no results are filled in, the Minimum as in the row below the element will apply

Identification of test methods:		
	Chemical elements:	
	Instrument:	ICP- OES Perkin Elmer Optima 3000
	Documentation:	

Date: 2003/11/26
Analysed by: K GOVENDER

Date: 2003/11/27
Authorised : K GOVENDER

Untitled:10

Label: Sample 1

kV:15.0 Tilt:0.0 Take-off:20.0 Det Type:SUTW Res:143 Tc:40

FS : 3531 Lsec : 108

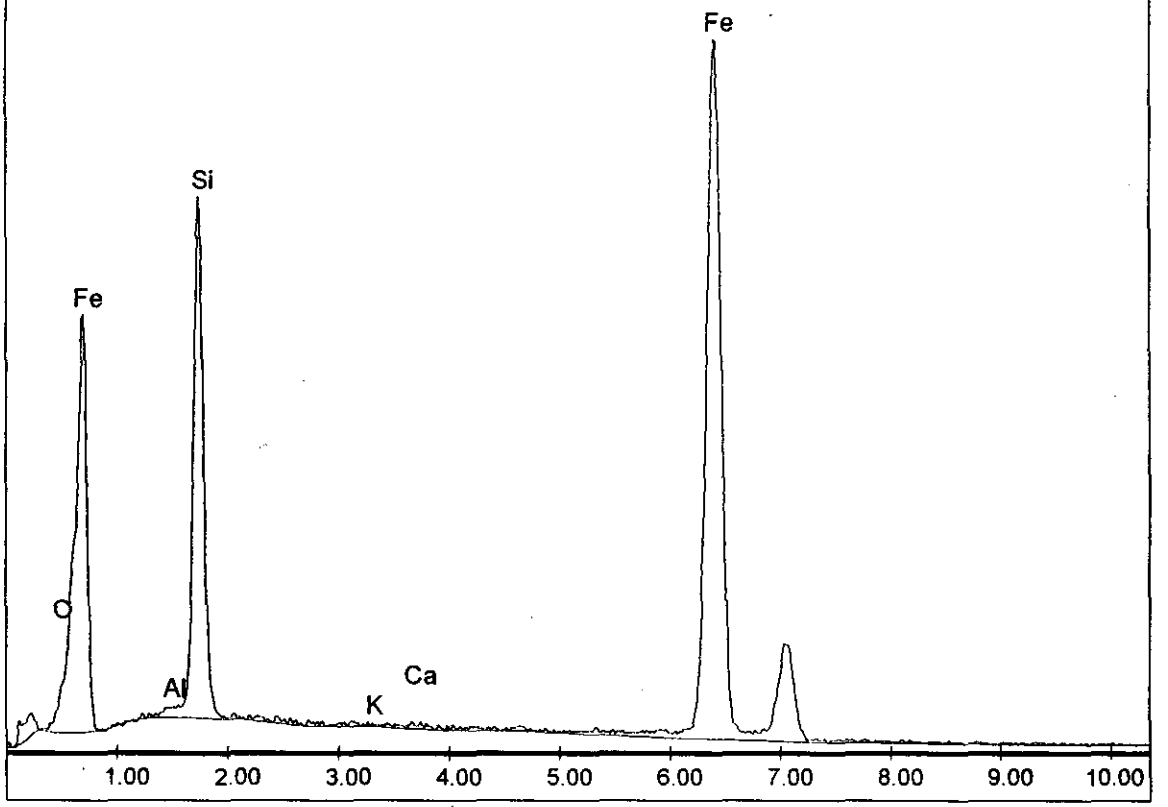

EDAX PhiZAF Quantification (Standardless)
Element Normalized
SEC Table : Default

Element	Wt %	At %	Z	A	F
O K	3.87	10.82	1.2073	0.3792	1.0035
AlK	0.45	0.74	1.0893	0.3704	1.0028
SiK	14.80	23.56	1.1160	0.4909	1.0006
K K	0.10	0.11	1.0474	0.8621	1.0129
CaK	0.23	0.25	1.0687	0.9043	1.0220
FeK	80.56	64.51	0.9607	0.9977	1.0000
Total	100.00	100.00			

Untitled:10

Label: Sample 2

kV:15.0 Tilt:0.0 Take-off:20.0 Det Type:SUTW Res:143 Tc:40

FS : 6185 Lsec : 110

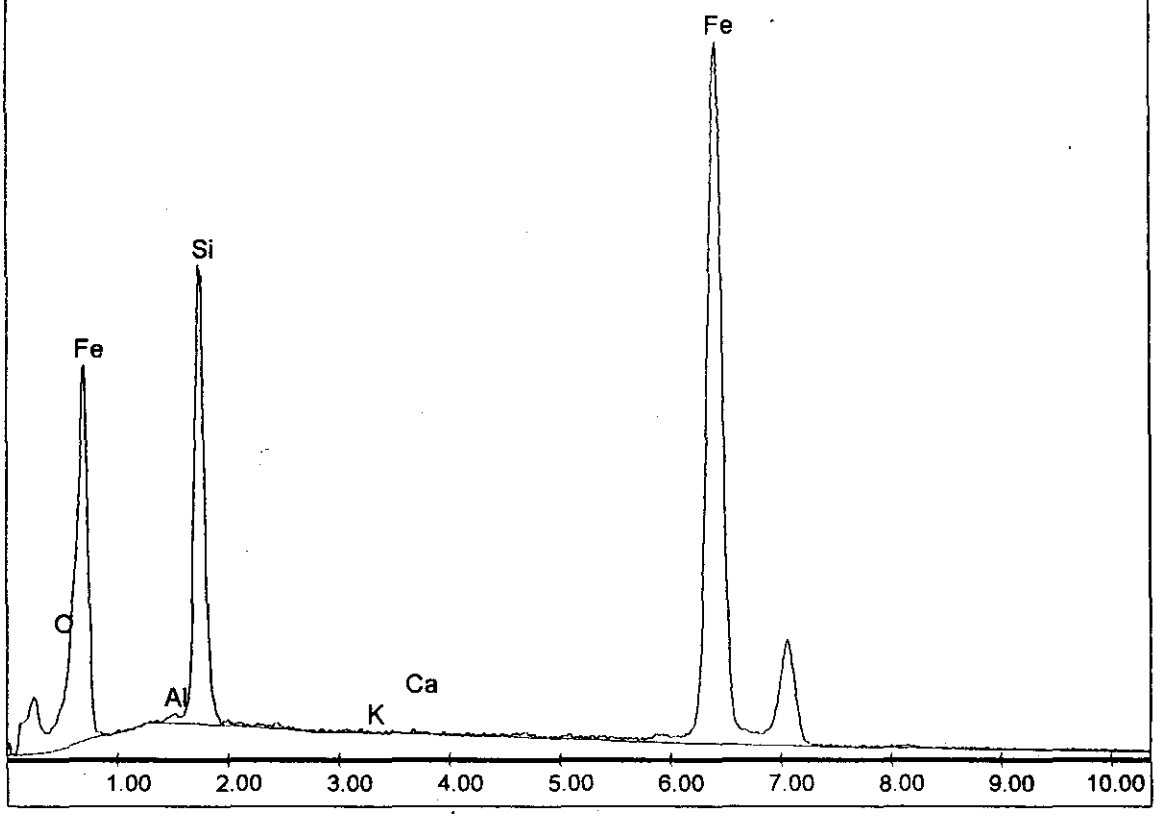

EDAX PhiZAF Quantification (Standardless)
Element Normalized
SEC Table : Default

Element	Wt %	At %	Z	A	F
O K	4.15	11.70	1.2096	0.3886	1.0036
AlK	0.33	0.55	1.0913	0.3656	1.0026
SiK	13.41	21.51	1.1180	0.4862	1.0006
K K	0.00	0.00	1.0494	0.8640	1.0131
CaK	0.09	0.10	1.0708	0.9063	1.0227
FeK	82.01	66.14	0.9627	0.9983	1.0000
Total	100.00	100.00			

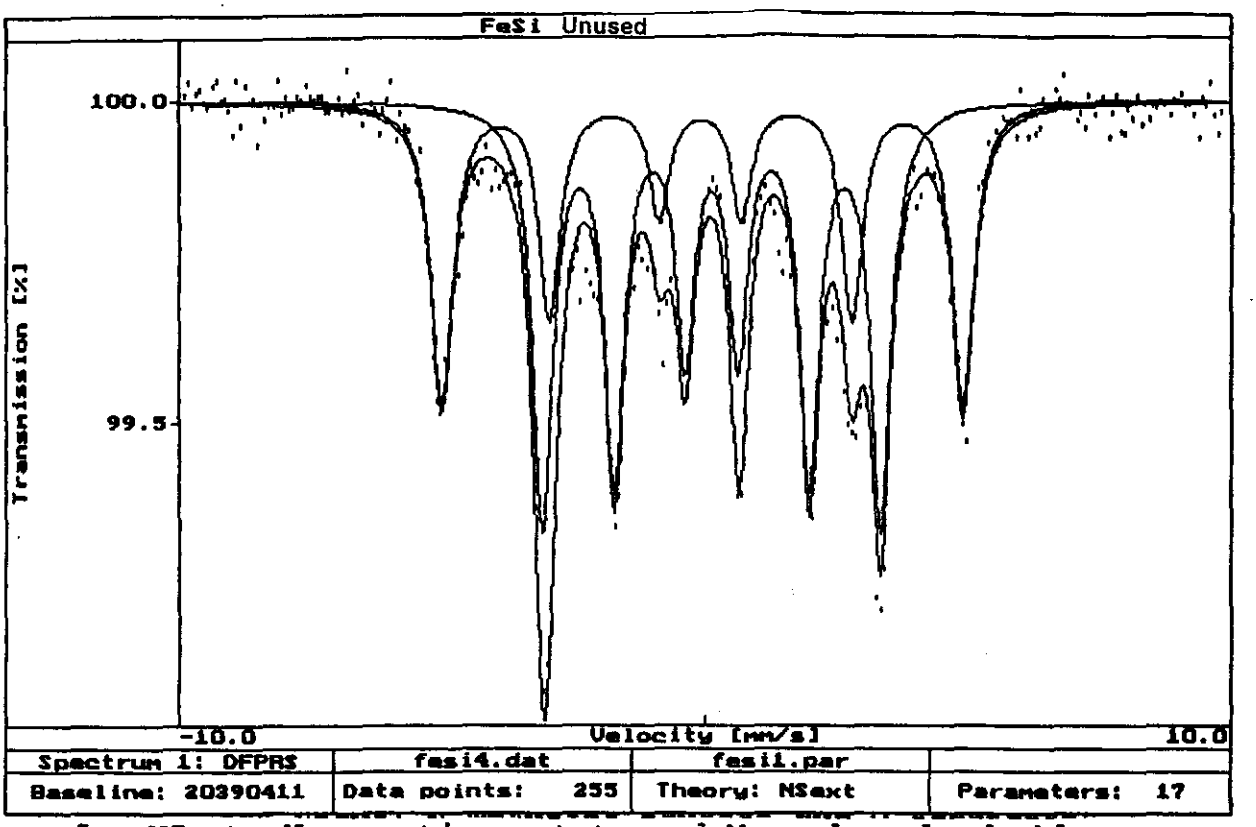

Parameters for NSext: N magnetic sextets and M quadrupole doublets
fitresults of data :
FeSi skoon en nuut

foldingpoint	256.0				
geometryeffect	0.033 %				
theory	C:\PCMOS\NSext.exe				
date	Tue Jan 07 10:25:27 2003				
flags	---CE-				
fitspectra	1				
chi2	2.6298				
chi2-test	0.0000 %				
corr-test	0.0001 %				
fitcycles	7				
maxiter	25				
parasig	1				
chi2sig	1				
fitparameter	17				
Baseline	20389426	20390411	460.85009	1.010	1.021
Total Area	0.01040	0.02404	0.00023	1.021	1.031
Sextets	2.00000	2.00000 F	0.00000	0.000	0.000
Doublets	0.00000	0.00000 F	0.00000	0.000	0.000
Mag Field 1	31.10000	30.67377	0.03094	0.915	1.015
Quad Mag 1	-0.00900	0.04345	0.00886	0.970	0.934
Shift Mag 1	-0.03300	-0.06822	0.00444	0.916	0.964
Width Out 1	0.50000	0.49148	0.01600	1.083	1.049
3:2:1 Corr	1.00000	1.02524	0.05157	0.775	0.794
WNat Mag 1	0.40000	0.44239	0.05419	0.659	0.692
Mag Field 2	20.20000	19.84596	0.02270	1.028	1.035
Quad Mag 2	-0.02000	-0.00236	0.00522	1.057	1.081
Shift Mag 2	0.11300	0.12317	0.00269	1.017	1.069
Width Out 2	0.30000	0.46921	0.01186	0.767	0.655
3:2:1 Corr	1.00000	1.27455	0.02154	0.948	0.911
Area 2	0.25000	0.60978	0.01305	0.785	0.741
WNat Mag 2	0.19000	0.42676	0.02053	0.828	0.706

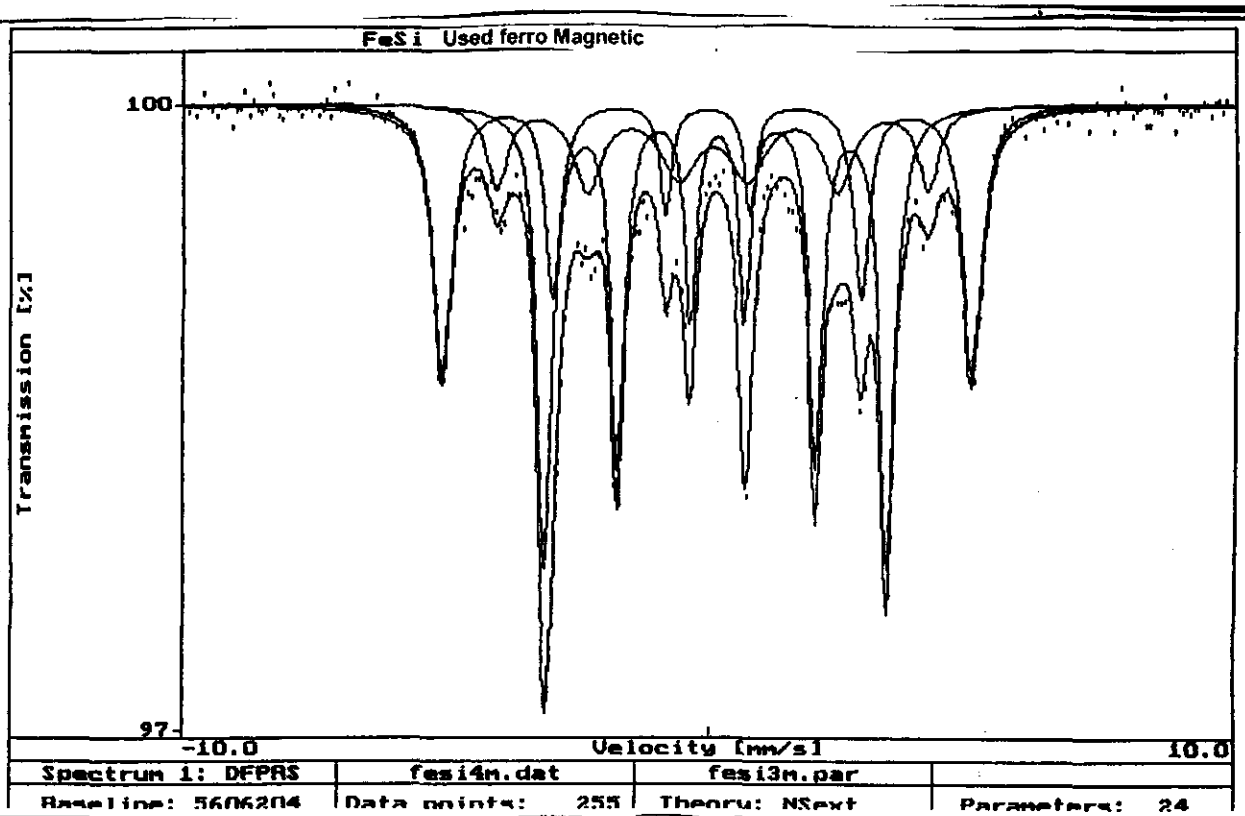

Parameters for NSext: N magnetic sextets and M quadrupole doublets
fitresults of data :
FeSi monster 4 mag na 5 dae in lus

foldingpoint	255.5				
geometryeffect	0.019 %				
theory	C:\PCMOS\NSext.exe				
date	Sun Aug 03 10:49:24 2003				
flags	---CE-				
fitspectra	1				
chi2	2.3233				
chi2-test	0.0000 %				
corr-test	0.0001 %				
fitcycles	5				
maxiter	25				
parasig	1				
chi2sig	1				
fitparameter	24				
Baseline	5605478	5606204	246.03065	0.972	1.033
Total Area	0.04840	0.06678	0.00046	0.962	1.042
Sextets	3.00000	3.00000 F	0.00000	0.000	0.000
Doublets	0.00000	0.00000 F	0.00000	0.000	0.000
Mag Field 1	31.22000	31.19306	0.02005	0.856	1.025
Quad Mag 1	0.02100	0.01126	0.00511	1.013	0.975
S ift Mag 1	-0.07300	-0.05982	0.00257	0.980	1.006
Width Out 1	0.50000	0.43337	0.01094	1.087	0.839
3:2:1 Corr	1.19940	0.86789	0.03590	1.109	1.026
WNat Mag 1	0.54000	0.23284	0.02694	1.038	0.882
Mag Field 2	20.07000	20.09783	0.01082	1.059	0.978
Quad Mag 2	-0.00700	-0.00915	0.00258	1.021	0.975
Shift Mag 2	0.12300	0.11727	0.00136	0.995	0.990
Width Out 2	0.30000	0.34881	0.00638	1.185	0.944
3:2:1 Corr	1.19000	1.03480	0.02620	1.167	1.132
Area 2	0.44000	0.47223	0.00883	1.182	0.918
WNat Mag 2	0.29000	0.26036	0.01460	1.133	1.049
Mag Field 3	25.46000	25.36802	0.06981	1.035	1.025
Quad Mag 3	-0.02100	-0.00147	0.01593	1.085	1.017
Shift Mag 3	0.00300	0.03563	0.00825	1.095	1.003
Width Out 3	0.49000	0.47191	0.04028	0.816	1.227
3:2:1 Corr	1.30000	2.11099	0.12723	1.249	0.998
Area 3	0.21000	0.22229	0.01263	0.833	1.171
WNat Mag 3	0.45000	0.91443	0.06111	1.009	0.824

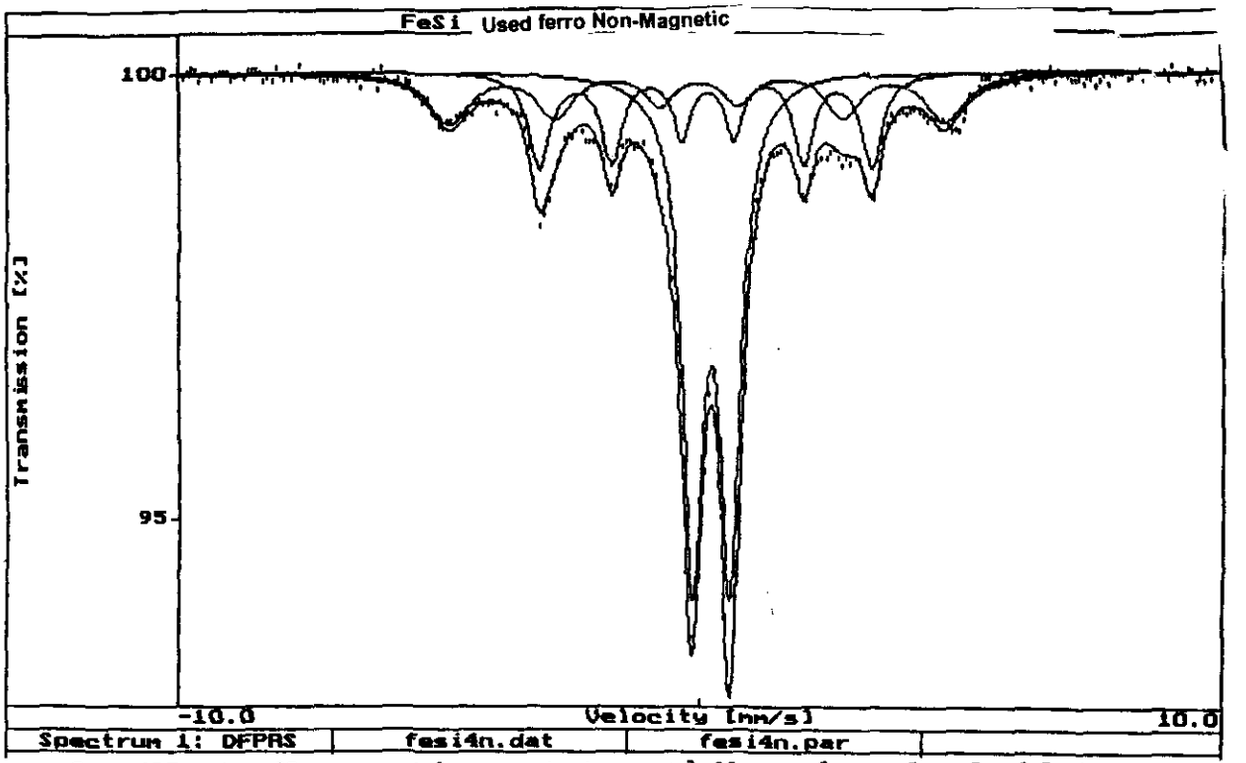

Parameters for NSext: N magnetic sextets and M quadrupole doublets
fitresults of data :
FeSi monster 4 nie magneties

foldingpoint	256.0				
geometryeffect	0.027 %				
theory	C:\PCMOS\NSext.exe				
date	Sun Aug 03 10:47:03 2003				
flags	---CE-				
fitspectra	1				
chi2	2.3542				
chi2-test	0.0000 %				
corr-test	0.0001 %				
fitcycles	7				
maxiter	25				
parasig	1				
chi2sig	1				
fitparameter	21				
Baseline	3048015	3046582	201.08986	1.113	1.075
Total Area	0.10900	0.10104	0.00074	1.177	1.115
Sextets	2.00000	2.00000 F	0.00000	0.000	0.000
Doublets	1.00000	1.00000 F	0.00000	0.000	0.000
Mag Field 1	30.26000	29.48644	0.09168	0.829	0.970
Quad Mag 1	0.02000	-0.02278	0.02114	0.897	0.922
Shift Mag 1	-0.05300	-0.05012	0.01112	0.917	0.877
Width Out 1	0.55000	0.93343	0.04928	1.360	1.148
3:2:1 Corr	1.30000	1.14998	0.10248	1.386	1.288
WNat Mag 1	0.40000	0.62432	0.11597	1.217	1.177
Mag Field 2	20.26000	19.69653	0.03647	1.063	1.083
Quad Mag 2	-0.00500	-0.03021	0.00817	1.039	1.027
Shift Mag 2	0.11300	0.11679	0.00417	1.036	1.034
Width Out 2	0.55000	0.51122	0.02171	0.768	0.832
3:2:1 Corr	1.30000	1.26713	0.05064	1.100	1.011
Area 2	0.30000	0.25841	0.01223	1.210	1.287
WNat Mag 2	0.40000	0.38813	0.03812	1.316	1.170
Quad Split 1	0.73000	0.71652	0.00352	0.805	0.882
Iso Shift 1	0.20000	0.19771	0.00140	0.930	0.966
Width 1	0.43000	0.47852	0.00456	1.101	1.114
Area 1	0.43000	0.50824	0.00646	1.087	1.137

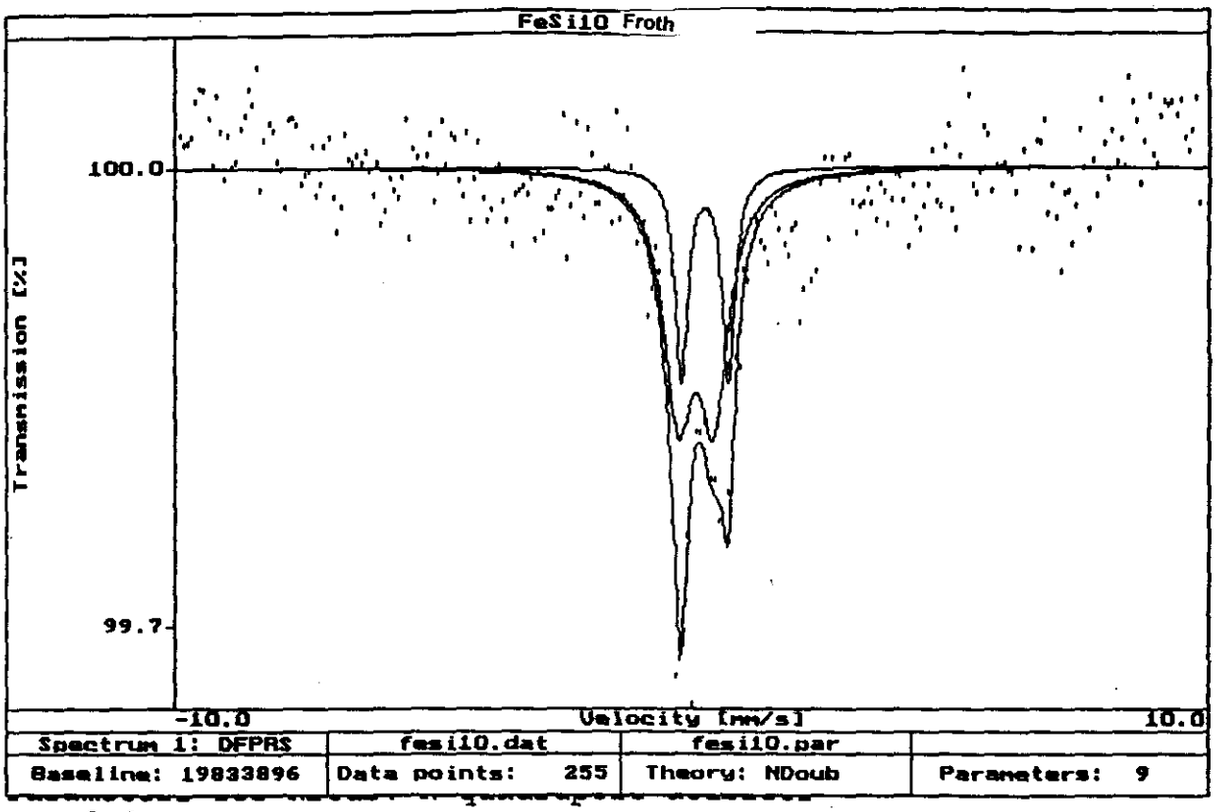

fitresults of data :
FeSi10 skuim

foldingpoint	255.0				
geometryeffect	0.005 %				
theory	C:\PCMOS\NDoub.exe				
date	Tue Apr 01 16:08:26 2003				
flags	---CE-				
fitspectra	1				
chi2	1.4675				
chi2-test	0.0002 %				
corr-test	0.0001 %				
fitcycles	9				
maxiter	25				
parasig	1				
chisig	1				
fitparameter	9				
Baseline	19833758	19833896	326.95264	1.098	0.870
Total Area	0.01000	0.00285	0.00012	1.215	0.720
Quad split 1	0.59000	0.69410	0.05955	-2.354	5.041
Iso shift 1	0.17030	0.06029	0.04603	2.946	1.056
Width 1	0.45440	0.68917	0.08433	1.719	-0.403
Quad split 2	0.65000	0.91837	0.04120	4.179	-1.084
Iso shift 2	0.16230	0.23499	0.02247	-2.979	4.956
Width 2	0.55000	0.43157	0.15597	3.928	0.240
Area 2	0.38700	0.28646	0.14177	3.772	0.295

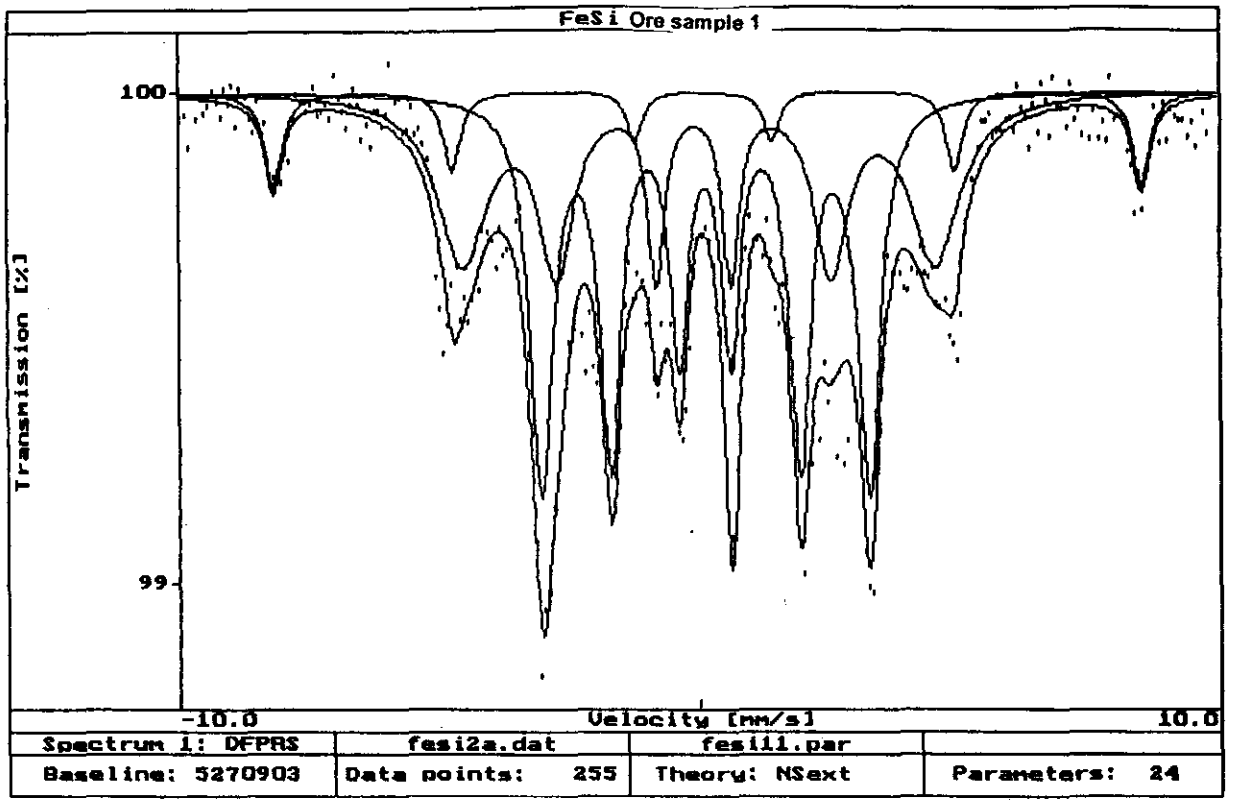

Parameters for NSext: N magnetic sextets and M quadrupole doublets
fitresults of data :
FeSi 2A

foldingpoint	255.5				
geometryeffect	0.020 %				
theory	C:\PCMOS\NSext.exe				
date	Mon Nov 10 16:46:09 2003				
flags	---CE-				
fitspectra	1				
chi2	1.9627				
chi2-test	0.0000 %				
corr-test	0.0049 %				
fitcycles	22				
maxiter	25				
parasig	1				
chi2sig	1				
fitparameter	24				
Baseline	5269322	5270903	347.66290	1.246	1.181
Total Area	0.01240	0.03953	0.00081	1.320	1.223
Sextets	3.00000	3.00000 F	0.00000	0.000	0.000
Doublets	0.00000	0.00000 F	0.00000	0.000	0.000
Mag Field 1	51.40000	51.86442	0.13106	1.198	0.491
Quad Mag 1	0.02100	0.08826	0.03308	1.111	0.567
Shift Mag 1	0.07300	0.12694	0.01654	0.496	1.176
Width Out 1	0.50000	0.41102	0.06793	1.587	1.269
3:2:1 Corr	1.19940	1.19940 F	0.00000	0.000	0.000
WNat Mag 1	0.40000	0.36477	0.09540	1.424	1.006
Mag Field 2	30.40000	28.29220	0.13396	0.566	0.822
Quad Mag 2	0.02100	0.10076	0.02473	0.937	0.674
Shift Mag 2	-0.07300	-0.04404	0.01263	0.962	0.690
Width Out 2	0.50000	1.16135	0.07306	1.553	1.336
3:2:1 Corr	1.19940	1.03405	0.06880	1.259	0.956
Area 2	0.55000	0.40571	0.02122	1.218	0.944
WNat Mag 2	0.40000	0.24335	0.06185	1.198	0.828
Mag Field 3	19.66000	19.55914	0.03723	1.104	1.111
Quad Mag 3	0.01100	0.00194	0.00836	1.117	1.048
Shift Mag 3	0.12300	0.11983	0.00435	1.061	1.111
Width Out 3	0.30000	0.53440	0.02120	0.652	0.762
3:2:1 Corr	1.00000	1.23946	0.03999	1.012	1.137
Area 3	0.25000	0.50394	0.02173	0.958	1.199
WNat Mag 3	0.29000	0.40833	0.03532	0.999	1.078

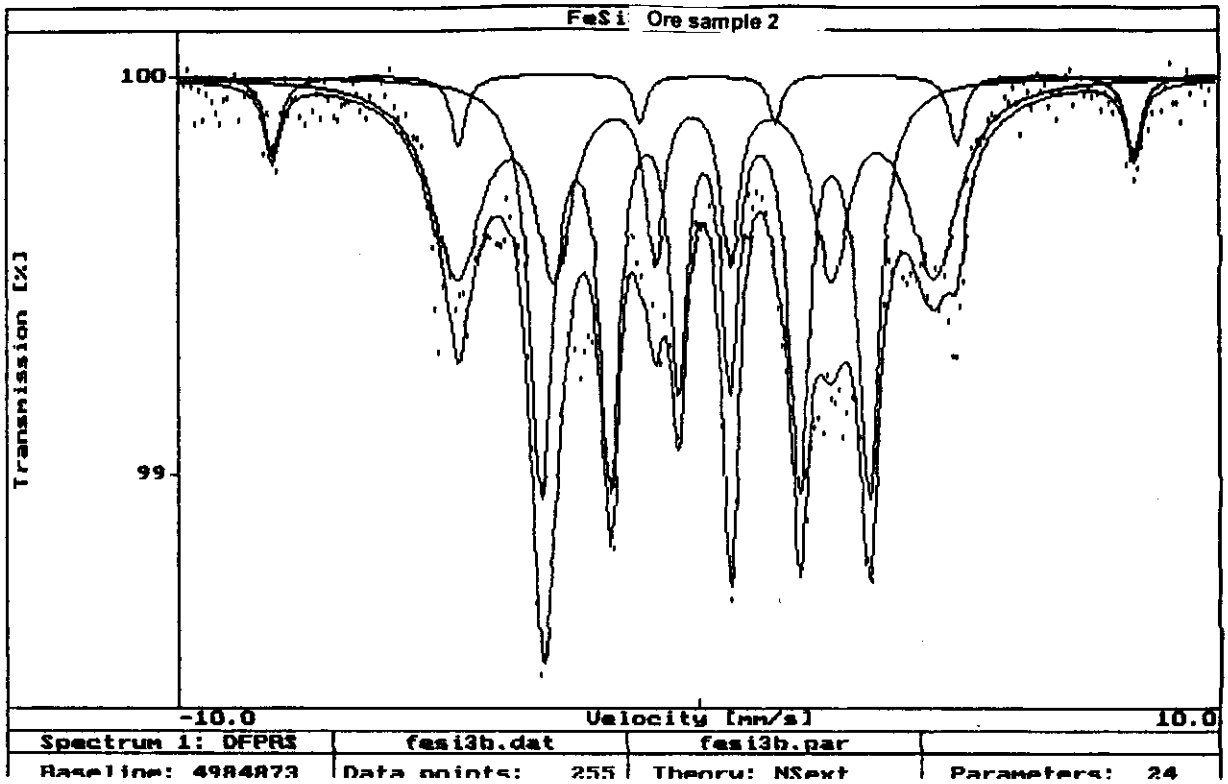

Parameters for NSext: N magnetic sextets and M quadrupole doublets
fitresults of data :
FeSi3b

foldingpoint	255.5				
geometryeffect	0.024 %				
theory	C:\PCMOS\NSext.exe				
date	Mon Nov 10 17:17:00 2003				
flags	---CE-				
fitspectra	1				
chi2	2.5810				
chi2-test	0.0000 %				
corr-test	0.0000 %				
fitcycles	16				
maxiter	25				
parasig	1				
chi2sig	1				
fitparameter	24				
Baseline	4983444	4984873	328.00022	1.166	1.195
Total Area	0.01240	0.04466	0.00072	1.258	1.163
Sextets	3.00000	3.00000 F	0.00000	0.000	0.000
Doublets	0.00000	0.00000 F	0.00000	0.000	0.000
Mag Field 1	51.40000	51.49542	0.11908	0.295	1.538
Quad Mag 1	0.08100	-0.07892	0.02992	0.665	1.160
Shift Mag 1	0.12300	0.14791	0.01496	1.268	0.522
Width Out 1	0.41000	-0.36464	0.06064	1.017	1.196
3:2:1 Corr	1.19940	1.19940 F	0.00000	0.000	0.000
WNat Mag 1	0.40000	-0.28306	0.07787	1.056	1.347
Mag Field 2	28.29000	28.56417	0.09835	0.939	0.303
Quad Mag 2	0.10100	0.04886	0.01947	0.573	0.982
Shift Mag 2	-0.04300	-0.08629	0.00978	0.584	1.014
Width Out 2	1.10000	1.18468	0.05453	1.498	1.505
3:2:1 Corr	1.03940	0.97496	0.05466	1.415	1.273
Area 2	0.40500	0.50391	0.02069	1.255	1.326
WNat Mag 2	0.34000	0.28552	0.05875	1.452	1.124
Mag Field 3	19.66000	19.54593	0.02896	1.116	1.087
Quad Mag 3	0.00100	0.01364	0.00651	1.103	1.050
Shift Mag 3	0.12300	0.12037	0.00335	1.136	1.035
Width Out 3	0.53000	0.52354	0.01690	0.913	0.660
3:2:1 Corr	1.20000	1.27025	0.03121	1.189	1.222
Area 3	0.50000	0.56979	0.02057	1.263	1.247
WNat Mag 3	0.40000	0.37656	0.02644	1.171	1.218

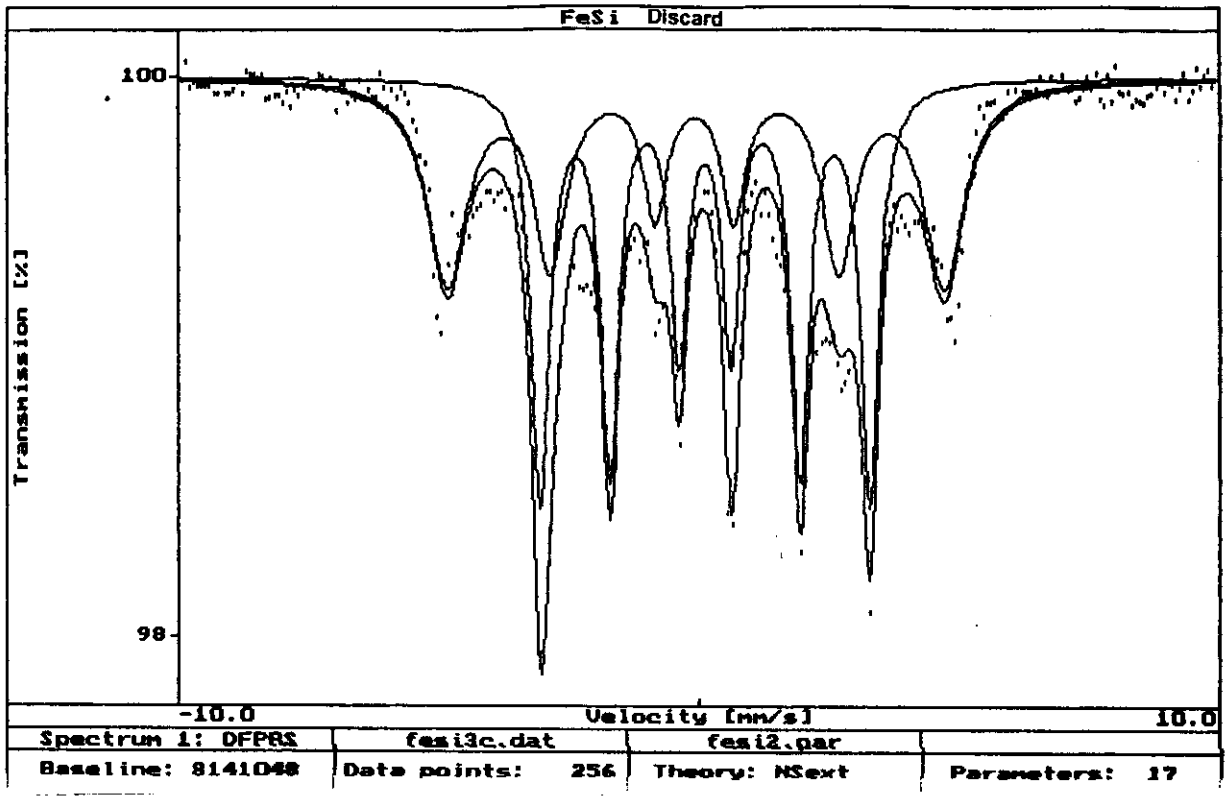

Parameters for NSext: N magnetic sextets and M quadrupole doublets
fitresults of data :
FeSi 3C

foldingpoint	255.5				
geometryeffect	0.021 %				
theory	C:\PCMOS\NSext.exe				
date	Mon Nov 10 16:50:06 2003				
flags	---CE-				
fitspectra	1				
chi2	6.1255				
chi2-test	0.0000 %				
corr-test	0.0000 %				
fitcycles	9				
maxiter	25				
parasig	1				
chi2sig	1				
fitparameter	17				
Baseline	8139081	8141048	313.64845	1.054	1.075
Total Area	0.01040	0.05969	0.00042	1.090	1.114
Sextets	2.00000	2.00000 F	0.00000	0.000	0.000
Doublets	0.00000	0.00000 F	0.00000	0.000	0.000
Mag Field 1	31.24000	29.72130	0.04157	1.277	0.639
Quad Mag 1	0.02560	0.02560 F	0.00000	0.000	0.000
Shift Mag 1	-0.07500	-0.07182	0.00467	1.004	1.068
Width Out 1	0.50000	0.91138	0.02190	1.037	1.176
3:2:1 Corr	1.08000	1.08000 F	0.00000	0.000	0.000
WNat Mag 1	0.48000	0.48000 F	0.00000	0.000	0.000
Mag Field 1	20.15000	19.65505	0.01373	1.068	1.099
Quad Mag 1	-0.02300	0.00541	0.00324	1.152	1.053
Shift Mag 1	0.11800	0.11948	0.00164	1.127	1.067
Width Out 1	0.30000	0.42787	0.00735	0.894	0.573
3:2:1 Corr	1.38000	1.33043	0.01344	0.932	0.953
Area 2	0.67000	0.53138	0.00675	1.081	0.863
WNat Mag 1	0.49000	0.38812	0.01007	0.852	0.833

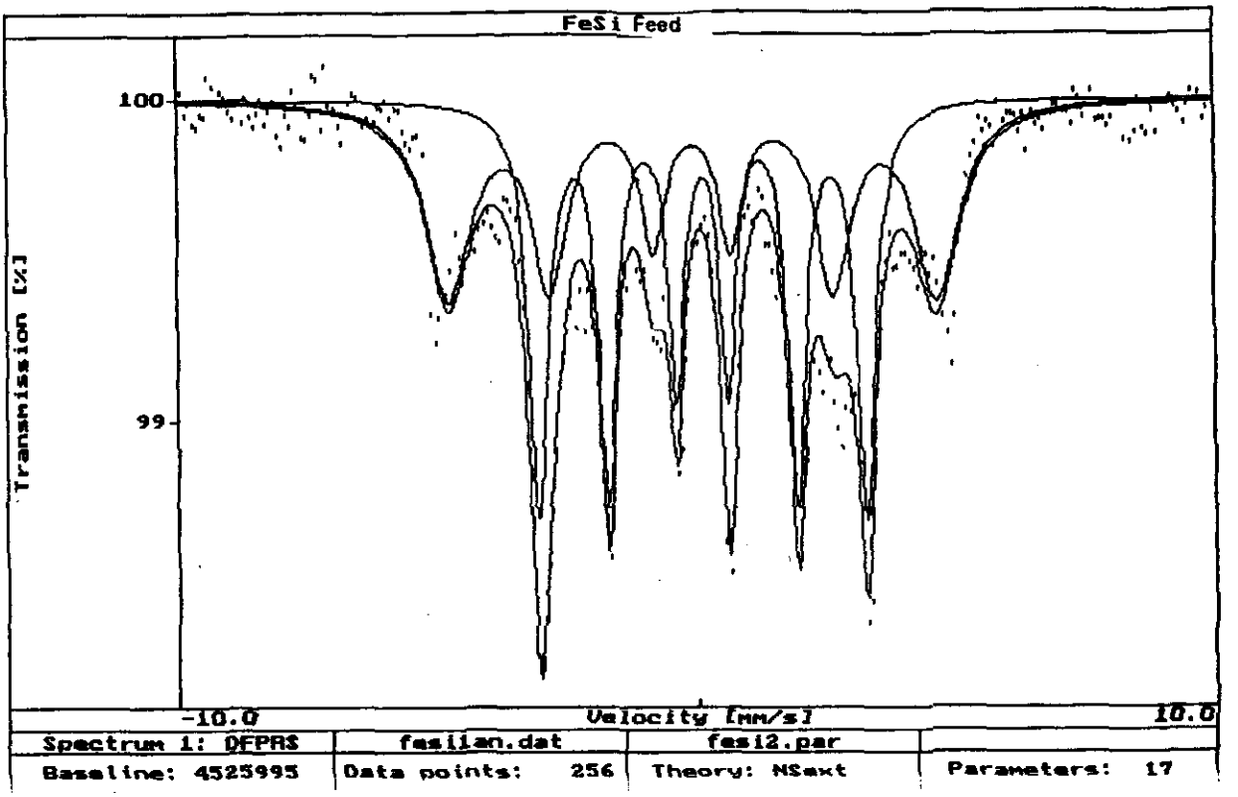

Parameters for NSext: N magnetic sextets and M quadrupole doublets
fitresults of data :
FeSi 1

foldingpoint	255.5				
geometryeffect	0.021 %				
theory	C:\PCMOS\NSext.exe				
date	Tue Nov 11 09:24:49 2003				
flags	---CE-				
fitspectra	1				
chi2	3.3165				
chi2-test	0.0000 %				
corr-test	0.0000 %				
fitcycles	8				
maxiter	25				
parasig	1				
chi2sig	1				
fitparameter	17				
Baseline	4525738	4525995	239.50323	0.682	1.565
Total Area	0.01040	0.05369	0.00059	0.643	1.745
Sextets	2.00000	2.00000 F	0.00000	0.000	0.000
Doublets	0.00000	0.00000 F	0.00000	0.000	0.000
Mag Field 1	31.24000	29.35123	0.07203	0.508	1.217
Quad Mag 1	0.02560	0.02560 F	0.00000	0.000	0.000
Shift Mag 1	-0.07500	-0.06257	0.00765	0.912	1.066
Width Out 1	0.50000	1.02918	0.03837	0.517	2.097
3:2:1 Corr	1.08000	1.08000 F	0.00000	0.000	0.000
WNat Mag 1	0.48000	0.48000 F	0.00000	0.000	0.000
Mag Field 1	20.15000	19.63692	0.02188	1.226	0.928
Quad Mag 1	-0.02300	0.00271	0.00504	0.912	1.282
Shift Mag 1	0.11800	0.12320	0.00256	0.925	1.267
Width Out 1	0.30000	0.44772	0.01197	0.982	0.526
3:2:1 Corr	1.38000	1.29335	0.02025	0.882	0.999
Area 2	0.67000	0.51345	0.01107	1.727	0.462
WNat Mag 1	0.49000	0.34981	0.01483	0.987	0.754

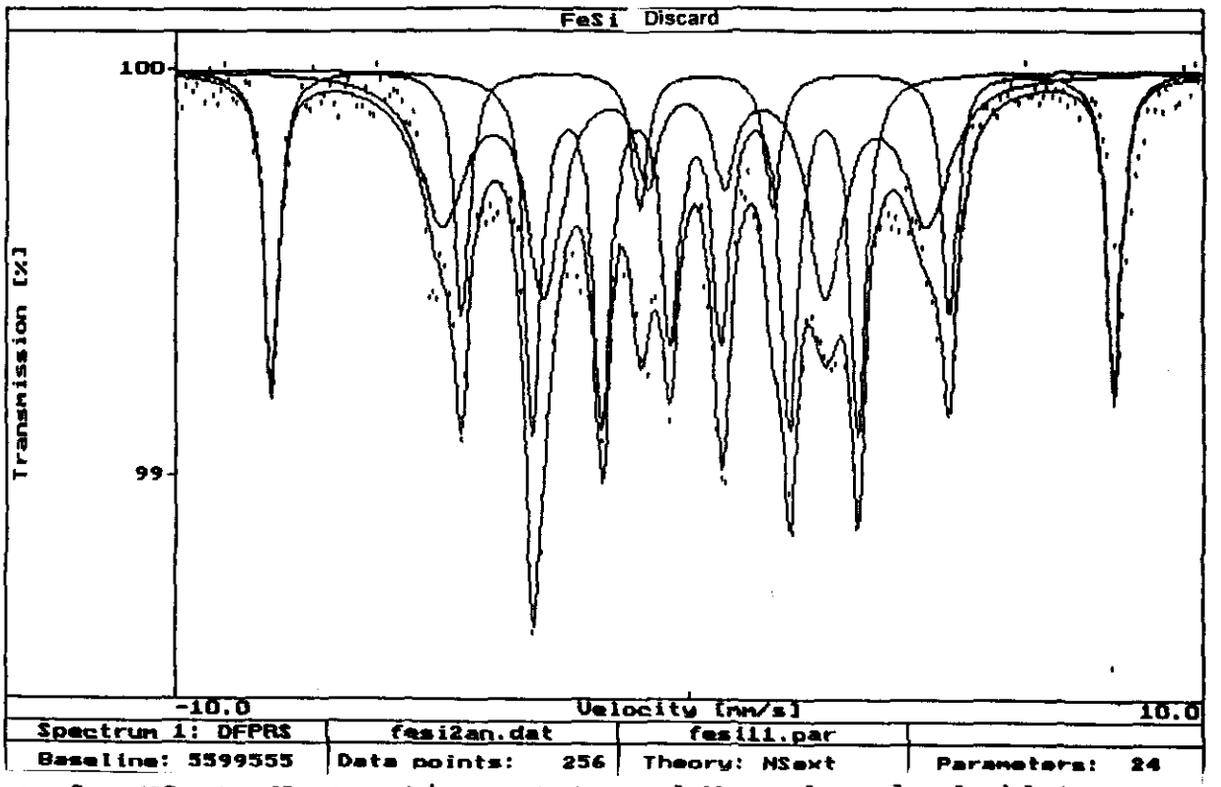

Parameters for NSext: N magnetic sextets and M quadrupole doublets
fitresults of data :
FeSi 2

foldingpoint	255.5				
geometryeffect	0.016 %				
theory	C:\PCMOS\NSext.exe				
date	Thu Nov 13 13:22:08 2003				
flags	---CE-				
fitspectra	1				
chi2	4.5364				
chi2-test	0.0000 %				
corr-test	22.5001 %				
fitcycles	11				
maxiter	25				
parasig	1				
chi2sig	1				
fitparameter	24				
Baseline	5599555	5599807	372.67676	1.797	0.590
Total Area	0.02540	0.05036	0.00082	1.912	0.565
Sextets	3.00000	3.00000 F	0.00000	0.000	0.000
Doublets	0.00000	0.00000 F	0.00000	0.000	0.000
Mag Field 1	51.04000	51.01821	0.03054	0.951	0.794
Quad Mag 1	-0.24000	-0.25726	0.00847	0.997	0.801
Shift Mag 1	0.19000	0.19661	0.00424	0.849	1.035
Width Out 1	0.50000	0.37568	0.01752	2.327	0.381
3:2:1 Corr	1.19940	0.98541	0.05316	0.767	1.565
WNat Mag 1	0.40000	0.26760	0.03809	1.094	1.565
Mag Field 2	29.41760	29.36663	0.09136	1.000	0.729
Quad Mag 2	-0.01700	0.04001	0.02299	0.876	0.909
Shift Mag 2	-0.07300	-0.08054	0.01114	0.873	0.893
Width Out 2	0.50000	0.98971	0.05652	1.777	0.842
3:2:1 Corr	1.19940	1.33385	0.07458	0.774	0.936
Area 2	0.55000	0.41018	0.01815	1.043	0.761
WNat Mag 2	0.40000	0.68570	0.08207	0.630	0.667
Mag Field 3	19.66000	19.61997	0.02652	0.992	1.198
Quad Mag 3	-0.00100	-0.00056	0.00619	1.187	0.992
Shift Mag 3	0.12300	0.12426	0.00306	1.122	0.984
Width Out 3	0.30000	0.41729	0.01477	0.753	0.787
3:2:1 Corr	1.00000	1.24898	0.04075	1.112	0.850
Area 3	0.25000	0.36824	0.01548	0.627	1.021
WNat Mag 3	0.43000	0.31849	0.02793	0.961	0.723

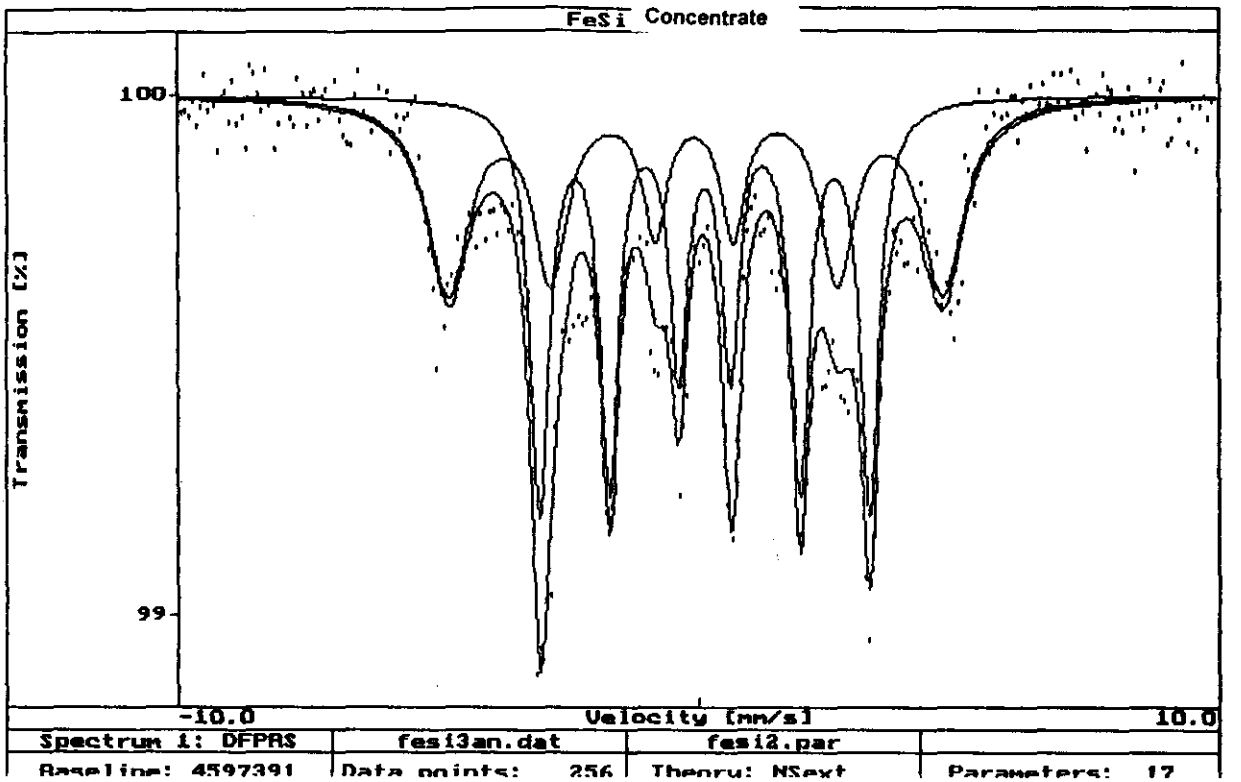

Parameters for NSext: N magnetic sextets and M quadrupole doublets
fitresults of data :
FeSi 3

foldingpoint	255.5				
geometryeffect	0.022 %				
theory	C:\PCMOS\NSext.exe				
date	Thu Nov 13 13:26:31 2003				
flags	---CE-				
fitspectra	1				
chi2	1.7634				
chi2-test	0.0000 %				
corr-test	0.0024 %				
fitcycles	8				
maxiter	25				
parasig	1				
chi2sig	1				
fitparameter	17				
Baseline	4596410	4597391	238.54043	0.799	1.356
Total Area	0.01040	0.03266	0.00058	0.777	1.466
Sextets	2.00000	2.00000 F	0.00000	0.000	0.000
Doublets	0.00000	0.00000 F	0.00000	0.000	0.000
Mag Field 1	31.24000	29.57666	0.11232	0.643	1.223
Quad Mag 1	0.02560	0.02560 F	0.00000	0.000	0.000
Shift Mag 1	-0.07500	-0.06123	0.01228	1.096	1.003
Width Out 1	0.50000	0.96638	0.05975	0.637	1.614
3:2:1 Corr	1.08000	1.08000 F	0.00000	0.000	0.000
WNat Mag 1	0.48000	0.48000 F	0.00000	0.000	0.000
Mag Field 1	20.15000	19.69199	0.03583	1.185	0.972
Quad Mag 1	-0.02300	0.00130	0.00838	0.973	1.227
Shift Mag 1	0.11800	0.12497	0.00427	0.983	1.212
Width Out 1	0.30000	0.44821	0.01934	0.900	0.569
3:2:1 Corr	1.38000	1.33963	0.03343	0.879	0.968
Area 2	0.67000	0.53752	0.01759	1.399	0.564
WNat Mag 1	0.49000	0.40943	0.02612	0.911	0.743